WASTEWATER TREATMENT AND WATER QUALITY ASSESSMENT THROUGH ELECTROCHEMICAL APPROACHES

A Thesis Presented to

The Faculty of Graduates Studies

Lakehead University

By

ZHAOYANG ZHANG

In partial fulfillment of the requirements for the degree of

Master of Science

September 2015

Lakehead UNIVERSITY

FACULTY OF GRADUATE STUDIES

NAME OF STUDENT: Zhaoyang Zhang

DEGREE AWARDED: Master of Science

ACADEMIC UNIT: Chemistry

TITLE OF THESIS: Wastewater Treatment and Water Quality Assessment Through Electrochemical Approaches

This thesis has been prepared

under my supervision

and the candidate has complied

with the Master's regulations.

Signature of Supervisor

Sept. 9, 2015

Date

Supervisor's Name (Printed) Aicheng Chen

Abstract

The protection of water resources is becoming one of the most critical issues afflicting people globally. Novel, robust, efficient, and environmentally compatible technologies for the treatment of wastewater and the analysis of water quality are urgently required. Fortunately, with the development of electrochemistry and new materials, promising and environmentally benign approaches for the treatment of wastewater and the assessment of water quality are currently available.

An advanced and efficient approach known as EDI was developed for the continuous separation and recovery of Cr(III) and Cr(VI). Firstly, we developed a new analytical method, which combines UV-Visible spectroscopy and Inductively Coupled Plasma Atomic Emission Spectroscopy (ICP-AES), for the determination of the concentrations of both Cr(VI) and Cr(III) in a mixed solution, and for monitoring the EDI process. Secondly, we determined the limiting current and systematically studied the effects of different applied currents on the removal of Cr(VI) as well as on the recovery of Cr(III) and Cr(VI). Thirdly, the influence of the level of saturation of the ion-exchange resins was assessed in terms of both removal efficiency and energy consumption. The use of fresh ion-exchange resins for the EDI process were initially found to be very effective for the removal of both Cr(VI) and Cr(III). Both resins became increasingly saturated with each subsequent cycle, resulting in a gradual lowering of the cell voltage. The continuous and highly efficacious removal of highly toxic Cr(VI) (> 99%), and low energy consumption make the EDI process attractive for the separation and recovery of Cr(VI) and Cr(III).

We also investigated the effective removal of nitrate from groundwater using EDI. An additional merit of this process was that hardness ions, such as Ca^{2+} and Mg^{2+}, were also simultaneously removed from the dilute compartment and recovered in the concentrate compartment. Furthermore, the impacts of different applied currents, water flow rates, and ratios of cationic and anionic exchange resins on the performance of nitrate removal were studied. When treating actual groundwater samples, the EDI system exhibited an excellent removal rate for all ions (>90%) under a low constant cell voltage. The results confirmed that the EDI process is suitable for the continuous and highly efficacious removal and recovery of nitrate and hardness ions in groundwater.

A novel, rapid, and environmentally compatible methodology for the determination of chemical oxygen demand (COD) using an electrochemically reduced nanoporous TiO_2 electrode was developed. A highly ordered nanoporous structure was grown directly onto a Ti plate through a three-step anodic oxidation process. Subsequent to electrochemical reduction, the nanoporous TiO_2 demonstrated a significant enhancement in photoelectrocatalytic activity. An advanced photoelectrochemical method based on the reduced nanoporous TiO_2 was successfully developed and employed to quantify COD values in both synthetic and actual wastewater samples. More importantly, the proposed method was in excellent agreement with the standard $K_2Cr_2O_7$ COD determination technique, albeit with a more rapid analysis period. Further merits included the negation of the necessity of any toxic ($Cr_2O_7^-$) and highly corrosive reagents (e.g. H_2SO_4), simple and automatic operation, and environmental compatibility.

Acknowledgements

First and foremost, I would like to express my sincere gratitude to my supervisor, Dr. Aicheng Chen, for all of his knowledge, advice and patience throughout the course of my M.Sc. degree. His support during my research has given me the confidence and encouragement required for a successful future in this field. I would also like to thank my committee members, Dr. Kinrade and Dr. MacKinnon, for their feedback on my thesis.

An extended thank you goes out to the entire Lakehead University Chemistry Department and to the Faculty of Graduate Studies. Thank you also to Dr. Guosheng Wu and Jiali Wen for their assistance in the Lakehead University Instrumentation Lab.

All of my fellow lab members in Dr. Chen's research group, both former and current, deserve special acknowledgement. For their direct aid in the development of my thesis I especially want to thank, Dr. Guosheng Wu, Jiali Wen, Dr. Sapanbir Thind, Shuai Chen, Xin Chang, Xiao Qu, Mona Amiri, Suresh Konda, Frank Boehm, and Daniel Liba.

Last, but not least, I would like to extend my deepest appreciation to my family and friends, especially my mother Hui Yang, my father Lingjie Zhang and my girlfriend Xiaochen Wang, for always being supportive, and helping me through the hard times that I have encountered.

List of abbreviations and symbols

Abbreviation	Name
AM	Anionic Membrane
BOD	Biological Oxygen Demand
CM	Cationic Membrane
COD	Chemical Oxygen Demand
CV	Cyclic Voltammetry
EC	Electrochemical
ED	Electrodialysis
EDI	Electrodeionization
EDS	Energy Dispersive Spectroscopy
ICP	Inductively Coupled Plasma
IX	Ion Exchange
LV	Linear Voltammetry
SEM	Scanning Electron Microscopy
UV	Ultraviolet
XRD	X-Ray Diffraction

Table of contents

Chapter 1 Introduction

1.1 Water pollution control and remediation technologies

Water is undoubtedly one of the most essential natural resources, and yet freshwater systems on the earth are threatened by human activities [1]. Considering the increasing quantities of pollutants that are being directly or indirectly discharged into water bodies (e.g., lakes, rivers, oceans, aquifers and groundwater), water pollution control and remediation have become issues of global concern [2]. It has been reported that the global demand for water has tripled since the 1950s, but the supply of fresh water has been declining [3]. Moreover, water contamination nowadays is one of the leading worldwide cause of deaths and diseases. Over 3,900 children die every day due to the diseases transmitted through unsafe drinking water, which accounts for the deaths of more than 14,000 people daily [4, 5]. In most cases, these deaths are related to waterborne enteric viruses and bacteria that cause intestinal parasitic infections and diarrheal diseases [6, 7]. It is therefore critical to have robust and efficient water pollution control systems and wastewater remediation technologies for human health.

Conventional methods of water quality control and water supply purification may be classified as physical methods (e.g., adsorption, filtration, solvent extraction.), chemical methods (e.g., chemical reduction, precipitation, desalination.) and biological methods (e.g., bacteria, microorganisms, invertebrates.). Although each of these methods possesses its own distinct advantages, they often require a considerable infusion of capital, as well as engineering expertise and appropriate system infrastructures for operation. Furthermore, the residues generated by intensive treatments may comprise a new source of freshwater

contamination if inappropriate disposal methods are used. In order to resolve wastewater remediation and water purification challenges for the benefit of human beings globally, the development of new, efficacious, low cost, sustainable and robust methods are urgently required.

1.2 General and new approaches for wastewater purification and water quality assessment

1.2.1 Wastewater purification

Wastewater purification involves processes that remove pollutants such as solids, algae, plants, bacteria, inorganic and organic compounds, and harmful ions to make water suitable for daily use, or for its return back to natural environments. Generally speaking, filtration [8] and extraction [9, 10] are often employed to remove solids, whereas adsorption [11], coagulation [12], flocculation [13] and sedimentation [14] are applied to remove inorganic and organic contaminants. Bacterial digestion [15] is another important technique for the removal of harmful pollutants. In recent years, technologies using ion exchange membranes known as "pressure-driven" and "electrically-driven" processes [16] have achieved great promise for the purification of wastewater without the intensive use of chemicals. Specifically, pressure-driven approaches (e.g., microfiltration, ultrafiltration, nanofiltration and reverse osmosis.) [17-19] are employed to remove suspended solids and bacteria, while electrically-driven processes (e.g., ion exchange, electrodialysis, electropermutation, donnan dialysis and electrodeionization, etc.) [20-23] are typically applied for the removal of harmful ions. Both of these approaches are based on the migration of ions through selective membranes. Permselective membranes can either facilitate anion exchange or cation

exchange. As depicted in Fig. 1.1, the anion exchange membrane contains a fixed matrix that is positively charged, with negative mobile ions residing within the pore spaces. When an electric field is applied, the anions from a solution may enter the pores, replace the mobile ions, and traverse the membrane, while the passage of cations is rejected by the positively charged matrix [24, 25]. Conversely, cation exchange membranes are permeable to cations and impermeable to anions.

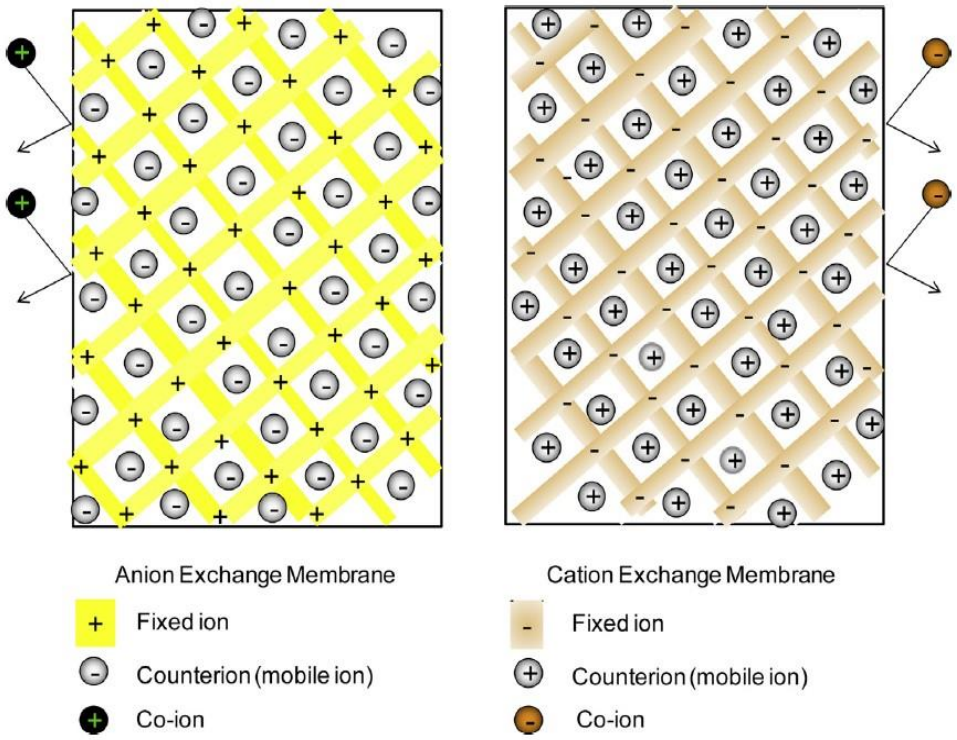

Fig. 1.1 Ion exchange membrane structure [16].

1.2.2 Water quality assessment

As for water quality assessment, hydrodynamic features, physical and chemical properties, and biological characteristics are the three major aspects that require monitoring. Particularly,

organic pollution monitoring is the focus of this thesis, as it is of critical importance for the protection of water resources. The concentration of organic compounds in wastewater is generally evaluated in terms of chemical oxygen demand (COD), biological oxygen demand (BOD), and total organic carbon (TOC). COD is the measurement of all the organics in water that can be oxidized; TOC is the measurement of the total organic carbons, whereas BOD measures the volume of organic carbons that may be oxidized via bacteria. For industrial wastewater assessment, BOD measurements are generally not suitable as the test duration is too long (five days) to measure organic constituent concentrations in wastewater with highly variable chemical compositions. The TOC measurement often requires expensive facilities and trained technicians, leaving COD widely used as one of the most prominent parameters in water quality assessment, which has been accepted as the national standard for organic pollution evaluation in many countries [26-30]. Furthermore, the COD index in drinking water has become of great concern globally, since water supplies cannot always meet quality requirements. The conventional COD test entails sampling, the addition of an oxidizer (e.g., potassium dichromate, potassium permanganate.), hydrothermal digestion, and optical measurement. It is not suitable for a simple automatic system, and secondary pollution is unavoidable when standard methods are employed [31]. Because of these limitations, rapid, continuous, inexpensive, environmentally compatible, and automated analysis methods for COD determination have become the focus of intense research [32-35]. Myriad developments have been driven by either electrocatalytic [36, 37] or photocatalytic [38-40] oxidation principles. Theoretically, with an appropriately applied voltage or irradiation and suitable electrodes, traditional oxidizing agents (e.g., $K_2Cr_2O_7$, $KMnO_4$) may be replaced. During the

process, the oxidation of organic compounds in an aqueous electrolyte in the presence of an electrode may be expressed as follows:

$$C_aH_bO_cN_d + (2a - c)H_2O \rightarrow aCO_2 + dNH_3 + (4a - 2c + b - 3d)H^+ + (4a - 2c + b - 3d)e^- \quad (1.1)$$

On the other hand, the complete oxidation of organic compounds with oxygen may be summarized as follows:

$$C_aH_bO_cN_d + yO_2 \rightarrow aCO_2 + (b/2)H_2O + dNO_2 \quad (1.2)$$

where a, b, c, and d represents the stoichiometric ratio of carbon, hydrogen, oxygen and nitrogen in organic compounds, respectively. Therefore, oxygen concentration changes can be measured as an electrical charge signal. Despite the advantages of an electrochemical monitoring system, such as rapidity of analysis, the directness of analytical signals, and the possibility of incorporation with online monitoring, which supersede conventional COD methods; these new approaches still require improvements due to the difficulty of oxidizing a wide spectrum of organic compounds, as well as low sensitivity of small changes in oxygen concentration during the process.

1.3 Wastewater treatment by the technology of electrodeionization (EDI)

1.3.1 Electrodialysis (ED)

Electrodialysis is an electrically-driven process which integrates ion exchange membranes in a stack under an electric field to separate ionic species in aqueous solutions. Fig. 1.2 demonstrates the basic principle of an ED system include cation exchange membranes (CM) and anion exchange membranes (AM) are alternately spaced between the anode and the

cathode. This arrangement serves to form individual concentrate and dilute solution compartments. Under the presence of an applied electric potential, anions migrate toward the anode, whereas cations migrate toward the cathode. However, cations may only pass through the CM and are rejected by the AM. Likewise, the AM allows anions to pass but the CM prevents anions from going through. As solution circulates through the system, the salt concentration will increase in another compartment, referred to as the concentrate compartment, while the remaining compartments, known as dilute compartments, is stripped of ions [41]. The reactions that take place at the electrodes are:

$$\text{Cathode: } 2H_2O + 2e^- \rightarrow H_2 + 2OH^- \qquad (1.3)$$

$$\text{Anode: } 2H_2O \rightarrow O_2 + 4H^+ + 4e^- \qquad (1.4)$$

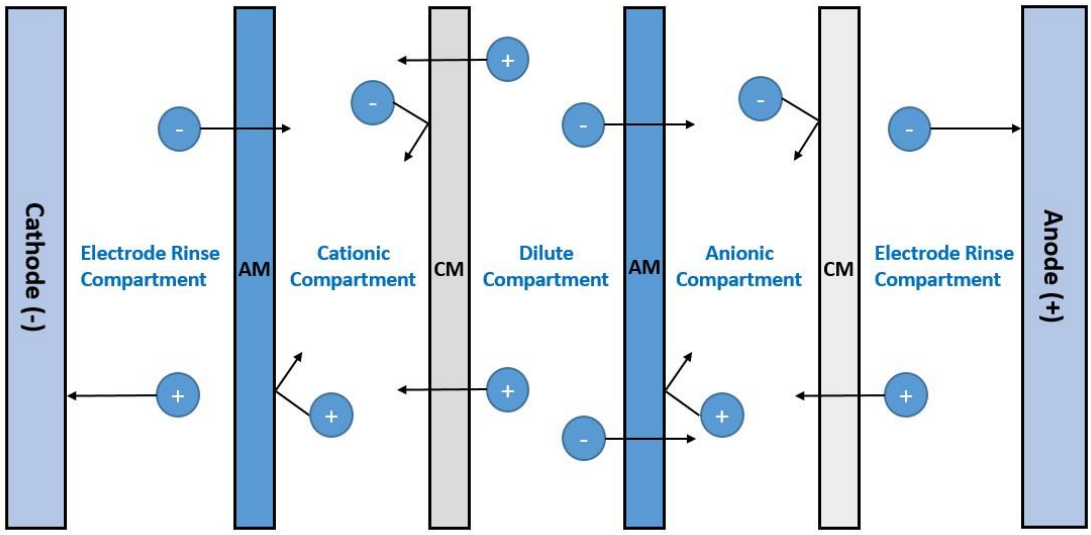

Fig. 1.2 Principle of the electrodialysis process.

Electrodialysis (ED) has been in commercial use for the desalination of brackish water over the last six decades, where an actual ED stack typically consists of hundreds of

membranes [42, 43]. Although ED is known to be superior for the separation and recovery of ionic species from aqueous solutions with the advantages of no chemicals being required, combined with low cost and continuous operation, there is an inherent drawback, which is known as concentration polarization, where a high cumulative resistance is built up within the cell, thus making the power consumption relatively high for the driving of the electric current through the ED stack [44].

1.3.2 Ion exchanger (IX)

Ion exchangers have the capacity to exchange cations or anions from solution, which is achieved due to a resin structure that consists of fixed charged exchange sites and mobile ions that may be substituted for other ions of the same polarity [45]. The structure of an anion exchanger at the molecular scale is represented in Fig. 1.3. Synthetic polystyrene beads contain a cross-linked chain matrix and fixed functional groups, as well as exchangeable anions. When a chemical potential gradient arises, anions in the solution will displace identical charged mobile species within the ion exchanger, which will then be retained as a result of intermolecular attractions. Analogously, cation exchangers enable the exchange of cations in aqueous solutions [46]. Typically, ion exchangers will exhibit some degree of ion selectivity, which is generally associated with its dimensions, pore sizes within the matrix, electrostatic interactions between the matrix and the mobile ions, ionic valences, and atomic numbers [47].

Ion exchangers have been widely applied to soften potable water, treat industrial wastewater, and prepare pure water for analytical chemistry and pharmaceutical applications [48-51], with the advantages that they require very little energy and have low running costs.

However, a number of limitations must be taken into account during the design stage. For instance, IX is not a continuous process since ion exchangers will become saturated when cations and anions have replaced most of the H^+ and OH^- active sites within the resins. Moreover, to accomplish the regeneration of ion exchangers, specific chemicals are required, which not only generate secondary pollution, but also increase the cost of the process.

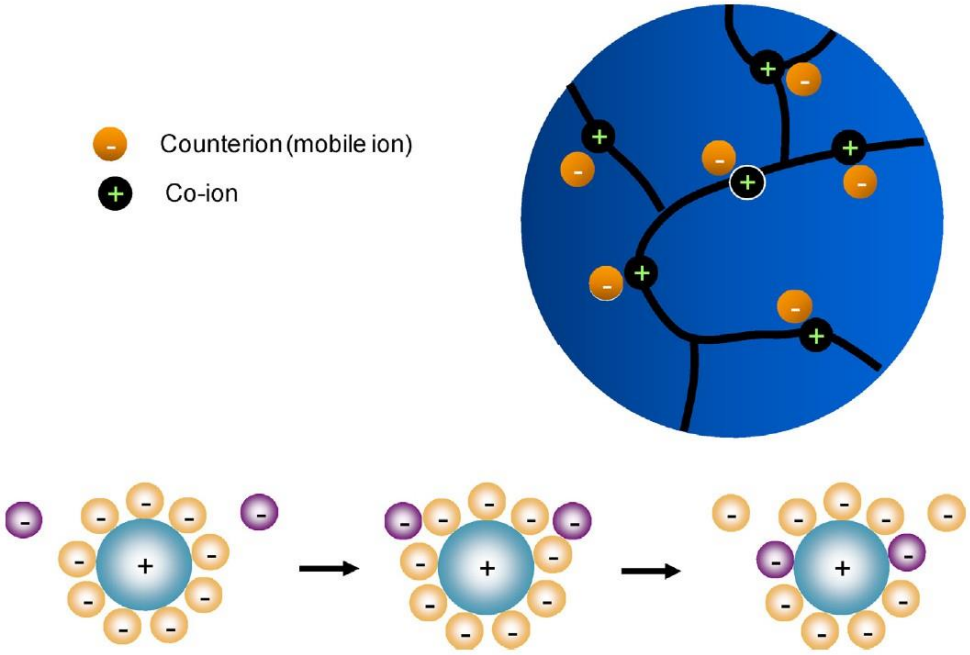

Fig. 1.3 Top: structure of an anion exchanger. Bottom: example of ion exchange process [16].

1.3.3 Electrodeionization (EDI)

Electrodeionization (EDI) is a hybrid technology that combines ion exchangers and electrodialysis to treat and purify wastewater of low conductivity at high efficiency. EDI was first studied in the mid 1950s, with the earliest publication ascribed to Walter et al. [52] who investigated resin regeneration by applying an electric field for the treatment of radioactive

wastewater. Subsequently, an EDI device incorporating an anionic and cationic resin mixture was developed by the Permutit Company, which allowed ion exchange resins to regenerate in situ without the addition of strong acids and bases as regeneration solutions. In 1959, Glueckauf [53] was the first to propose a theoretical mechanism for the continuous operation of the EDI process via two stages. The first stage was the diffusion of ions to the ion exchanger, and the second was ionic conduction of the solid phase to the border of the membranes. Further studies followed: Sammons and Watts (1960) investigated sodium salt deionization through an EDI device and the relationships between concentration values, flow rates and applied current. The continuous production of high purity water through the application of EDI was first achieved by Matejka in 1971 [54]; EDI reliability experiments were conducted with solutions that contained iron, calcium, phosphates, and detergents. In the late 1980's, EDI was commercially employed for the production of ultrapure water. Through the application of digital simulations, Verbeek and Neumeister [55] proposed a model based on Nernst-Planck equations and interfacial solid-liquid equilibrium to predict ion exchange bed behavior. Over the last ten years, the modification of ion exchange materials [56-58] and their combination with other treatment systems, such as ultraviolet (UV) [59], reverse osmosis (RO) [60] and electrochemical oxidation (EO) [61], have enabled significant improvements in this technology to be achieved, thus expanding its range of applications beyond ultrapure water production.

By incorporating a mixture of anionic and cationic resins in the dilute compartment of an ED cell, the strengths of both electrodialysis and ion exchangers are combined in a single technology known as electrodeionization. Fig. 1.4 presents a schematic of EDI for the production of ultrapure water, where the dilute compartment is packed with mixed ion

exchange resins. These serve as a conductor between the membranes and play a role as a substrate for electrical activity, which provides supplemental conductivity to the dilute compartment [62].

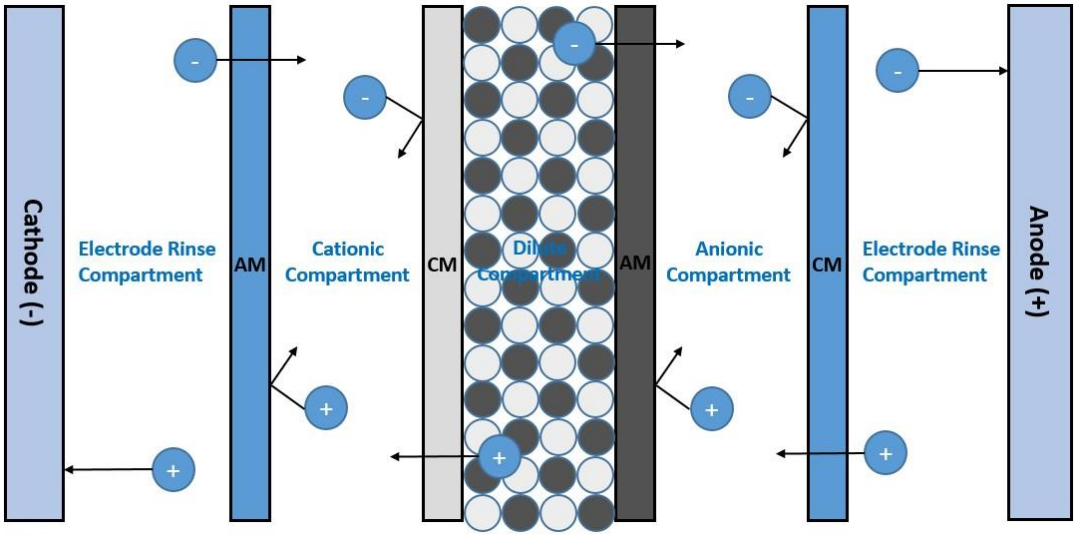

Fig. 1.4 A schematic of the EDI process for ultrapure water production.

This arrangement allows the resin bed to collect and discharge the ionic species and transport them to different compartments under an applied electric field, thereby initiating mass transport between the membranes and resins [63]. Furthermore, the ion exchange resins are continuously regenerated by the applied electric field, which water dissociation occurs simultaneously at the interface of anionic and cationic materials within the dilute compartment, creating hydrogen and hydroxyl ions to regenerate the ion exchange bed in situ. Thus, no additive chemicals are required to run the EDI process.

Conversely, the removal mechanism for ionic species in EDI process may be explained by the theory of two distinct regimes of operation by Ganzi [64, 65]. In the “enhanced transfer regime”, ion exchange resins are saturated with salt ions within the dilute compartment. The mixed ion exchange bed serves as a conductor, which can lower the cell resistance as well as

reduce the energy consumption of the process. In this regime, the current efficiency is high; however, the water dissociation rate is low. In the second regime, called the "electroregeneration regime", the dissociation of water occurs acutely in the dilute compartment where anionic and cationic exchange materials are in contact, and the ion exchange bed is continuously regenerated in situ by H^+ and OH^- that are produced by water dissociation. The water dissociation is due to rapid ion transport within the membrane, which is much higher than that within the solution. Thus, when the applied current increases, there exists a threshold where the population of ions at the membrane/solution interface is insufficient to carry current flow. At this point, water splitting is forced to compensate for the lost conductivity. Therefore, the H^+ and OH^- ions generated from the water dissociation begin to conduct electrical current and regenerate the ion exchange resins [66]. The optimal applied current of the EDI process is selected as the juncture of these two regimes, where both ionic removal and water dissociation occur simultaneously.

EDI is a chemical-free green technology that can significantly remove ionic species from liquids, which requires only electricity and proper ion exchange materials. As an environmentally compatible technology, EDI is capable of continuously treating solutions and includes the merits of no chemical disposal, low energy consumption, inexpensive and safe operation. It overcomes the limitations of conventional electrodialysis and ion exchange processes and synergistically combines their strengths in a single process. In terms of its applications, it may be used for the removal of heavy metals and other ions, and the production of ultrapure water for power generation and the manufactural of pharmaceuticals, foods and semiconductors.

1.4 Chemical oxygen demand determination by electrochemical methods based on TiO_2

Chemical oxygen demand (COD) is a metric that indicates soluble organics in aqueous environments (e.g., industrial water, rivers/lake water), and is one of the most important indexes of water quality. Secure and reliable sources of potable water are of critical and growing concern globally, particularly in the developing world. In order to evaluate drinking water quality, COD determination has quickly become a research focus. There are various methods for COD tests [67-70], and anatase phase TiO_2 nanomaterials have exhibited superior properties for COD sensors due to their strong capacity for the oxidation of organics under UV irradiation as well as to their chemical stability and non-toxicity. TiO_2 is known as an excellent photocatalyst as it possesses a deep valence band of 3.2 eV, and free electrons may easily harvest photon generated holes located on the surface of nanomaterials under illumination, which function as an oxidizer. Additionally, TiO_2 possesses photovoltaic properties when UV irradiation is applied, which makes TiO_2 based sensors self-cleanable, thereby increasing their longevity [71]. The basic principle of TiO_2 nanomaterials as COD sensors is that with appropriate illumination, organic substances may be fully oxidized to carbon dioxide by photoholes and photoelectrons produced by TiO_2 [72]. As shown in Fig. 1.5, when TiO_2 is exposed to UV light, the free photoelectrons in the conduction band (CB) and free photoholes in the valence band (VB) are generated (eq. 1.5). Photoholes possess a strong capacity for oxidation (E_g = +3.2 eV) and will therefore participate in redox reactions with organic compounds (eq. 1.6) [73]. In the meantime, photoholes oxidize water that is adsorbed on the surfaces of the TiO_2 nanoparticles to generate potent hydroxyl radical oxidizing agents (eq. 1.7) [74], which will oxidize organics (eq. 1.8) until they are completely

degraded [75]. The reactions are represented as follows, and are recognized as the foundation of TiO_2 based COD sensors.

$$TiO_2 + h\upsilon \rightarrow h^+ + e^- \quad (1.5)$$

$$h^+ + R \rightarrow R^{\cdot} \quad (1.6)$$

$$TiO_2 + h^+ + H_2O \rightarrow TiO_2(^{\cdot}OH) + H^+ \quad (1.7)$$

$$TiO_2(^{\cdot}OH) + R \rightarrow TiO_2 + R^{\cdot} + H^+ + e^- \quad (1.8)$$

Because of its advantages, including superb photocatalytic oxidative ability, low cost of fabrication, chemical stability, and environmental compatibility, this promising TiO_2 nanoparticle-based COD sensor has emerged as a ground breaking technology in recent years.

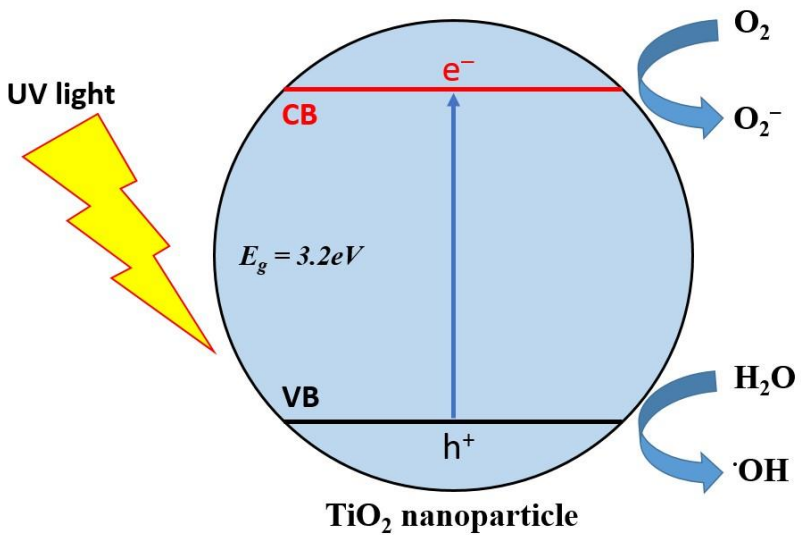

Fig. 1.5 Process of photocatalytic oxidation and reduction at a TiO_2 nanoparticale.

The electrochemical measurement principle for COD determination based on TiO_2 nanoparticles is by tracing the photocurrent during the degradation of organics under UV illumination to indicate sample COD values. Since the photocurrent generated during the photoelectrocatalytic oxidation of organic compounds is proportional to the substance concentration [76], it can be easily converted into equivalent COD values. In a three-electrode system where TiO_2 serves as the working electrode, an external UV light source is applied, and the resulting photocurrent signals analysed. During photoelectrocatalytic processes based on TiO_2 nanoparticle electrodes, photoholes and photoelectrons will participate in the photocatalytic oxidation of organic compounds that are present in the solution under UV irradiation. The decomposed organic matter will release electrons to the external circuit and to the auxiliary electrode at which the photocurrent is monitored, and thus impart a direct analytical signal indicated the COD values [77].

TiO_2 based COD sensors were first investigated by Karube's group [78] in 2000, who used TiO_2 nanoparticles to degrade organics and to measure COD values in water through changes in dissolved oxygen concentrations. Although the results were close to theoretical COD values, the narrow linear range and inadequate sensitivity restricted its applications in practice. To overcome the drawbacks of traditional systems, studies showed that with the application of electric field, the separation of photogenerated electron/hole pairs may be expedited, which enhanced the photocatalytic efficiency. Furthermore, charge alterations may appear in the form of current, which varies in accordance with the organic concentrations during the photoelectrocatalytic process. In this way, low cost, rapid response, adaptable and environmentally compatible methods for the quantification of COD values were proposed [79-81].

1.5 Stimulus and scope of this thesis

An overview of urgent anthropogenic water resource issues, including wastewater treatment and water quality assessment were introduced in this chapter. Since conventional wastewater treatment and quality assessment technologies no longer meet the requirements of sustainable development and restrict themselves within their inherent limitations, the core intent of this M.Sc. thesis is to develop novel, rapid, highly efficient, cost-effective, and environmentally compatible water remediation and monitoring technologies toward addressing this global challenge. The primary objectives in this study include:

1) Propose an advanced and efficient approach to continuously separate and recover Cr(III) and Cr(VI) based on electrodeionization (EDI), and systematically investigate the saturation influences of ion exchange resins.

2) Investigate the simultaneous removal of nitrate and hardness ions from groundwater via electrodeionization (EDI), as well as the influence of system variables (applied current, water flow rate, and resins ratio) on the performance of this process.

3) Develop a novel and rapid photoelectrochemical method to determine chemical oxygen demand (COD) based on reduced nanoporous TiO_2 electrodes.

This thesis is comprised of six chapters. The following chapter, which describes experimental methods, will discuss the fabrication of electrodes for EDI systems and COD tests, as well as the assembly of EDI cells and the methods employed to analyze their structures and physical properties. Chapter 3 and Chapter 4 will present a complete study of the simultaneous removal and recovery of Cr(III) and Cr(VI), nitrate, and hardness ions through electrodeionization (EDI). Chapter 5 will discuss the results of a novel, rapid, and

environmentally compatible methodology for COD determination based on reduced nanoporous (NPs) TiO_2 electrodes. The final chapter, Chapter 6, will provide a synopsis of the results and outlook for future work.

References

[1] Meybeck, M. *Phil. Trans. R. Soc. Lond. B* **2003**, *358*, 1935.

[2] Vörösmarty, C. J.; McIntyre, P. B.; Gessner, M. O.; Dudgeon, D.; Prusevich, A.; Green, P.; Davies, P. M. *Nature* **2010**, *467*, 555.

[3] Gleick, P. H. *Science* **2003**, *302*, 1524.

[4] Shannon, M. A.; Bohn, P. W.; Elimelech, M.; Georgiadis, J. G.; Mariñas, B. J.; Mayes, A. M. *Nature* **2008**, *452*, 301.

[5] World Water Assessment Programme. Water in a Changing World. *The United Nations World Water Development Report 3* (UNESCO, **2009**).

[6] Lima, A. A. M. *J. Infect. Dis.* **2000**, *181*, 1643.

[7] Behrman, J. R.; Alderman, H.; Hoddinott, J. *Global Crises, Global Solutions: First Edition* (Cambridge University Press, **2004**)

[8] Hamoda, M. F.; Al-Ghusain, I.; Al-Mutairi, N. Z. *Desalination* **2004**, *164*, 203.

[9] Colin, X.; Farinet, J. L.; Rojas, O.; Alazard, D. *Bioresource Technol*. **2007**, *98*, 1602.

[10] Xu, J.; Chen, Y. Q.; Zhang, H. J.; Tang, L.; Wang, K.; Zhang, J. H.; Mao, Z. G. *Bioprocess Biosystems Eng.* **2014**, *37*, 1659.

[11] Gupta, V. K.; Sadegh, H.; Yari, M.; Shahryari Ghoshekandi, R.; Maazinejad, B.; Chahardori, M. *J. Environ. Sci. Manage.* **2015**, *1*, 149.

[12] Gungor, K.; Karakaya, N.; Gunes, Y.; Yatkin, S.; Evrendilek, F. *Desalin. Water Treat*. **2015**, *(ahead-of-print)*, 1. DOI: 10.1080/19443994.2015.1007489

[13] Liang, C. Z.; Sun, S. P.; Li, F. Y.; Ong, Y. K.; Chung, T. S. *J. Membr. Sci.* **2014**, *469*, 306.

[14] Domopoulou, A. E.; Gudulas, K. H.; Papastergiadis, E. S.; Karayannis, V. G. *Mod. Appl. Sci.* **2015**, *9*, 137.

[15] Rizzo, L.; Manaia, C.; Merlin, C.; Schwartz, T.; Dagot, C.; Ploy, M. C.; Fatta-Kassinos, D. *Sci. Total Envir.* **2013**, *447*, 345.

[16] Alvarado, L.; Chen, A. C. *Electrochim. Acta.* **2014**, *132*, 583.

[17] Tice, J. D.; Desai, A. V.; Bassett, T. A.; Apblett, C. A.; Kenis, P. J. *RSC Adv.* **2014**, *4*, 51593.

[18] Efligenir, A.; Déon, S.; Fievet, P.; Druart, C.; Morin-Crini, N.; Crini, G. *J. Chem. Eng.* **2014**, *258*, 309.

[19] Richards, P. J.; Norris, S. E. *J. Wind Eng. Ind. Aerodyn.* **2015**, *142*, 43.

[20] Zhang, Z. Y.; Liba, D.; Alvarado, L.; Chen, A. C. *Sep. Purif. Technol.* **2014**, *137*, 86.

[21] Lu, H.; Wang, Y.; Wang, J. *J. Clean. Prod.* **2015**, *92*, 257.

[22] Hu, J.; Fang, Z.; Jiang, X.; Li, T.; Chen, X. *Sep. Purif. Technol.* **2015**, *144*, 90.

[23] Alvarado, L.; Torres, I. R.; Chen, A. C. *Sep. Purif. Technol.* **2013**, *105*, 55.

[24] Sata, T. Ion exchange membranes: preparation, characterization, modification and application. Royal Society of chemistry. **2004**.

[25] Tanaka, Y. *Membr. Sci. Technol. Series, 12, 1st ed., Elsevier, Amsterdam* **2007**, 251.

[26] Kumar, U. K.; KM Pandey, B. *J. Res. Eng.* **2014**, *14*, 6.

[27] Kondo, T.; Tamura, Y.; Hoshino, M.; Watanabe, T.; Aikawa, T.; Yuasa, M.; Einaga, Y. *Anal. Chem.* **2014**, *86*, 8066.

[28] Jirka, A. M.; Carter, M. J. *Anal. Chem.* **1975**, *47*, 1397.

[29] Dobbs, R. A.; Williams, R. T. *Anal. Chem.* **1963**, *35*, 1064.

[30] Xiao, Y.; De Araujo, C.; Sze, C. C.; Stuckey, D. C. *J. Hazard. Mater.* **2015**, *286*, 15.

[31] A. P. H. Association, A. W. W. Association and W. E. Federation, *Washington, D.C.19th ed.* **1995**.

[32] Qiu, J. X.; Zhang, S. Q.; Zhao, H. J. *J. Hazard. Mater.* **2012**, *381*, 211.

[33] Zendehdel, M.; Zendehnam, A.; Hoseini, F.; Azarkish, M. *Polym. Bull.* **2015**, *72*, 1281.

[34] Gaehr, F.; Hermanutz, F.; Oppermann, W. *Water Sci. Technol.* **2014**, *30*, 255.

[35] Hu, D. X.; Tian, Y.; Chen, Z. B.; Ge, H.; Cui, Y. B.; Ran, C. Q. *Water Sci. Technol.* **2015**, *71*, 21.

[36] Ai, S.; Gao, M.; Yang, Y.; Li, J.; Jin, L. *Electroanal*. **2004**, *16*, 404.

[37] Silva, C. R.; Conceição, C. D.; Bonifácio, V. G.; Fatibello Filho, O.; Teixeira, M. F. *J. Solid State Electrochem.* **2009**, *13*, 665.

[38] Lee, K. H.; Kim, Y. C.; Suzuki, H.; Ikebukuro, K.; Hashimoto, K.; Karube, I. *Electroanal.* **2000**, *12*, 1334.

[39] Li, X. J.; Yin, W. P.; Li, J. Y.; Bai, J.; Huang, K.; Li, J. H.; Zhou, B. X. *Water Environ. Res.* **2014**, *86*, 532.

[40] Wang, H.; Zhong, S.; He, Y.; Song, G. *Sens. Actuators, B* **2011**, *160*, 195.

[41] Fritzmann, C.; Löwenberg, J.; Wintgens T.; Melin, T. *Desalination* **2007**, *216*. 1.

[42] Mintz, M. S. *Ind. Eng. Chem.* **1963**, *55*, 18.

[43] AlMadani, H. M. N. *Renewable Energy* **2003**, *28*, 1915.

[44] Ochoa Gómez, J. R. *Electrosíntesisy Electrodiálisis, 1st ed.* **1996**, 340.

[45] Alchin, David. *Ion Exchange Resins nzic.org.nz.* **2010**.

[46] Helfferich, F. *Ion Exchange ISBN 0-486-68784-8*, **1995**.

[47] Park, J. S.; Chilcott, T. C.; Coster, H. G. L.; Moon, S. H. *J. Membr. Sci.* **2005**, *246*. 137.

[48] Faylor, T. L.; Martin, R. W. *U.S. Patent No. 3-870-033. Washington, DC. U.S. Patent and Trademark Office* **1975**.

[49] Yamanaka, K. *Encyclopedia of Polymeric Nanomaterials* **2015**, 1019.

[50] Lamprou, A.; Storti, G.; Soos, M.; Morbidelli, M. *J. Chromatogr. A* **2015**, *1407*, 90.

[51] Gao, W.; Liang, H.; Ma, J.; Han, M.; Chen, Z. L.; Han, Z. S.; Li, G. B. *Desalination* **2011**, *272*, 1.

[52] Walters, W. R.; Weiser, D. W.; Marek, L. J. *Ind. Eng. Chem*. **1955**, *47*, 61.

[53] Glueckauf, E. *British Chem. Eng.* **1959**, *4*, 646.

[54] Matejka, Z. *J. Appl. Chem. Biotechnol.* **1971**, *21*, 117.

[55] Verbeek, H. M.; Fürst, L.; Neumeister, H. *Computers Chem. Eng.* **1998**, *22*, 913.

[56] Chruściel, J. J.; Leśniak, E. *Prog. Polym. Sci.* **2015**, *41*, 67.

[57] Taheri-Behrooz, F.; Maher, B. M.; Shokrieh, M. M. *Comput. Mater. Sci.* **2015**, *96*, 411.

[58] Hoque, M. I.; Chowdhury, D. A.; Holze, R.; Chowdhury, A. N.; Azam, M. S. *J. Environ. Chem. Eng.* **2015**, *3*, 831.

[59] Yen, H. Y.; Kang, S. F.; Lin, C. P. *Water Environ. Res.* **2015**, *87*, 312.

[60] Hu, J.; Fang, Z.; Jiang, X.; Li, T.; Chen, X. *Sep. Purif. Technol*. **2015**, *144*, 90.

[61] Peng, C.; Jin, R.; Li, G.; Li, F.; Gu, Q. *Sep. Purif. Technol*. **2014**, *136*, 42.

[62] Danielsson, C. O. *Electropermutation assisted by ion-exchange textile: removal of nitrate from drinking water* **2006**.

[63] DiMascio, F.; Ganzi, G. C. *U.S. Patent No. 5-858-191. Washington, DC: U.S. Patent and Trademark Office* **1999**.

[64] Ganzi, G. C.; Egozy, Y.; Giuffrida, A. J.; Jha. A. D. *Ultrapure Water.* **1987**, *4*, 43.

[65] Ganzi, G. C.; Jha, A. D.; DiMascio, F.; Wood. J. H. *Ultrapure Water.* **1997**, *14*, 64.

[66] Danielsson, C.; Dahlkild, A.; Velin, A.; Behm, M. *Electrochim. Acta*. **2009**, *54*, 2983.

[67] Díaz, V.; Ibáñ za, R.; Gñme , P.; Urtiaga, A. M.; Ortiz, I. *Water Res.* **2011**, *45*, 125.

[68] Ramavandi, B.; Farjadfard, S. *K. J. Chem. Eng.* **2014**, *31*, 81.

[69] Chen, B.; Wu, H.; Li, S. F. Y. *Talanta* **2014**, *120*, 325.

[70] Kameswari, K. S. B.; Kalyanaraman, C.; Thanasekaran, K. *Clean Technol. Environ. Policy* **2014**, *16*, 369.

[71] Kim, Y. G.; Walker, J.; Samuelson, L. A.; Kumar, J. *Nano Lett.* **2003**, *3*, 523.

[72] Qiu, J. X.; Zhang, S. Q.; Zhao, H. J. *J. Hazard. Mater.* **2012**, *381*, 211.

[73] Bai, J.; Li, J. H.; Liu, Y. B.; Zhou, B. X. *Appl. Catal. B* **2010**, *95*, 408.

[74] Comninellis, C. *Electrochim. Acta.* **1994**, *39*, 1857.

[75] Konstantinou, I. K.; Albanis, T. A. *Appl. Catal. B* **2004**, *49*, 1.

[76] Bai, J.; Zhou, B. *Chem. Rev.* **2014**, *114*, 10131.

[77] Zhao, H.; Jiang, D.; Zhang, S.; Catterall, K.; John, R. *Anal. Chem.* **2004**, *76*, 155.

[78] Lee, K. H.; Kim, Y. C.; Suzuki, H.; Ikebukuro, K.; Hashimoto, K.; Karube, I. *Electroanal.* **2000**, *12*, 1334.

[79] Liang, L. H.; Zhang, Z. H.; Yuan, Y.; Zeng, L. P.; Jin, L. T. *Chem. Sens.* **2008**, *28*, 57.

[80] Zhang, S.; Li, L.; Zhao, H. *Environ. Sci. Technol.* **2009**, *43*, 7810.

[81] Qu, X.; Tian, M.; Chen, S.; Liao, B. Q.; Chen, A. C. *Electroanal.* **2011**, *23*, 1267.

Chapter 2 Experimental methods

2.1 Introduction

In the previous chapter, several types of electrically-driven technologies for wastewater purification and different COD measurement based on TiO_2 were introduced. Also, the objectives for this thesis research were outlined. In this chapter, the main experimental methodologies and techniques that were used in this M.Sc. project will be discussed. Details of the experimental procedures and equipment pertaining to each specific study will be presented in Chapters 3-5.

2.2 Chemicals and materials

The following chemicals were used as received from Sigma-Aldrich: H_2SO_4 (≥98%); $K_2Cr_2O_7$ (99.5%); $Cr_2(SO_4)_3$•n H_2O; $NaNO_3$ (≥99.0%); $Ca(NO_3)_2$ •$4H_2O$ (99.0%); $Mg(NO_3)_2$•$6H_2O$ (99.0%); $IrCl_3$•n H_2O; $TaCl_5$ (99.99%); D-glucose (≥99.5%); potassium hydrogen phthalate (≥99.95%); lactic acid (≥98.0%); phenol (≥99.0%); acetic acid (≥ 99.0%); hydrochloric acid (37.5%); ethylene glycol (≥99%); hydrofluoric acid (50%); ammonium fluoride (99.99%) and Amberlite® ion exchange resins (sodium form and chloride form).

The following materials were used as received from Alfa-Aesar: titanium wire (99.7%, 2 mm diameter); titanium strip (99.2%, 1.25 cm x 0.5 mm); Pt wire (99.9%, 0.5 mm diameter); Pt mesh (99.9%, 1.0 cm x 1.0 cm).

The following gas was used throughout this thesis research: argon (PRAXAIR, UHP, 99.999%).

The cation exchange membranes (CMI-7000S) and anion exchange membranes (AMI-7001S) were provided by Membranes International Inc.

Pure water (18 MΩ cm) obtained from a Nanopure® Diamond^{TM} UV ultrapure water purification system was used for cleaning purposes and preparation of all solutions and electrolytes.

2.3 Fabrication of electrodes

2.3.1 Preparation of the Ti/Ta_2O_5-IrO_2 electrode

A thermal decomposition technique was employed to fabricate the Ti/Ta_2O_5–IrO_2 anode. Firstly, A Ti mesh substrate was immersed in acetone in an ultrasonic bath for 15 min. Subsequently, the mesh was etched in a 32% HCl solution at 85 ^oC for 15 min and rinsed with ultrapure water. Then, the Ta_2O_5–IrO_2 coating was prepared by combining tantalum and iridium precursor solutions, according to an established protocol [1]. Afterwards, the coating solution was painted manually onto the Ti substrates with a brush and the process was repeated until an oxide coating load of 30 g/m^2 was attained. Lastly, the fabricated electrode was annealed at 450 ^oC for 1 hour.

2.3.2 Fabrication of the nanoporous TiO_2 electrode

The nanoporous TiO_2 electrode was prepared utilizing a three-step anodic oxidation process. The pure titanium plates were initially sonicated in acetone for 15 min and then

etched in an 18% HCl solution at 85 ºC for 10 min. The etched titanium plates were then anodized in a one-compartment, two-electrode (a titanium plate as the anode and a platinum mesh as the cathode) cell in a solution containing ethylene glycol, 0.3 wt.% NH_4F and 2 wt.% H_2O at 50 V for 5 hours. Afterwards, the roughly grown nanoporous TiO_2 layer on the surface was removed by masking tape, and the same titanium plate was treated by a second-step anodization at 50 V for another 2 hours. The fabricated nanoporous layer was peeled away by masking tape again and then a third anodization was performed on the titanium plate at 50 V for 15 min. Finally, the fabricated NPsTiO_2 electrode underwent thermal treatment at 450 °C for 3 hours [2].

2.4 Assembly of the EDI stack

The EDI stack setup is a plate-and-frame module, which was configured by an array of acrylic sheets and membranes between the two electrodes to separate the concentrated and diluted compartments. Sandwiched between the acrylic sheets were ion exchange membranes (cationic and anionic) and two acrylic sheets housed the two electrodes to form the electrode rinse compartments. The dilute compartment was filled with mixed ion exchange resins between the cationic and anionic membranes. Rubber gasket spacers were positioned on both sides of the ion exchange membranes to distribute the pressure. Auxiliary components such as tanks, pumps, flow-meters and power supply were also equipped with the laboratory EDI stack [3].

2.5 Surface analysis

The surface morphology of the synthesized electrodes was observed using a JEOL 5900LV scanning electron microscope (SEM). The surface composition was characterized by an Oxford Links ISIS energy dispersive X-ray spectroscopy (EDS). The X-Ray diffraction (XRD) spectra of the electrodes were recorded with a Philips PW 1050-3710 diffractometer using a Cu K-alpha radiation source.

2.6 Electrochemical experiments

The electrodeionization experiments were carried out in an EDI stack cell utilizing a stainless steel plate as the cathode, and the as-prepared Ti/Ta_2O_5-IrO_2 as the anode. A Voltalab PGZ402 potentiostat was used in this work. The COD determination experiments were performed in a three-electrode cell reactor connected with an electrochemical workstation (PGZ301 Universal Potentiostat). The synthesized reduced NPsTiO_2 electrode was used as the working electrode. A platinum coil and a Ag/AgCl (saturated KCl) electrode were utilized as the counter and reference electrodes, respectively. The UV illumination source was a CureSpot 50 (ADAC systems) equipped with an Hg lamp with measured light irradiance of 2.0 mW cm^{-2}. All the experiments were carried out at room temperature (20 ± 2 ^{o}C).

2.7 Water quality measurements

The concentrations of different species in the solutions were determined by inductively coupled plasma atomic emission spectroscopy (ICP-AES) (Varian Vista Pro) and UV-Visible

spectrophotometer (Cary 50). The pH of the aqueous solutions was measured with an Oakton Acorn® pH meter.

References

[1] Tian, M.; Wen, J. L; MacDonald, D.; Asmussen, R. M.; Chen, A. C. *Electrochem. Commun.* **2010**, *12*, 527

[2] Chang, X.; Thind, S. S.; Tian, M.; Hossain, M. M.; Chen, A. C. *Electrochimica. Acta*. **2015**, *173*, 728.

[3] Zhang, Z. Y.; Liba, D.; Alvarado, L.; Chen, A. C. *Sep. Purif. Technol.* **2014**, *137*, 86.

Chapter 3 Separation and recovery of Cr(III) and Cr(VI) using electrodeionization as an efficient approach*

3.1 Introduction

Chromium is naturally occurring in soils, rocks, plants and animals and is of importance for the environment, human health, and in industry. However, it is also a waste product that is excessively generated by various industries, such as in stainless-steel production, leather tanning, paint and pigment fabrication [1-3]. The most useful form of chromium is metallic chromium, which is widely used to provide wear, abrasion and corrosion resistance for metals via the process of electroplating. For metallic chromium, chemically inert Cr_2O_3 forms on the surface, which is deemed as safe for the environment and human health. However, the remaining forms of chromium, subsequent to the electroplating process, are its only stable ions: Cr(III) and Cr(VI). Cr(VI) ions are extremely toxic, and have been classified as a carcinogenic agent in humans by the IARC (International Agency for Research of Cancer). Cr(VI) exists primarily as an anionic species in aqueous solutions such as $HCrO_4^-$, CrO_4^{2-}, $HCr_2O_7^-$ and $Cr_2O_7^{2-}$ [4]. In contrast, Cr(III) is less soluble and much less toxic than Cr(VI). One strategy that is utilized in industry to treat Cr(VI) involves its reduction to less toxic Cr(III), which is then precipitated out by forming $Cr(OH)_3$ at near neutral to high pH [5]. Other techniques for the treatment of chromium waste involve coagulation, ion exchange, reverse osmosis and solvent extraction. Both Cr(III) and Cr(VI) species may often be found in industrial effluents [6-8]. In addition, Cr(III) and Cr(VI) can be exchanged via oxidation and reduction [9]. It is therefore critical to develop a novel approach that can effectively treat both Cr(III) and Cr(VI).

Various techniques, for instance co-precipitation [10], solvent extraction utilizing different reagents [11], ion exchange [12], electrochemical reduction [13] and solid-phase extraction [14], have been used for the preconcentration, conversion and separation of Cr(III) and Cr(VI) species. Ion exchange resins have been employed for the removal of Cr(VI) from wastewater [15]; however, this is not a continuous process, as the resins may easily become exhausted (saturated). Therefore, they require the regeneration of their ion exchange sites with acids or bases, which creates a secondary chemical waste in the process [16]. Electrodialysis (ED) has been successfully utilized in the past as a method for the removal of metal ions from wastewater through the application of an electrical current or potential in conjunction with ion exchange membranes. The limitation of electrodialysis, however, is that once the ion concentration becomes low, higher levels of energy are consumed in conjunction with low ion removal efficiencies [17]. The synergistic combination of these two technologies is called electrodeionization (EDI) [18-22], which has been found to generally resolve issues that are inherent to these two technologies when each is applied on its own.

Electrodeionization has been used for the production of high-purity water, and it has also been investigated for the removal of heavy metals within diluted electroplating rinse waters [23-29]. The dual driving forces that have enabled this hybrid technology to outperform ion exchange resins and electrodialysis include the efficient regeneration of ion exchange sites, and the high level of conductivity that is maintained in the dilute compartment from the ion exchange resins, which leads to more rapid, energy efficient and extensive separation [30]. The regeneration of the ion exchange sites is accomplished through a process called electroregeneration, which electrically induces water splitting reactions via the formation of H^+ and OH^-, to regenerate the resins to their proton and hydroxide forms [31]. The water

splitting reaction was found to be enhanced at the bipolar interfaces of ion-exchange materials (cationic resin - anionic resin, cationic resin - anionic membrane, anionic resin - cationic membrane) [32, 33]. By virtue of having a mixed bed of ion exchange resins, water-splitting might theoretically be evenly dispersed across the entire dilute compartment, thus regenerating the ion-exchange resins in a uniform manner [34]. It was also experimentally discovered that mixed beds of resins in EDI were the most efficacious [18]. Although electrodeionization has an issue with metal hydroxide precipitation due to large OH^- ion populations that are formed as the result of water splitting, this might be avoided by lowering the pH to conditions where the precipitation does not occur [35].

Although EDI has been widely investigated for the removal of Cr(VI) from wastewater [36-39], to the best of our knowledge there is no report on the simultaneous separation of Cr(III) and Cr(VI). In the present study, we have explored EDI as an advanced approach for the continuous separation and recovery of Cr(III) and Cr(VI). A new analytical method, which integrates UV-Visible spectroscopy and Inductively Coupled Plasma Atomic Emission Spectroscopy (ICP-AES) has been developed for monitoring the concentrations of both Cr(VI) and Cr(III) in a mixed solution. We have also determined the limiting current and systematically studied the effects of different applied currents of EDI on the removal of Cr(VI) as well as Cr(III). Moreover, the influence of the level of saturation within the ion-exchange resins has been assessed in terms of both removal efficiency and energy consumption. The improved configuration of the EDI membrane stack described in this study may also be employed to simultaneously separate other anions and cations.

3.2 Experimental

3.2.1 Materials

The cationic exchange membranes (CMI-7000S) and anionic exchange membranes (AMI-7001S) were purchased from Membranes International Inc. As for the AMI-7001S, the polymer structure was comprised of cross-linked gel polystyrene and DVB (Divinylbenzene), with $-N^{+}(CH_3)_3$ functional groups and a total exchange capacity of 1.3 Eq/L. The polymeric structure of the CMI-7000S was also cross-linked gel polystyrene and DVB (Divinylbenzene), with $-SO_3^{-}$ functional groups and a total exchange capacity of 1.6 Eq/L. A strong basic macroreticular anion exchange resin (Amberlite® IRA900RF Cl) and a strong acidic macroreticular cation exchange resin (Amberlite® 200C Na) were purchased from Rohm and Haas Co. The matrix of IRA900RF Cl was a styrene DVB (Divinylbenzene) copolymer, with $-N^{+}(CH_3)_3$ functional groups and a total exchange capacity of >1.0 Eq/L (Cl^{-} form). The matrix of 200C Na consisted of a styrene DVB copolymer, with $-SO_3^{-}$ functional groups and a total exchange capacity of >1.7 Eq/L (Na^{+} form). Solutions containing Cr(VI) were prepared from analytical grade $K_2Cr_2O_7$ (99.5% purity; Sigma Aldrich). Solutions containing Cr(III) were prepared from 'Baker Analyzed' Reagent $Cr_2(SO_4)_3 \bullet n\ H_2O$. The 0.1 M H_2SO_4 electrolytes were prepared from ACS reagent grade H_2SO_4 (95.0 - 98.0% purity; Sigma Aldrich). The water used in the preparation of all the solutions was purified by a Nanopure® Diamond Water System (18 MΩ cm). All of the experiments were carried out at 20 ± 2 ^{o}C.

3.2.2 Ion exchange resin and membrane pre-treatment

The anion exchange resin (Amberlite® IRA900RF Cl) and a strong acidic macroreticular cation exchange resin (Amberlite® 200C Na) were treated with 0.1M H_2SO_4 for 60 min, rinsed with nanopure water for 30 min, treated with 0.1M KOH for an additional 60 min, rinsed once again with pure water for 30 min, and then dried at 60 ^oC. The membranes were immersed in 0.1 M KOH for 24 h prior to use, and subsequently rinsed with deionized water to remove any excess KOH just prior to their installation into the electrochemical cell system.

3.2.3 Analysis of Cr(III) and Cr(VI)

The total Cr(VI) and Cr(III) concentrations in solutions were determined by ICP-AES (Varian Vista Pro). The Cr(VI) for the Cr mixture experiments was analyzed using a UV-Visible spectrophotometer (Cary 50). The pH of the aqueous solutions was measured with an Oakton Acorn® pH meter.

3.2.4 Electrochemical set-up

Our previous studies have shown that Ta_2O_5-IrO_2 coatings possess robust electrocatalytic activity and stability as an anode material [40, 41]. The ED and EDI were carried out in an electrochemical cell utilizing a stainless steel plate (5 cm x 8 cm) as the cathode, and Ti/Ta_2O_5-IrO_2 as the anode, whereas Ti mesh was employed as the substrate. To determine the optimized current for the EDI process, a polarization curve was recorded using a Voltalab PGZ 402 Universal Potentiostat.

3.2.5 Preparation of the Ti/Ta_2O_5-IrO_2 electrode

A thermal decomposition technique was employed in the preparation of the Ti/Ta_2O_5–IrO_2 anode. A Ti mesh substrate (5cm x 8cm) was immersed in acetone in an ultrasonic bath for 15 min. Subsequently, the mesh was etched in 32% HCl at 85 ^oC for 15 min and rinsed with ultrapure water. The Ta_2O_5–IrO_2 coating was prepared by combining iridium and tantalum precursor solutions, according to an established protocol [42]. The precursor solution was prepared by mixing the iridium precursor solution (dissolution of 0.30 g of $IrCl_3 \bullet 3H_2O$ in 2.5 mL of ethanol) and the tantalum precursor solution (0.13 g $TaCl_5$ dissolved in 7.5 mL of isopropanol). The coating solution was painted manually onto the Ti substrates using a brush technique. This process was repeated until an oxide coating load of 30 g/m^2 was attained. The electrode then underwent thermal treatment under 450 ^oC for 1 h.

3.2.6 ED and EDI treatment of Cr(VI) and a mixture of Cr((III) and Cr(VI)

The ED stack setup, as shown in the top of Scheme 3.1 (designated as “unexpanded cell”), was configured by using two acrylic sheets of 18 mm in thickness, which housed the two electrodes as well as the electrodic compartment solution, and by integrating three acrylic sheets of 6 mm thickness, which served as the concentrate and dilute compartments. Rubber gasket spacers (3.5 mm) were positioned on either side of the ion exchange membranes, between the concentrate and electrodic compartments. Sandwiched between the acrylic sheets were ion exchange membranes (cationic and anionic) with a dimension of 5cm x 8cm. The EDI stack setup was identical to the ED configuration described above, except for the dilute compartment, which was filled with approximately 15 g of mixed resins (cationic and

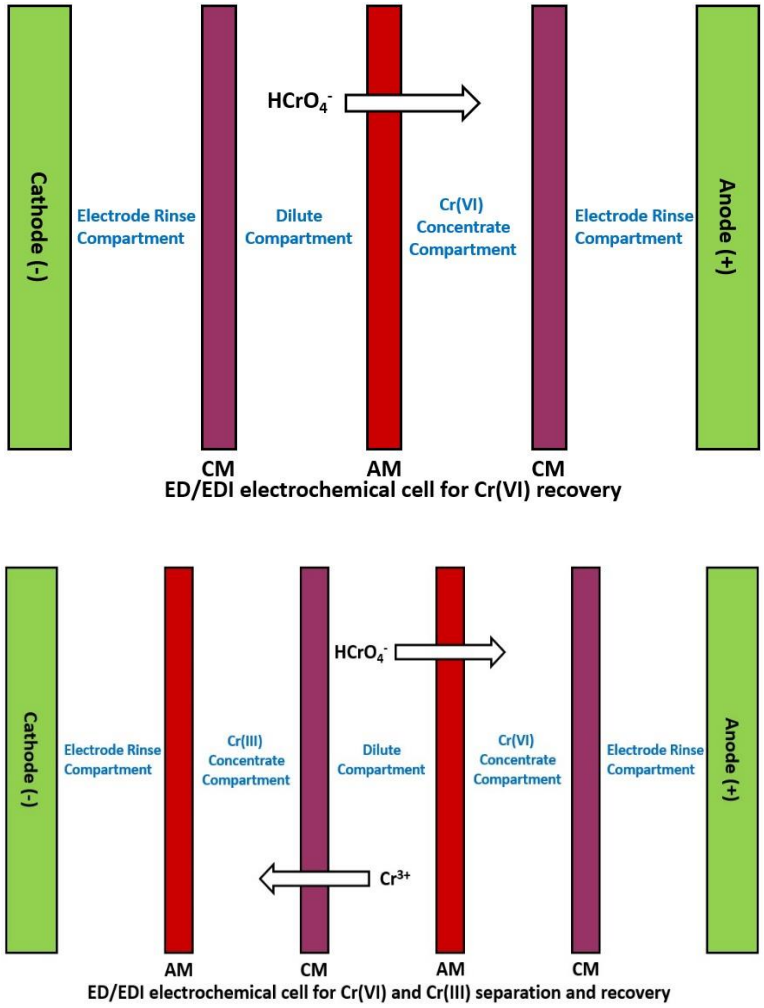

Scheme 3.1. Schematic diagram illustrating the electrodialysis/electrodeionization cells for Cr(VI) recovery and Cr(VI), Cr(III) mixture separation.(AM: Anionic membrane; CM: Cationic membrane).

anionic) at a 1:1 ratio by weight. For mixing the Cr(III) and Cr(VI), a concentrate compartment of Cr(III) was added, as shown in the bottom of Scheme1 (designated "expanded cell"). The ED and EDI experiments were performed in batch mode. For the removal of Cr(VI), the unexpanded cell was used, where the dilute compartment solutions were initially 100 ppm Cr(VI) with a volume of 150 mL at pH ~3.0, which resulted in a dominant $HCrO_4^-$ species in the solution. The solution that was cycled in the concentrate compartment was also 100 ppm Cr(VI), with a volume of 150 mL. The electrode rinse compartments were fed using 0.1 M H_2SO_4, with a volume of 200 mL. All the solutions were fed from the bottom of the cell and came out from the top of the cell at a continuous flow rate of 4.5 mL/min.

For the separation and recovery of Cr(III) and Cr(VI), the expanded cell system was employed, where the mixed resins were packed into the dilute compartment. A mixture of Cr(III) and Cr(VI), with an initial concentration of 100 ppm each, was used as the feed solution to the dilute compartment at a flow rate of 4.5 mL/min. The concentrate compartments were supplied simultaneously using 0.1 M H_2SO_4 in order to avoid precipitation via the lowering of the pH during the process [35]. Additionally, 200 mL of a 0.1 M H_2SO_4 solution was recirculated into the electrode rinse compartment. To study the influence of saturation, the resins were initially saturated in a solution containing 1000 ppm Cr(III) and 1000 ppm Cr(VI). The EDI experiments were subsequently repeated under identical conditions in order to compare the effects of the saturated and unsaturated resins.

3.3 Results and discussion

3.3.1 Determination of Cr(III) and Cr(VI) concentration by ICP-AES and UV-Vis spectroscopy

A method for quantifying the distinct concentrations of both Cr(VI) and Cr(III) in the same solution was developed by employing UV-Vis spectroscopy and ICP-AES. Fig. 3.1 presents the UV-Vis spectra of the blank solution, 100 ppm Cr(III) and 100 ppm Cr(VI). There is no notable UV-Vis absorption at a wavelength higher than 250 nm for Cr(III). In contrast, two intense absorption bands were centred at 277 and 352 nm, which are characteristic for the O-Cr^{6+} electronic charge transfer of chromate species in a tetrahedral conformational structure. As a result, the concentration of Cr(VI) may be determined in a mixture of Cr(III) and Cr(VI) by UV-Vis spectroscopy, while the total chromium concentration can be determined via ICP-AES. Thus, the difference between the total Cr and Cr(VI) might be interpreted as the Cr (III) concentration. To develop the calibration curve for the determination of Cr(VI) concentration in our study, a series of standard solutions containing n ppm Cr(VI) as well as n ppm Cr(III) were made, where n was varied, from 0.0 to 100.0. The UV-Vis spectra of these standard solutions are displayed in Fig. 3.2A; the intensity of the two absorption peaks at 277 and 352 nm, increased linearly with elevated concentrations. As the absorption peak at 277 nm was noisy at high concentrations, the calibration plot of Cr(VI) absorption was plotted at 352 nm with a co-efficient of $R^2 = 0.9999$, as depicted in Fig. 3.2B. For comparison, another series of standard solutions containing m ppm Cr(VI) in the absence of Cr(III) were prepared, where m was varied, from 0.0 to 100.0. The obtained calibration plot of Cr(VI) absorption was

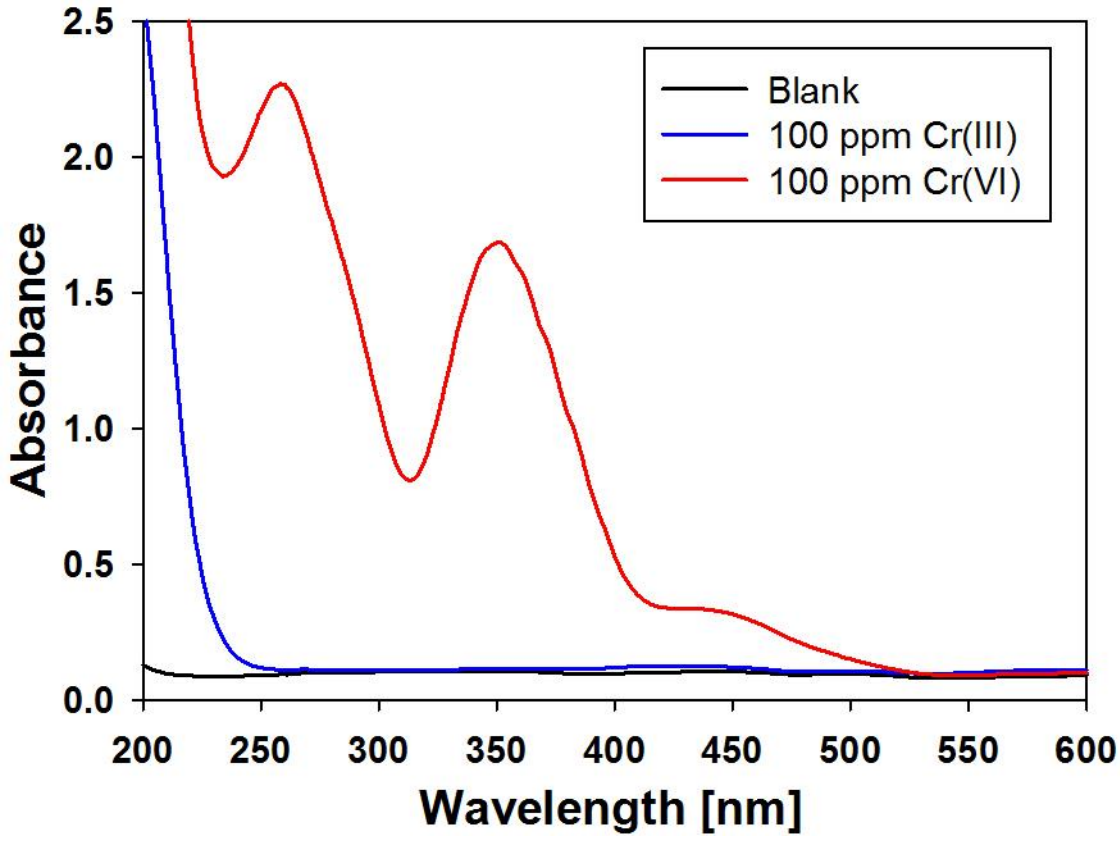

Fig. 3.1. Absorption spectra of Cr(VI) and Cr(III) in solution with $K_2Cr_2O_7$ and $Cr_2(SO_4)_3 \cdot n\ H_2O$ respectively.

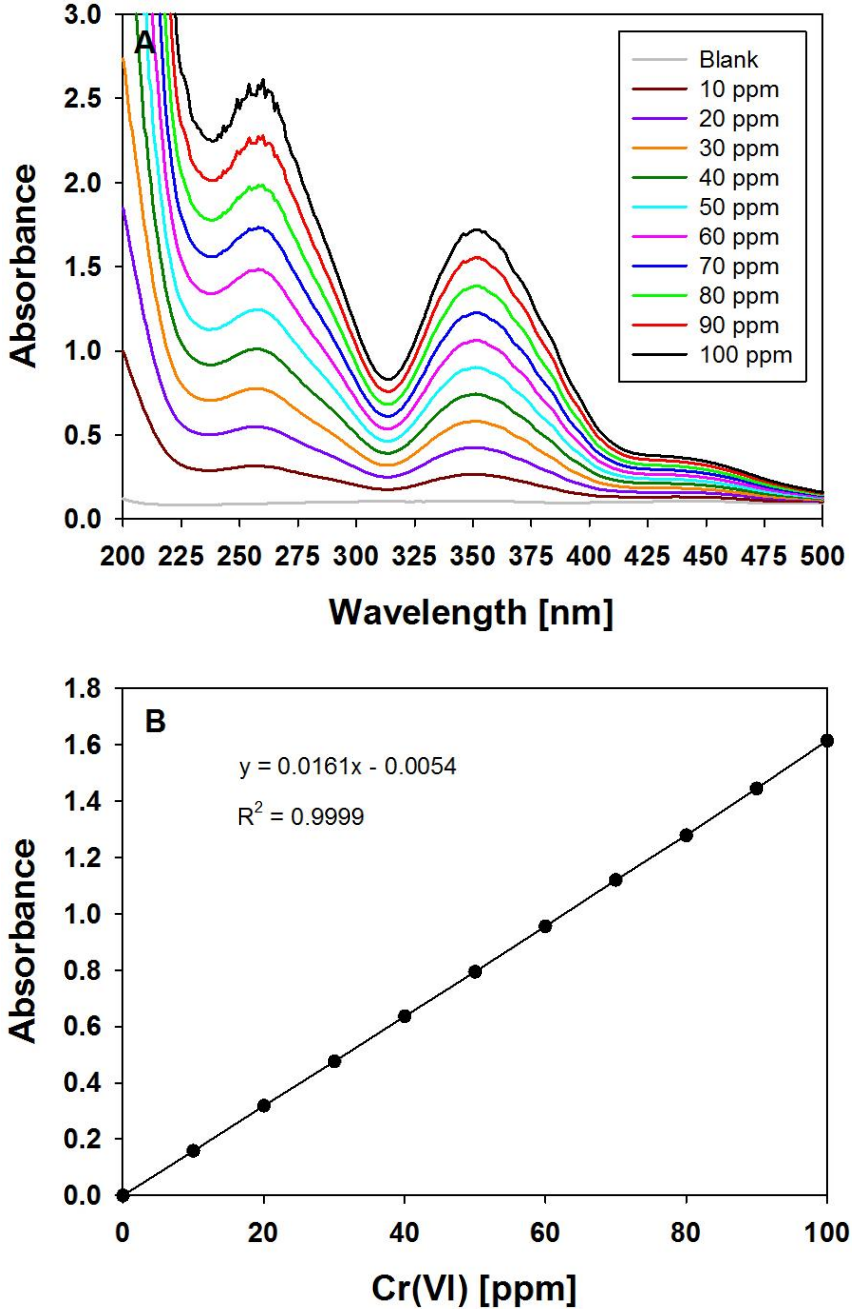

Fig. 3.2. (A) Absorption spectra of Cr(VI) in solution with $K_2Cr_2O_7$ and $Cr_2(SO_4)_3$• n H_2O. (B) Calibration curve of Cr(VI) absorption at 352 nm.

identical to the one presented in Fig. 3.2B, showing that UV-Vis spectroscopy may effectively be used for the detection of Cr(VI), and that there is no interference from Cr(III).

3.3.2 Polarization curve

Prior to the EDI experiments, a current – voltage (I vs E) polarization curve was recorded in order to determine the limiting current in the absence of resin. For the unexpanded electrochemical cell system, a 150 mL volume of 100 ppm Cr(VI) solution was circulated through the dilute compartment at a flow rate of 4.5 mL min^{-1}, while a 200 mL volume of 0.1 M H_2SO_4 solution was recirculated within the electrode rinse compartments. The cell voltage was scanned from 1.0 to 5.0 V at a sweep rate of 1 mV s^{-1}; with the resulting I vs E curve presented in Fig. 3.3A. The current was almost zero when the cell voltage was below 1.0 V, revealing that the input energy was consumed primarily for the charging of the membranes and the electrodes. The current increased only slightly when the cell voltage was scanned from 1.0 to 1.4 V, indicating that the driving force behind the transport of ions from the bulk material to the membrane/solution interface was small. The current increased significantly with the increase of the applied cell voltage from 1.4 to 3.0 V. However, the current increased slowly with further voltage elevation from 3.0 to 5.0 V. The limiting current may be estimated with the tangents crossing corresponding to the straight portions of polarization curve [22, 43] As illustrated in Fig. 3.3A, the limiting current was determined to be approximately 11.5 mA. The same approach was employed to determine the limiting current of the expanded electrochemical cell system. Rather than the 100 ppm Cr(VI) solution, a 150 mL mixture of 100 ppm Cr(VI) and 100 ppm Cr(III) was circulated through the dilute compartment at a flow rate of 4.5 mL min^{-1}. The recorded I vs E curve is displayed in Fig.

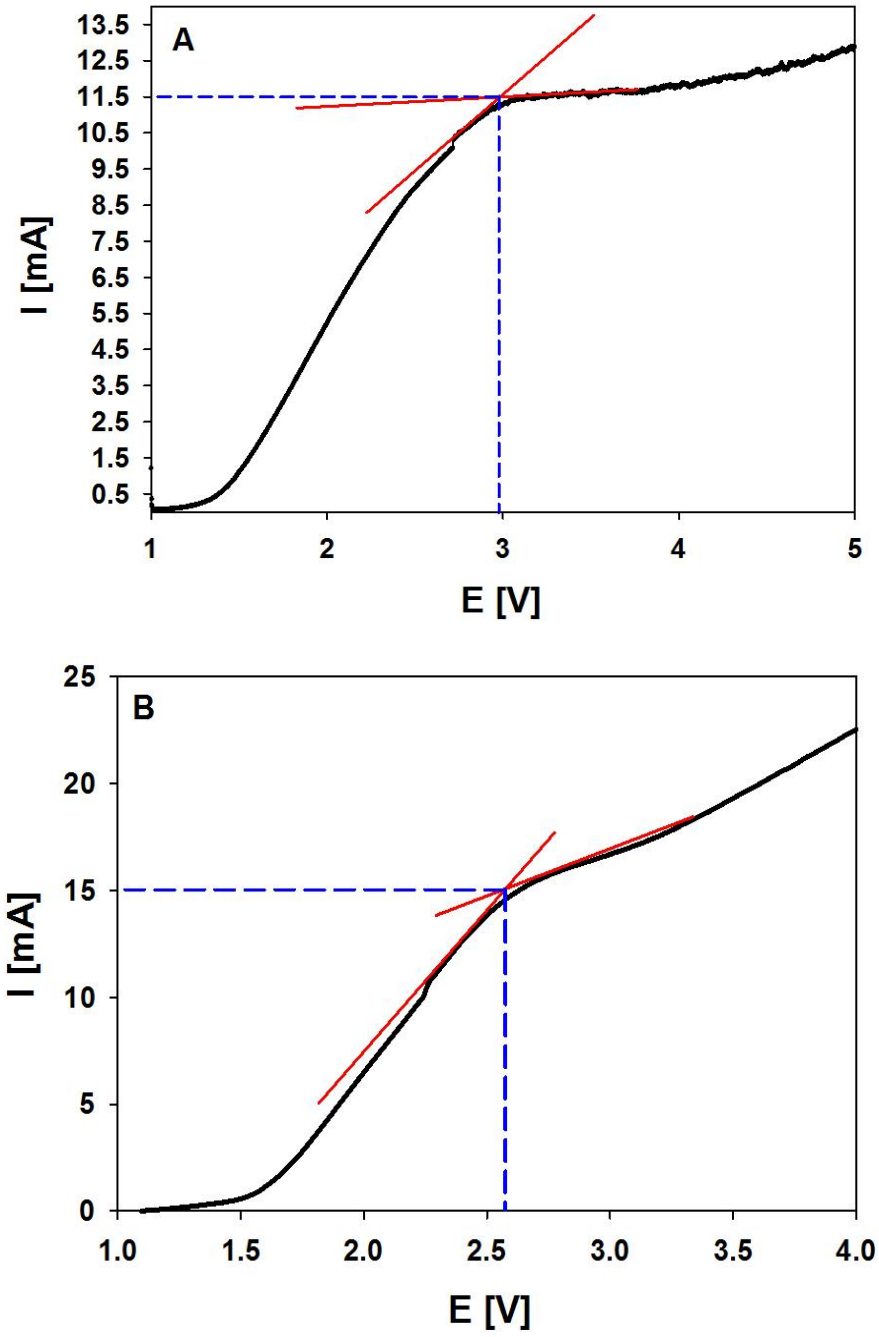

Fig. 3.3. (A) Cr(VI) - Unexpanded ED cell limiting current determination at a flow rate of 4.5 mL min^{-1} and a voltage scanning rate of 1 mV s^{-1}. (B) Cr(VI) and Cr(III) - Expanded length ED cell limiting current determination at a flow rate of 4.5 mL min^{-1} and a voltage scanning rate of 1 mV s^{-1}.

3.3B. The limiting current of the expanded cell was thus determined to be approximately 15 mA. The increase of the limiting current, in comparison with the unexpanded electrochemical cell system, can be attributed to the increase of amounts of the ions in the solution which was fed to the dilute compartment. The limiting current is the maximum current in the electrodialysis process where the ion concentration at the surface of ion exchange membranes approaches to zero [44]. It depends on membrane and solution properties as well as on the electrodialysis stack construction and various operational parameters such as the flow rate. It has been shown that the limiting current increases with the increase of the electrolyte concentration [45]. For the unexpanded electrochemical cell, the dilute compartment was fed with a 100 ppm Cr(VI) solution containing $HCrO_4^-$ and K^+ ions. In contrast, the dilute compartment of the expanded electrochemical cell was fed with a mixture of 100 ppm Cr(VI) and 100 ppm Cr(III). The additional ions (e.g., Cr^{3+}, SO_4^{2-}) in the fed solution resulted in the increase of the limiting current of the expanded electrochemical cell.

3.3.3 Effect of applied EDI current on the removal of Cr(VI)

To understand the influence of current on the performance of the EDI process, resins and ion exchange membranes used in the unexpanded cell were completely saturated with Cr(VI). The applied current was varied from 80% to 120% of the limiting current in order to determine the optimal current for the EDI process. Fig. 3.4 presents Cr(VI) concentration changes at the five different applied currents during a 120 min EDI treatment, showing that the performance of the system decreased in the following order: 100% of limiting current (11.5 mA) > 110% (12.65 mA) > 90% (10.35 mA) > 120% (13.80 mA) > 80% of limiting current (9.20 mA). When 100% of the limiting current was applied, the most rapid removal

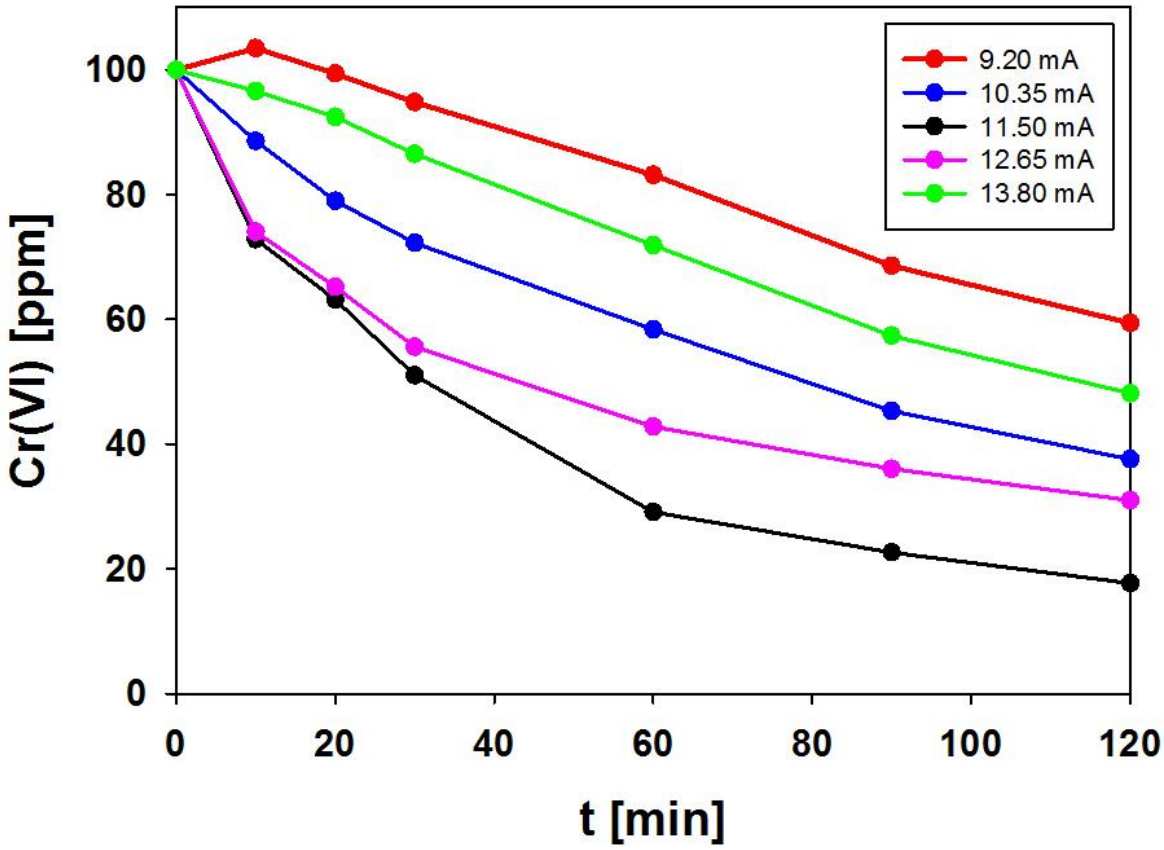

Fig. 3.4. Cr(VI) - Electrodeionization at different current regimes with initially saturated membranes and resins at a flow rate of 4.5 mL min^{-1}.

and highest level of separation were achieved. In contrast, the poorest performance was found to be at 80% of the limiting current, as it gave the lowest level of separation, having an even higher concentration of Cr(VI) than the initial effluent during the initial 20 min. This is primarily due to Cr(VI), from the initially saturated resins and ion exchange membranes, being transferred into the dilute effluent at a faster rate than the ion transfer from the dilute compartment into the concentrate compartment, which resulted in a net increase of the Cr(VI) concentration within the dilute effluent. It is known that the ionic species removal mechanism in an EDI process may be explained by the theories of two different regimes of operation [46, 47]. When the applied current is lower than the limiting current, known as an 'enhanced transfer regime', the ion exchange resins in the dilute compartment are generally exhausted via salt ions. The mixed-bed serves as a conducting spacer, which reduces the stack resistance, as well as to increase the current efficiency. At the limiting current and above, defined as 'electroregeneration regime', water splitting occurs in the dilute compartment, and the ion exchange bed is continuously regenerated by H^+ and OH^- that are formed by in situ water dissociation. When 120% of the limiting current (13.80 mA) was applied, the number of the generated H^+ and OH^- ions from the water dissociation could be too high, not only regenerating the ion exchange resins, but also participating in the ion exchange through membranes. As a result, as seen in Fig. 3.4, the performance for the removal of Cr(VI) at the 120% of the limiting current was dramatically decreased in comparison with the operation, at either 100% or 110% of the limiting current, indicating that the applied current between 100% and 110% of the limiting current achieved optimal Cr(VI) separation.

3.3.4 Separation and recovery of Cr(III) and Cr(VI) via EDI with fresh resins

To investigate the effect of unsaturated resins on removal efficiency and energy consumption, the dilute compartment of the expanded cell was initially filled with fresh anionic and cationic resins. Twelve continuous cycles were carried out at 100% of the limiting current (15.0 mA) for the separation and recovery of Cr(III) and Cr(VI). Each cycle began with a 150 mL mixture of 100 ppm Cr(VI) and 100 ppm Cr(III), and ran for a period of 60 min. The concentrations of the remaining Cr(III) and Cr(VI), as well as the removal efficiency, are listed in Table 3.1. It was revealed that the overall removal efficiency for both Cr(VI) and Cr(III) was very high, although it gradually declined over the 12-cycle operation, from 98.57% to 95.79%, and from 99.30% to 90.36%, for Cr(VI) and Cr(III), respectively. For the duration of the initial several cycles, Cr(III) was slightly better separated than Cr(VI),

Table 3.1. Cr(VI) and Cr(III) mixture EDI unsaturated resins experiment; concentrations and removal efficiency (£) of chromium at 60 min of EDI treatments.

Cycle	Cr(VI) (ppm)	Cr(III) (ppm)	£ (Cr(VI)%)	£ (Cr(III)%)
1st	1.43	0.70	98.57	99.30
2nd	1.42	0.72	98.58	99.28
3rd	1.67	1.28	98.31	98.73
4th	1.80	1.79	98.20	98.21
5th	1.96	2.19	98.04	97.81
6th	2.37	2.22	97.63	97.78
7th	2.59	2.46	97.41	97.54
8th	2.90	3.95	97.10	96.05
9th	2.98	4.05	97.02	95.95
10th	2.46	8.50	97.54	91.50
11th	3.61	8.76	96.39	91.24
12th	4.21	9.64	95.79	90.36

which might be attributed to the larger ion exchange capacity of the cationic resin Amberlite® 200C Na relative to the anionic ion exchange resin Amberlite® IRA900RF Cl. However, in subsequent treatments it was revealed that the Cr(VI) species exhibited improved separation, which might be due to the stronger affinities between the anionic resin ion exchange groups, $-N^{+}(CH_3)^3$ and $HCrO_4^-$ relative to the cationic resin ion exchange groups $-SO_3^-$ and Cr^{3+}, as well as the net charge of the species, one for $HCrO_4^-$ and three for Cr^{3+}. Both resins became more saturated following each cycle, resulting in a decrease of the removal efficiency.

The cell voltage vs time (E vs t) curves for the 1st, 3rd, 5th and 10th cycle are presented in Fig. 3.5. For comparison, the E vs t plots are also included in Fig. 3.5 when no resins were loaded into the dilute compartment of the expanded cell system (Curve a) (known as electrodialysis (ED), as well as when it was filled with the saturated resins (Curve f). As expected, the cell voltage of the EDI system was lower than that of the ED system, which is the primary advantage of EDI over ED. This is due to the enhanced conductivity in the dilute compartment that is provided by the ion exchange resins. Also, a gradual decrease in the cell voltage was observed as additional cycles were performed. As the resins became increasingly saturated, it was observed that they became more conductive, and thus contributed to a lower cell voltage. This might be explained by the replacement of mobile phase species that are resident in the unsaturated resins, with additional ions in solution (e.g., Cr^{3+}, $HCrO_4^-$). Within the fresh resins, there are essentially only H^+ and OH^- groups that are attached to the ion exchange functional groups ($-SO_3^-$, $-N^{+}(CH_3)_3$), which ionize only when they are dissociated (equilibrium between resins and solution). However, when H^+ and OH^-

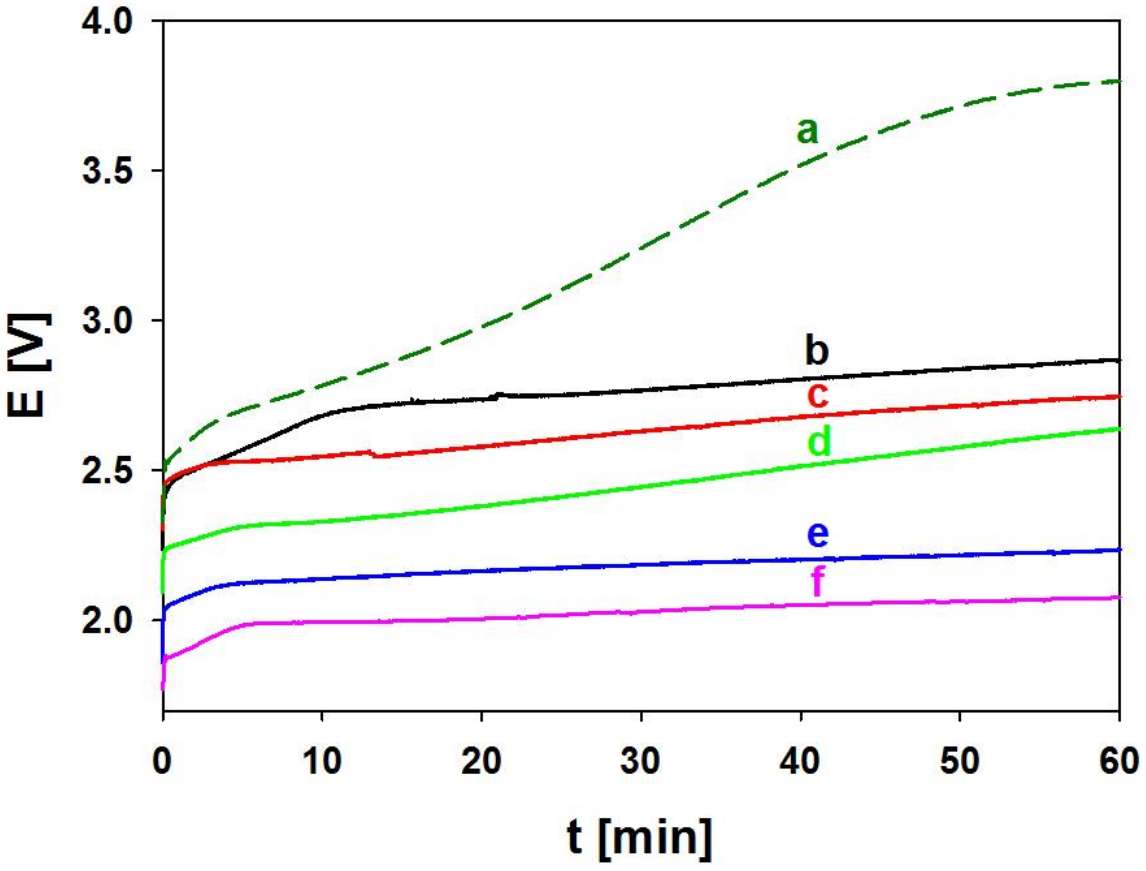

Fig. 3.5. Cell voltage vs. time – electrodeionization (EDI) and electrodialysis (ED) of Cr(VI) and Cr (III) mixture, with current applied at limiting current (15.0 mA) and a flow rate at 4.5 mL min^{-1}. (a) ED treatment (dashed line), (b) EDI 1st treatment (black line), (c) EDI 3rd treatment (red line), (d) EDI 5th treatment (green line), (e) EDI 10th treatment (blue line), (f) EDI following resin saturation treatment (pink line).

groups are substituted by other ionic species in solution, the bonding that occurs is typically ionic in nature. This provides for the inclusion of other ions within the resins, in addition to the H^+ and OH^- groups, which consequently increases conductivity, thus lowering both the resistance and cell voltages. When the dilute compartment of the expanded cell was filled with the saturated resins, the lowest cell voltage was achieved (as can be seen in Curve f of Fig. 3.5), leading to the lowest energy consumption.

3.3.5 Continuous separation and recovery of Cr(III) and Cr(VI) by EDI with saturated resins and ion exchange membrane

In order to determine the efficacy of the EDI system under saturated conditions, the resins were completely saturated with a Cr(VI) and Cr(III) concentrate solution. Four cycles were run using the expanded cell at 100% of the limiting current (15 mA). Each cycle began with a 150 mL of 100 ppm Cr(VI) and 100 ppm Cr(III) solution, at a flow rate of 4.5 mL/min. The concentrations of Cr(VI) and Cr(III), as well as the changes of the cell voltage were monitored over the course of the 120-min EDI treatment. The standard deviation (*s*) of the Cr(VI) and Cr(III) removal, including the cell voltages over the four cycles were calculated using the following formula:

$$s = \sqrt{\frac{1}{N-1}\sum_{i=1}^{N}(x_i - \overline{x})^2} \qquad (3.1)$$

where N is the total number of data points (i.e., the number of cycles); x_i is the value of each data point; and $\overline{x}$ is the average of the data. The removal of Cr(VI) and Cr(III) with error bars are depicted graphically in Fig. 3.6A and Fig. 3.6B, respectively. The R^2 was determined to be 96.15% and 95.38% for the removal of Cr(VI) and Cr(III), respectively, indicating that

the efficiency of the chromium removal remained constant over the four cycles. The removal of Cr(VI) was much more rapid than the removal of Cr(III), which might be due to the differences in the affinities of resins, and as relates to the net charge per Cr(III) and Cr(VI) species. The binding of Cr(VI) via anion exchange resins involved a predominantly electrostatic interaction, with a secondary hydrophobic interaction. The low charge density of $HCrO_4^-$ (one negative charge for every six atoms) explains its strong affinity for the hydrophobic polystyrene-DVB matrix (Amberlite® IRA900RF Cl). Unlike the anionic resin, the hydrophobic character of the cationic resin (Amberlite® 200C Na) is weaker due to the presence of $-SO_3^-$ functional groups, which have the capacity to form hydrogen bridges with water molecules [48]. Fig. 3.6C presents the EDI cell voltages of four treatment cycles, demonstrating that the energy consumption remained stable after the resins were saturated, and that the cell voltage was fairly low at ~2.03 V.

As Cr(VI) is highly toxic, we carried out an eight-hour EDI treatment using the completely saturated mixed resins at 100% of the limiting current (15 mA). As shown in Fig. 3.7A, the concentration of Cr(VI) decreased sharply during the first 120 min, and then gradually diminished to 0.70 ppm. After 4 h, close to 99.0% of the Cr(VI) was successfully removed, indicating that four hours is the optimal duration for this EDI treatment. Fig. 3.7B displays the cell voltage over the eight-hour treatment period, which remained nearly constant at about 2.0 V, even when the Cr(VI) concentration was very low. This indicates that the EDI process developed in this study for the continuous separation and recovery of Cr(VI) and Cr(III) exhibited high efficacy, while having low energy consumption.

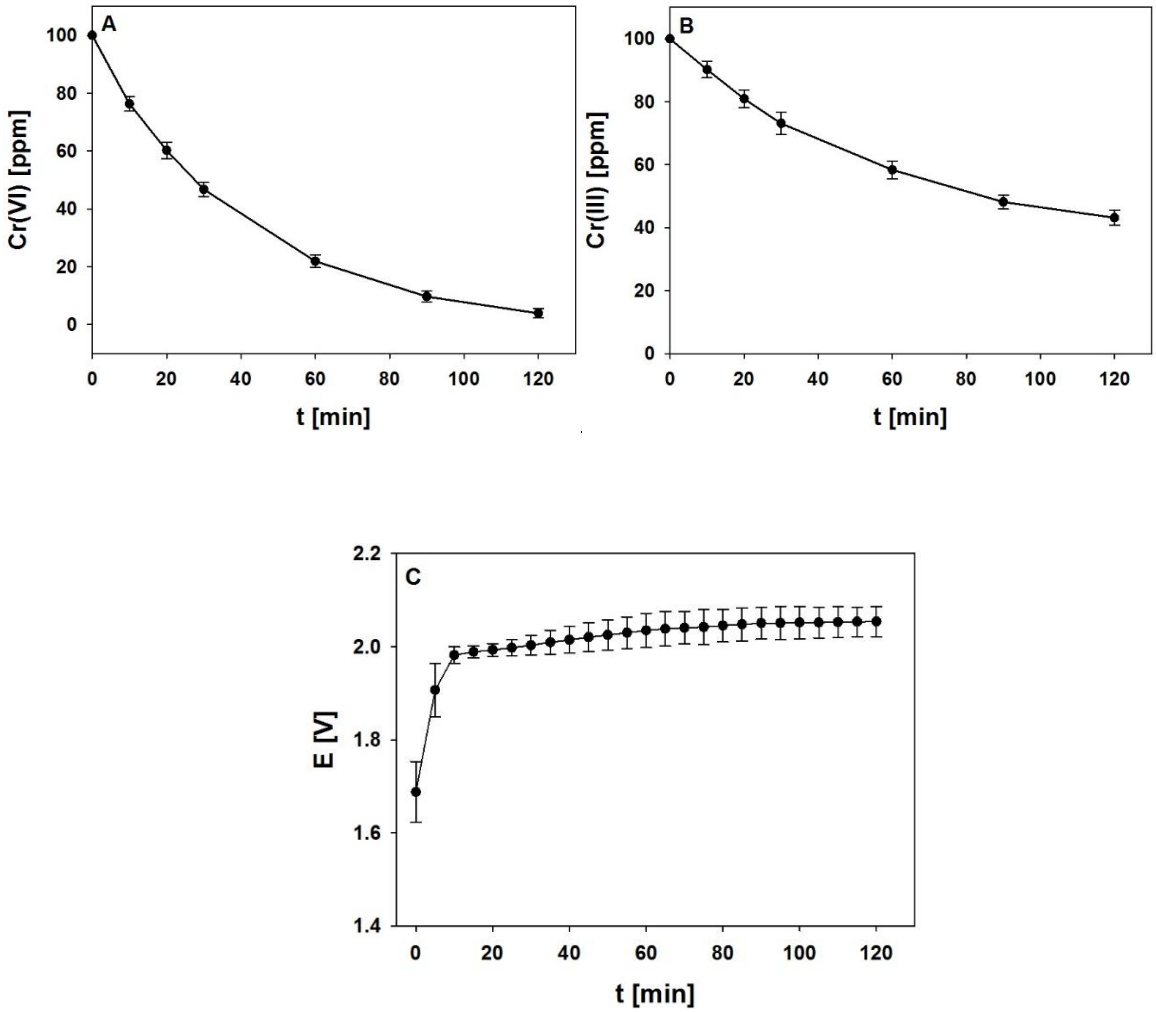

Fig. 3.6. Electrodeionization at 15 mA with saturated resins and a flow rate at 4.5 mL min^{-1} for two hours. (A) Cr(VI). (B) Cr(III). (C) Cell voltage vs. time, 15 mA current applied EDI treatments of Cr(VI) and Cr(III) mixture with saturated resins.

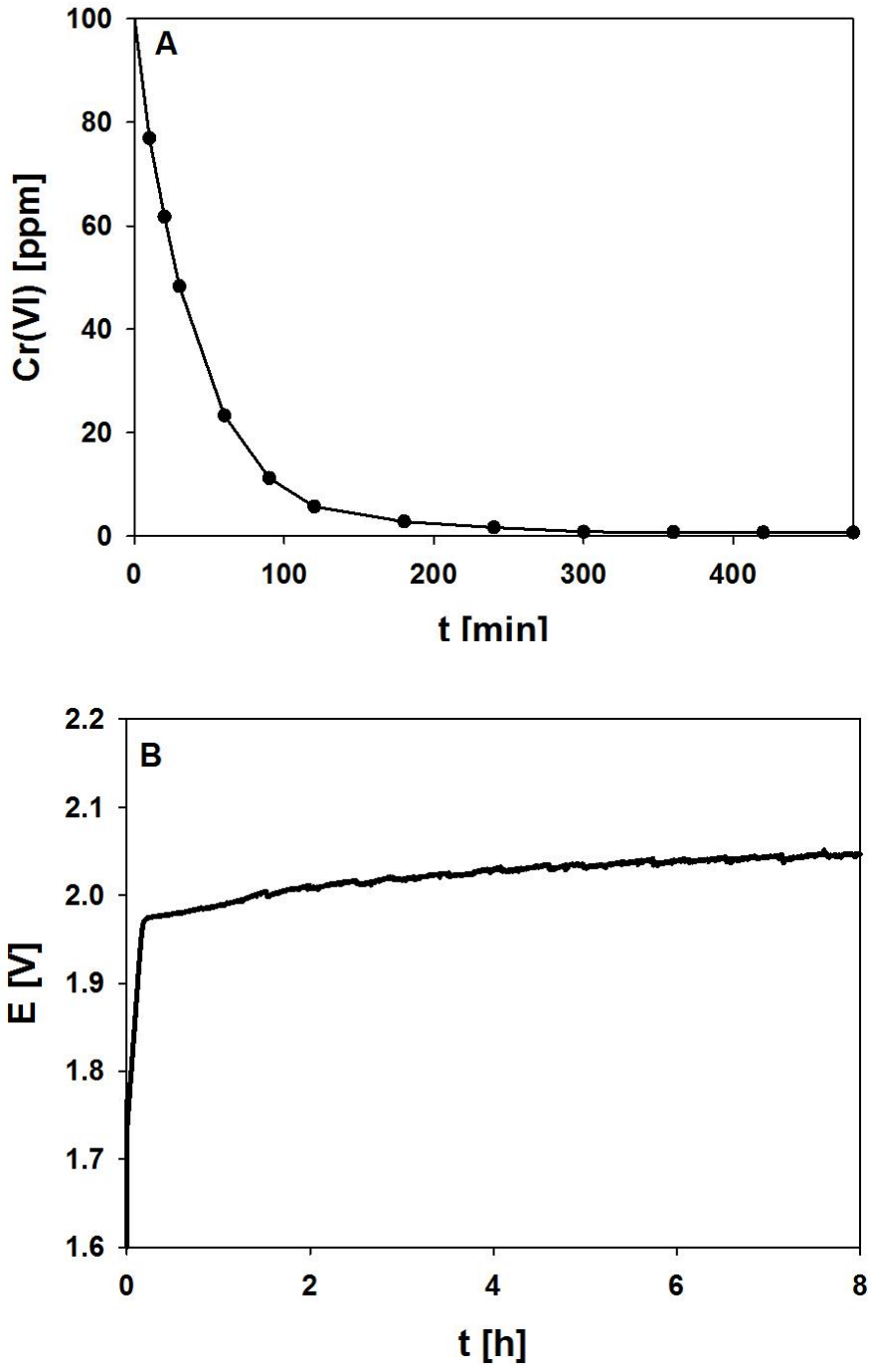

Fig. 3.7. Electrodeionization (EDI) at 15 mA with saturated resins. (A) Cr(VI) concentration vs. time. (B) Cell voltage vs. time.

3.4 Conclusions

In summary, we have developed a new method that effectively combined UV-vis spectroscopy and ICP-AES for the determination of Cr(VI) and Cr(III) concentrations, where UV-vis spectroscopy was used to measure the concentration of Cr(VI), and ICP-AES was employed to quantify the concentration of total chromium. The continuous removal of Cr(VI), as well as the separation and recovery of Cr(VI) and Cr(III), were systemically investigated using the advanced EDI approach. The limiting current was successfully determined to be 11.5 mA for the unexpanded cell, and 15.0 mA for the expanded cell, by measuring the current - voltage relationship. It was found that with the saturated resins and ion exchange membranes, the optimal current was between 100% and 110% of the limiting current. The effect of unsaturated resins was investigated, initially with fresh ion exchange resins. The EDI process demonstrated the very effective removal of both Cr(VI) and Cr(III), in the range of from 95.5% to 98.5%, and from 90.0% to 99.0% within 60 min., respectively. However, both resins became more saturated subsequent to each cycle, resulting in the degradation of the removal efficiency. On the other hand, a gradual decrease in the cell voltage was observed when additional cycles were performed, as the resins became more conductive and thus contributed to a lower cell voltage. Further treatments showed that after the resins were fully saturated, the removal efficiency and energy consumption remained stable; however, the removal of Cr(VI) was higher than Cr(III) mainly due to the net charge of Cr(VI) and Cr(III) species. The continuous and highly efficient removal of highly toxic Cr(VI) (over 99%), and low energy consumption make the EDI process very promising for the treatment of Cr(VI) containing wastewater. Moreover, the configuration of the EDI

membrane stack system described in this study may be employed to separate other species of anions and cations simultaneously.

References

[1] Mihçiokur, H.; Peker, I. *Desalination and Water Treat*. **2013**, *51*, 2116.

[2] Malaviya, P.; Singh, A. *Environ. Sci. Technol.* **2011**, *41*, 1111.

[3] Agrawal, A.; Kumar, V.; Pandey, B. D. *Miner. Processing and Extractive Metall. Rev.* **2006**, *27*, 99.

[4] Catalin, B.; Irina, V.; Doina, B. *Chem. Ind. Chem. Eng. Q.* **2013**, *19*, 615.

[5] Martínez, S.A.; Rodríguez, M.G.; Aguilar, R.; Soto, G. *Water Sci. Technol.* **2004**, *49*, 115.

[6] Alvarado, L.; Torres, I. R.; Chen, A. C. *Sep. Purif. Technol.* **2013**, *105*, 55.

[7] Korngold, E.; Belayev, N.; Aronov, L. *Sep. Purif. Technol.* **2003**, *33*, 179.

[8] Xing, Y.; Chen, X.; Yao, P.; Wang, D. *Sep. Purif. Technol.* **2009**, *67*, 123.

[9] Bielicka, A.; Bojanowska, I.; Wiśniewski, A. *Pol. J. Environ. Stud.* **2005**, *14*, 5.

[10] Golder, A.K.; Chanda, A.K.; Samanta, A.N.; Ray, S. *Sep. Purif. Technol.* **2011**, *76*, 345.

[11] Aeungmaitrepirom, W.; Hagege, A.; Asfari, Z.; Vicens, J.; Leroy, M. *J. Inclusion Phenom. Macrocyclic Chem.* **2001**, *40*, 225.

[12] Basha, C.A.; Ramanathan, K.; Rajkumar, R.; Mahalakshmi, M.; Kumar, P. S. *Ind. Eng. Chem. Res.* **2008**, *47*, 2279.

[13] Jin, W.; Zhang, Z. Y.; Wu, G. S.; Tolba, R.; Chen, A. C. *RSC Adv.* **2014**, *4*, 27843.

[14] Barrera-Díaz, C.; Colín-Cruz, A.; Ureña-Nuñez, F.; Romero-Romo, M.; Palomar-Pardavé, M. *Environ. Technol.* **2004**, *25*, 907.

[15] Gode, F.; Pehlivan, E. *J. Hazard. Mater.* **2005**, *119*, 175.

[16] Coca, M.; Mato, S.; Gonzalez-Benito, G.; Urueña, M. A.; Garcia-Cubero, M. T. *J. Food Eng.* **2010**, *97*, 569.

[17] Nataraj, S. K.; Hosamani, K. M.; Aminabhavi, T. M. *J. Appl. Polym. Sci.* **2006**, *99*, 1788.

[18] Alvarado, L.; Ramírez, A.; Rodríguez-Torres, I. *Desalination* **2009**, *249*, 423.

[19] Arar, Ö.; Yüksel, Ü.; Kabay, N.; Yüksel, M. *Desalination* **2014**, *342*, 16.

[20] Lee, H. J.; Hong, M. K.; Moon, S. H. *Desalination* **2012**, *284*, 221.

[21] Arar, Ö.; Yüksel, Ü.; Kabay, N.; Yüksel, M. *Desalination* **2014**, *342*, 23.

[22] Alvarado, L.; Chen, A. C. *Electrochim. Acta.* **2014**, *132*, 583.

[23] Bouhidel, K. E.; Lakehal, A. *Desalination* **2006**, *193*, 411.

[24] Wang, J.; Wang, S.; Jin, M. *Desalination* **2000**, *132*, 349.

[25] Spoor, P. B.; Koene, L.; Veen, W. R.; Janssen, L. J. J. *J. Appl. Electrochem.* **2002**, *32*, 1.

[26] Spoor, P. B.; Koene, L.; Veen, W. R.; Janssen, L. J. J. *J. Chem. Eng.* **2002**, *85*, 127.

[27] Rozhdestvenska, L. M.; Dzyazko, Y. S.; Belyakov, V. N. *Desalination* **2006**, *198*, 247.

[28] Arar, Ö.; Yüksel, Ü.; Kabay, N.; Yüksel, M. *Desalination* **2011**, *277*, 296.

[29] Semmens, M. J.; Dillon, C. D.; Riley, C. *Environ. Prog.* **2001**, *20*, 251.

[30] Mahmoud, A.; Hoadley, A. F. A. *Water Res.* **2012**, *46*, 3364.

[31] Meng, H.; Peng, C.; Song, S.; Deng, D. *Surf. Rev. Lett.* **2004**, *11*, 599.

[32] Wood, J.; Arba, J.; Shaw, M. *Desalination* **2010**, *250*, 973.

[33] Simons, R. *Electrochim. Acta*. **1984**, *29*, 151.

[34] Dermentzis, K. *J. Hazard. Mater.* **2010**, *173*, 647.

[35] Taghdirian, H. R.; Moheb, A.; Mehdipourghazi, M. *J. Membr. Sci.* **2010**, *362*, 68.

[36] Xing, Y.; Chen, X.; Wang, D. *Sep. Purif. Technol.* **2009**, *68*, 357.

[37] Dzyazko, Y. S.; Rozhdestvenskaya, L. M.; Vasilyuk, S. L.; Belyakov, V.N.; Kabay, N.; Yuksel, M.; Arar, O.; Yuksel, U. *Chem. Eng. Commun.* **2009**, *196*, 3.

[38] Dzyazko, Y. S.; Rozhdestvenskaya, L. M.; Vasilyuk, S. L.; Belyakov, V.N.; Kabay, N.; Yuksel, M.; Arar, O.; Yuksel, U. *Chem. Eng. Commun.* **2009**, *196*, 22.

[39] Bergmann, M. E.; Lourtchouk, T.; Rittel, A.; Zuleeg, H. *Electrochim. Acta.* **2009**, *59*, 2417.

[40] Chen, A. C.; Miller, B. *J. Phys. Chem. B,* **2004**, *108*, 2245.

[41] Asmussen, R. M.; Tian, M.; Chen, A. C. *Environ. Sci. Technol.* **2009**, *43*, 5100.

[42] Tian, M.; Wen, J. L; MacDonald, D.; Asmussen, R. M.; Chen, A. C. *Electrochem. Commun.* **2010**, *12*, 527.

[43] Martí-Calatayud, M. C.; García-Gabaldón, M.; Pérez-Herranz, V.; Ortega, E. *J. Membr. Sci.* **2011**, *379*, 449.

[44] Krol, J. J.; Wessling, M.; Strathmann, H. *J. Membr. Sci.* **1999**, *162*, 145.

[45] Lee, H. J.; Strathmann, H.; Moon, S. H. *Desalination* **2006**, *190*, 43.

[46] Lee, J. W.; Yeon, K. H.; Song, J. H.; Moon, S. H. *Desalination* **2007**, *207*, 276.

[47] Cuan, S.; Wang, S. C. *Sep. Sci. Tech.* **2007**, *42*, 949.

[48] Xiong, Z.; Zhao, D.; Harper Jr. W. F. *Ind. Eng. Chem. Res.* **2007**, *46*, 9213.

Chapter 4 Simultaneous removal of nitrate and hardness ions from ground water using electrodeionization

4.1 Introduction

Increased levels of nitrate in surface and groundwaters have become a significant environmental problem on a global scale. Contamination with high nitrate concentrations is the result of industrial activity, wastewater treatment plants, domestic sewage, landfills, agricultural fertilizers, as well as human and animal wastes. [1]. One of the primary health hazards regarding nitrate is that it is reduced to nitrite within the human body, which reacts with red blood cells to cause methemoglobinemia (also known as blue-baby syndrome). Nitrite oxidizes hemoglobin to methemoglobin, which impacts the capacity of blood to transport oxygen to cells and tissues [2, 3]. In addition, due to their low gastric acidity, infants are particularly sensitive to the nitrate contamination. Therefore, it is critical to develop an effective approach for nitrate removal from potable water. According to the Guidelines for Canadian Drinking Water Quality, as well as World Health Organization's recommendation, the maximum acceptable concentration (MAC) in drinking water has been set at 10 mg/L nitrogen as NO_3^- [4], which corresponds to 45 mg/L of nitrate.

In order to remove nitrate from water, several techniques have been proposed: biological processes [5-7], chemical precipitation [8], reverse osmosis [9, 10], ion exchange [11, 12], electrodialysis [13-16] and catalytic reduction [17]. Among them, biological denitrification has been successfully utilized for the treatment of municipal and industrial wastewater. However, large installations are required and biological processes are quite slow. Moreover, since bacterial responses for nitrate transformation are very sensitive, ambient parameters

such as pH and temperature must be maintained within a certain range. Conventional ion exchange resins have also been employed for the removal of nitrate. Advantages of this strategy in comparison to biological denitrification include the capability of achieving very low nitrate concentrations, low operating cost, reduced time consumption, and relative insensitivity to temperature fluctuations [18]. However, this is a non-continuous operation as the resins become exhausted. This necessitates their regeneration using concentrated acidic or basic solutions, which creates secondary chemical wastes as well as increased operational costs [19]. Membrane processes such as electrodialysis (ED) have proven their reliability and efficacy when large volumes are to be treated. This is an electrochemical separation process that combines an electric field with ion exchange membranes to separate ionic species from aqueous solutions. The limitation of electrodialysis, however, is that high levels of energy are consumed plus ion removal is efficient once ion concentrations become too low [20].

A hybrid ion-exchange resin/electrodialysis process is referred to as electrodeionization (EDI) [21-24]. This synergistic combination allows EDI to overcome the inherent drawbacks of these two technologies when they are applied on their own. Systems that integrate EDI have the capacity to continuously treat solutions with low conductivity due to the incorporation of ion exchange resins between the membranes that are contained within the dilute compartment of the electrodialysis system. The ion exchange resins are continuously regenerated by the applied electric field, which can dissociate water in situ to form H^+ and OH^- thus, no additive chemicals are required [25]. Further, added ion exchange resins provide supplementary conductivity to the dilute compartment, which leads to more rapid, energy efficient, and extensive separation [26]. Electrodeionization was initially investigated in 1956 by Walter et al. [27], and in the late 1950s Glueckauf conducted theoretical

investigations into these hybrid processes [28]. Currently, EDI is widely used for the generation of high-purity water, removal and recovery of heavy metals, organic compound separation, and production of rinse water for the microelectronics industry [29-36].

Very few researchers have investigated the removal of nitrate using EDI to produce potable water [14, 24, 37, 38], and actual water streams typically contain hardness ions such as Ca^{2+} and Mg^{2+}. The aims of this investigation were to evaluate the impact of the presence of hardness ions on the removal of nitrate and energy consumption, and to select the optimal operating parameters of EDI technologies. In the present work, we have explored EDI as an advanced approach for the continuous removal of nitrate and hardness ions. UV-Visible spectroscopy was applied to monitor nitrate concentrations, while Inductively Coupled Plasma Atomic Emission Spectroscopy (ICP-AES) was used to determine Ca^{2+} and Mg^{2+} concentrations in mixed solutions. Furthermore, the effects of different operational parameters (e.g., current density, water flow, and ion exchange material ratios) have been systematically investigated. Meanwhile, in this study, we have improved the configuration of the EDI membrane stack, which might be employed to simultaneously separate and recover other cations and anions.

4.2 Experimental

4.2.1 Materials

A strong acidic macroreticular cation exchange resin (Amberlite® 200C Na) and a strong basic macroreticular anion exchange resin (Amberlite® IRA900RF Cl) were purchased from Rohm and Haas Co. Cationic exchange membranes (CMI-7000S) and anionic exchange membranes (AMI-7001S) were provided by Membranes International Inc. The properties of

the membrane are listed in Table 4.1. Inorganic chemicals were supplied by Sigma Aldrich as analytical grade reagents, and standard nitrate solutions were prepared using $NaNO_3$. Solutions containing Ca^{2+} and Mg^{2+} were prepared through the dissolution of $Ca(NO_3)_2$ and $Mg(NO_3)_2$, respectively. The 0.1 M H_2SO_4 electrolyte was prepared from ACS reagent grade H_2SO_4 (95.0 - 98.0% purity). The water used in the preparation of all the solutions was purified by a Nanopure® Diamond Water System (18.2 MΩ cm), and all of the experiments were carried out at 20 ± 2 ^oC.

Table 4.1. Properties of the anionic and cationic exchange materials.

Materials	Cationic Resin	Anionic Resin	Cationic Membranes	Anionic Membranes
Name	Amberlite® 200C Na	Amberlite® IRA900RF Cl	CMI-7000	AMI-7001S
Matrix	Styrene DVB copolymer	Styrene DVB copolymer	Gel polystyrene crosslinked, DVB	Gel polystyrene crosslinked, DVB
Functional Groups	$-SO_3^-$	$-N^+(CH_3)_3$	$-SO_3^-$	$-N^+(CH_3)_3$
Total Exchange Capacity (Eq/L)	> 1.7 (Na^+ form)	> 1.0 (Cl^- form)	1.6	1.3

4.2.2 Instruments for measurements

Nitrate concentrations in solution were monitored by a UV-Visible spectrophotometer (Cary 50) with a 4 cm^3 quartz cuvette, whereas the Ca^{2+} and Mg^{2+} concentrations were determined by Inductively Coupled Plasma Atomic Emission Spectroscopy (ICP-AES) (Varian Vista Pro). A pH meter (Oakion Acorn®) was employed to measure the pH of solutions. The current-voltage curve and time-voltage curve were recorded by a Voltalab PGZ 402 Universal Potentiostat and the conductivity experiments were carried out using a multimeter (Oakton).

4.2.3 Ion exchange materials pre-treatment

All of the ion exchange materials were treated prior to the EDI process in order to minimize any inaccuracies due to the initial exchange capacities of resins and membranes. Specifically, the anion and cation membranes were immersed in 0.1 M NaOH and 0.1 M H_2SO_4 for 24 h, respectively, and subsequently rinsed with deionized water to remove any excess reagents just prior to their installation into the EDI cell system. The anion exchange resins (Amberlite® IRA900RF Cl) were treated with 0.1 M NaOH and stirred for 1 h while the cation exchange resins (Amberlite® 200C Na) were immersed in 0.1M H_2SO_4 and stirred for 1 h. They were subsequently to be rinsed twice with pure water, separated from the water via filtration, and dried completely at 60 ^oC.

4.2.4 Electrodes for EDI cell

The EDI process was carried out in a custom-fabricated electrochemical cell, utilizing a stainless steel plate (6 cm x 10 cm) as the cathode and Ti/Ta_2O_5-IrO_2 (6 cm x 10 cm) as the

anode. Our previous work has verified that Ta_2O_5-IrO_2 coatings possess robust electrical and electrocatalytic properties as an anode material [39, 40].

In order to fabricate the Ti/Ta_2O_5-IrO_2 electrode, a thermal decomposition technique was employed. Briefly, a pure Ti mesh substrate with area of 6 cm x 10 cm was initially immersed in acetone in an ultrasonic bath for 15 min, rinsed with pure water, etched in a 18% HCl solution at 85 ^oC for 15 min, and then rinsed again with ultrapure water. According to an established protocol published by our group [41], the Ta_2O_5-IrO_2 coating was prepared by combining tantalum and iridium precursor solutions. The tantalum precursor solution contained 0.13 g of $TaCl_5$ dissolved in 7.5 mL of isopropanol, while the iridium precursor solution was prepared by dissolving 0.30 g of $IrCl_3 \bullet 3H_2O$ in 2.5 mL of ethanol. Subsequent to mixing both the tantalum and iridium precursor solutions, the Ti substrates were manually painted with the coating solution using a brush. This process was repeated until an oxide coating load of 30 g/m^2 was attained. The fabricated Ti/Ta_2O_5–IrO_2 electrodes were then annealed at 450 °C for 1 h.

4.2.5 Description of the EDI cell and experimental scheme

The experiments were performed with a laboratory EDI cell, as shown in Scheme 4.1, which is a plate-and-frame module with ion exchange layers. The EDI stack setup was configured as an array of acrylic sheets and membranes between the two electrodes to separate the concentrate and dilute compartments. Sandwiched between the acrylic sheets were ion exchange membranes (cationic and anionic) with an effective area of 60 cm^2 (6 cm x 10 cm), and two acrylic sheets of 20 mm in thickness housed the two electrodes to form

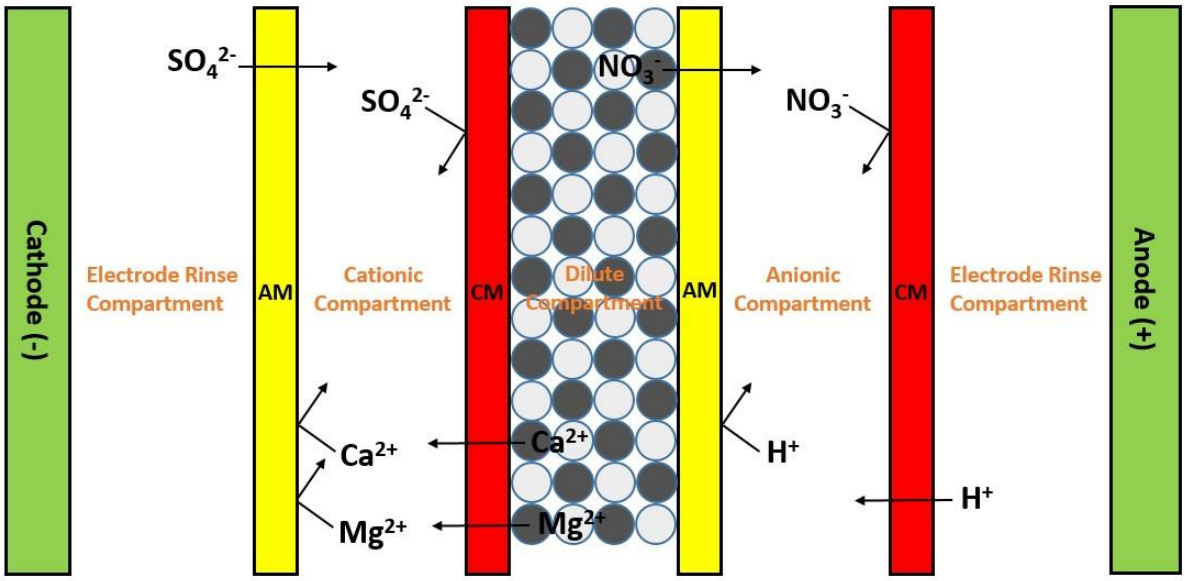

Scheme 4.1. Schematic diagram of the electrodeionization (EDI) cell for NO_3^-, Ca^{2+} and Mg^{2+} separation and recovery. (AM: Anionic membrane; CM: Cationic membrane).

the electrode rinse compartments. The dilute compartment was filled with ~ 20 g of mixed ion exchange resins between the cationic and anionic membranes. Rubber gasket spacers (3.5 mm thick) were positioned on both sides of the ion exchange membranes to distribute the pressure. The EDI stack was also equipped with auxiliary components such as tanks, pumps, flow-meters and a power supply.

In this EDI system, the thicknesses of the dilute, concentrate and electrode rinse compartments were 10 mm, 10mm and 5 mm, respectively. The cation concentrate compartment and anion concentrate compartment were positioned on each side of the dilute compartment and adjacent to the electrode rinse compartments. A continuous flow of solution passed from the bottom to the top of all the compartments contained within the EDI cell.

As saturated and unsaturated resins have different influences on the performance of EDI [23], cation resins were saturated with calcium and magnesium ions, while anion resins were

saturated with nitrate ions prior to the operation of the EDI. Afterwards, the EDI experiments were repeated multiple times until the ion exchange equilibrium of the resins was attained.

For the removal of nitrate and hardness ions, such as Ca^{2+} and Mg^{2+}, a constant current was applied to the cell using a Voltalab PGZ 402 Universal Potentiostat. One L of nitrate and Ca^{2+}, Mg^{2+} mixture was pumped through the dilute compartment at specific flow rates and cycled in the same tank as the feed solution. Simultaneously, 0.1 M H_2SO_4 with a volume of 250 mL was circulated through the concentrate compartments to increase the conductivity of the EDI cell, and to avoid the precipitation of $Ca^{2+}$and Mg^{2+}. Meanwhile, 250 mL of a 0.1 M H_2SO_4 solution was recirculated into the electrode rinse compartments as a continuous flow. As depicted in Scheme 1, when a current was introduced to the cell in response to the presence of the electric field, NO_3^- migrated to the anode, whereas $Ca^{2+}$and Mg^{2+} moved toward the cathode. Nevertheless, due to the interposed permselective membranes between different compartments, the concentration of NO_3^- increased in the anionic compartment, while the concentrations of $Ca^{2+}$and Mg^{2+} increased in the cationic compartment. The reactions which took place on the electrodes are presented as follows:

$$\text{Cathode: } 2H_2O + 2e^- \rightarrow H_2 + 2OH^-$$

$$\text{Anode: } 2H_2O \rightarrow O_2 + 4H^+ + 4e^-$$

At the end of the process, cations and anions in the dilute compartment were stripped from solution, while becoming more populated in the concentrate compartments. The EDI experiments were performed in batch mode and samples were intermittently extracted from both the dilute and concentrate compartments to determine the concentrations of NO_3^-, Ca^{2+} and Mg^{2+}.

4.3 Results and discussion

4.3.1 Monitoring of ionic species

In this investigation, a quantitative analysis of nitrate was performed using UV-Vis spectroscopy, while hardness ions, such as $Ca^{2+}$and Mg^{2+}, were determined by ICP-AES. Fig. 4.1A presents the UV-Vis spectra of the standard nitrate solutions where the nitrate concentration was varied from 0.0 to 200.0 ppm. To facilitate the development of the calibration curve for the determination of nitrate concentrations in this study, the most intensive absorbance value at a wavelength of 305 nm was selected, and the calibration curve was plotted. As depicted in Fig. 4.1B, the absorbance value increased linearly with elevated concentration, and the equation of the best fit line is calculated to be $y = (1.23e^{-4})x - 1.24e^{-4}$, with $R^2 = 0.9998$. To compare with standard nitrate solutions containing $Ca^{2+}$and Mg^{2+}, another parallel experiment was performed, with the results showing that there was no interference from them.

4.3.2 Limiting current determination

In EDI, the applied electric field was the driving force of the process, as it determined the migration speed of ions (e.g., NO_3^-, Ca^{2+}, Mg^{2+}) across the membranes. Additionally, it was used for water dissociation, which was the reason for resin regeneration. Therefore, a current – voltage (I vs E) polarization curve was recorded in order to establish the limiting current. During the experiments, the cell voltage was scanned from 1.0 to 4.0 V at a sweep

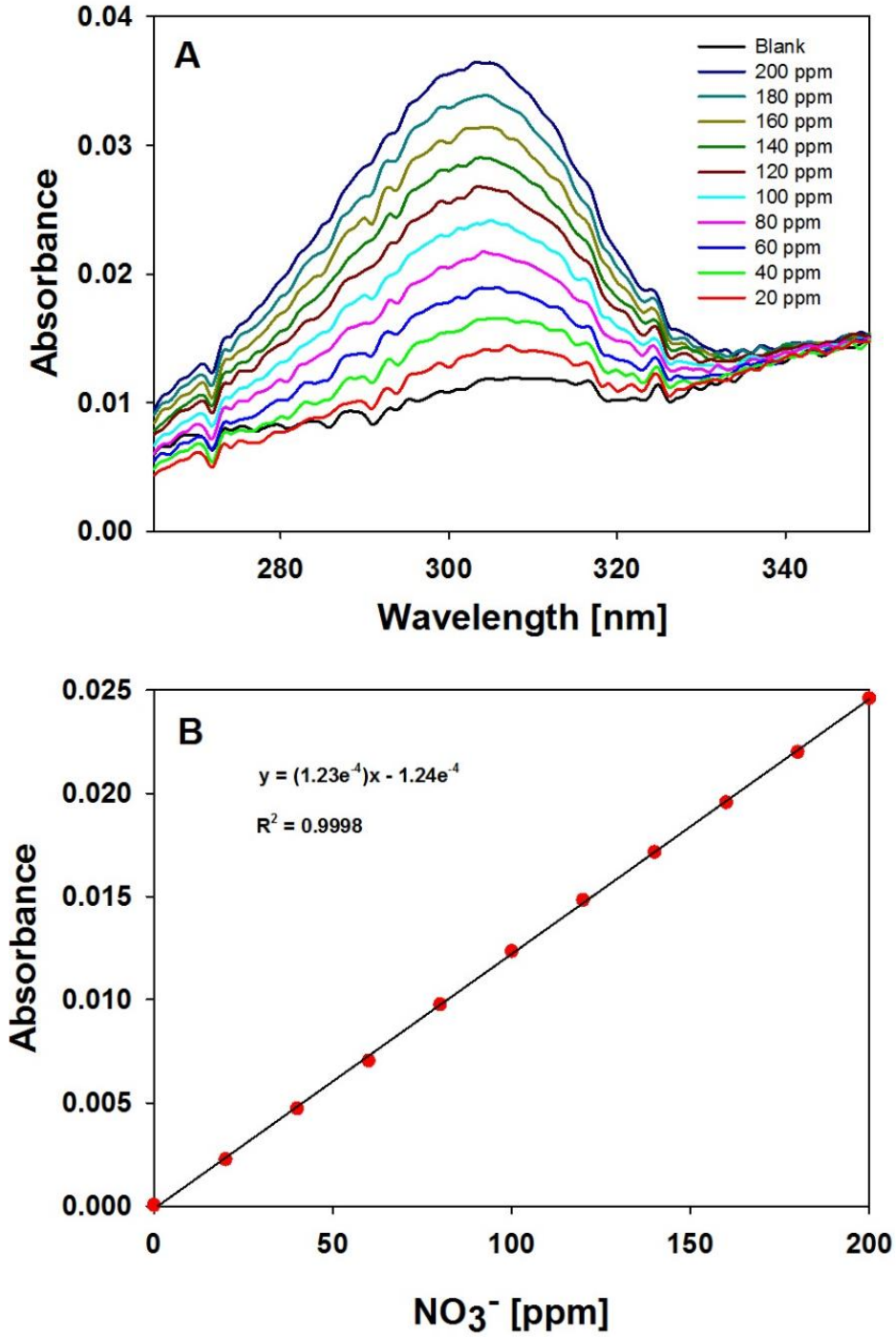

Fig. 4.1. (A) UV-Vis absorption spectra of variable nitrate concentration. (B) Calibration curve for nitrate at wavelength 305 nm.

rate of 1 mV s^{-1}. As shown in Fig. 4.2, at the beginning of the EDI process. The current was nearly zero before the cell voltage attained 1.0 V, as the input energy was used primarily to charge the cell membranes and electrodes. From 1.0 V to 1.5 V, the current increased slightly, revealing that the ion transportation from the bulk solution to the membrane/resin interface slowly began. The current was elevated linearly with the increase of the applied cell voltage from 1.5 V to 2.7 V, but exhibited a more shallow rise from 2.7 V to 4.0 V. The limiting current could be evaluated with the tangents crossing, which corresponded to the straight portions of the current – voltage curve [42]. As displayed in Fig. 4.2, the limiting current of the EDI cell was determined to be 19.0 mA.

The removal mechanism for ionic species via the EDI process might be explained by the theory of two distinct regimes of operation [43, 44]. In the "enhanced transfer regime" from 0.0 V to 2.7 V, the ion exchange resins were exhausted with salt ions and strongly ionized substances were removed in the dilute compartment. The mixed ion exchange resins served as a conductive spacer, which increased the cell conductivity and reduced power consumption. In addition, the rate of water dissociation in this regime was low. The second regime (from 2.7 V to 4.0 V) is referred to as the "electroregeneration regime", where water dissociation occurred acutely in the dilute compartment and the ion exchange bed was continuously regenerated in situ by the resulting H^+ and OH^- ions. The limiting current of the EDI process was selected as the intermediate regime (2.9 V), where both ionic removal and water dissociation occurred simultaneously.

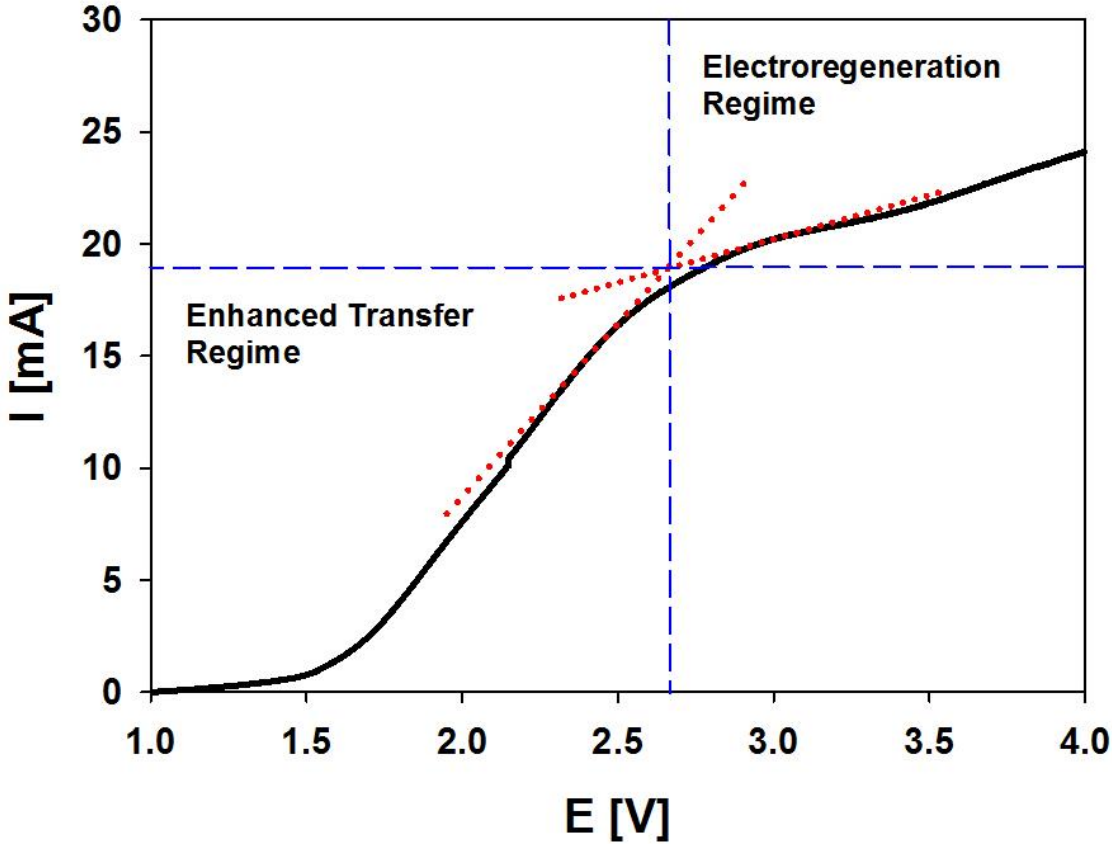

Fig. 4.2. Current-voltage curve of the EDI cell for limiting current determination at a scan rate of 1 mV s^{-1}.

4.3.3 Variable effects on the performance of EDI for the nitrate removal

4.3.3.1 Effect of applied current

The effect of the applied current on the performance of EDI was investigated since it is a critical operational variable for the process. All of the ion exchange resins were saturated with nitrate prior to each experiment, whereas other parameters were fixed. Fig. 4.3A depicts the variations of the nitrate removal rate under different applied currents from 15 mA to 22 mA over a four-hour treatment. As anticipated, the applied current had the capacity to significantly affect the removal of nitrate. Specifically, at an applied current of 19 mA-i.e., the limiting current-the highest nitrate removal rate (96.3%) was achieved. If the applied current either exceeded or was lower than the limiting current, the nitrate removal rate was decreased. When the applied current exceeded the limiting current, the number of H^+ and OH^- ions generated via water dissociation increased accordingly, not only regenerating the ion exchange resins, but also participating in ion exchange through the membranes, resulting in a decreased nitrate removal rate. On the other hand, an applied current that was lower than the limiting current probably provided an insufficient driving force for migration of NO_3^- ions from the dilute compartment to the anionic concentrate compartment. Based on the overall analysis, 19.0 mA was determined as the optimal operating current.

4.3.3.2 Effect of flow rate

It is necessary to investigate the influence of flow rate on the removal of nitrate, as it may vary from time to time in industrial applications. Fig. 4.3B represents variations in the removal rate of nitrate under different flow rates, from 6 mL/min to 12 mL/min. The applied

current was 19 mA, whereas the initial concentration of NO_3^- was 200 ppm, the ratio of mixed cation and anion exchange resins was 1:1, and the operational time was 4 hours. As can be seen in Fig. 4.3B, the nitrate removal rate was initially increased by the elevated flow rate. When the flow rate was 9 mL/min, the optimal nitrate removal rate was attained. However, beyond a flow rate of 9 mL/min, the nitrate removal rate began to decline. The initial improvement in the removal rate was due to an increase in the flow rate, where more NO_3^- ions were transferred to the concentrate compartment. Subsequently, the removal rate was improved, as too rapid a flow rate would result in a shorter residence time of ions in the permselective membranes, such that portions of the NO_3^- ions would be discharged prior to treatment, which reduced the removal efficiency. As a result, for EDI process, the optimum water flow rate was determined to be 9 mL/min.

4.3.3.3 Effect of mixed resins ratio

EDI experiments were also carried out using differently mixed resin ratios in the dilute compartment. Anion and cation exchange resins at variable ratios (1:1, 1:2, 2:1, 1:3, and 3:1) by weight were loaded into the EDI cell. After 4 hours, the highest nitrate removal rate of 95.8% was observed at the resin ratio of 1:1, as shown in Fig. 4.3C. Along with either the anion exchange resin or cation exchange resin taking up a larger portion of the mixed-bed, the performance of nitrate removal was further degraded. It is known that the regeneration of ion exchange resins is accomplished through water dissociation, which generates H^+ and OH^- ions. It was revealed that, at the bipolar interfaces of ion exchange materials (e.g., cation resin - anion resin, cation resin - anion membrane, anion resin - cation membrane), the dissociation

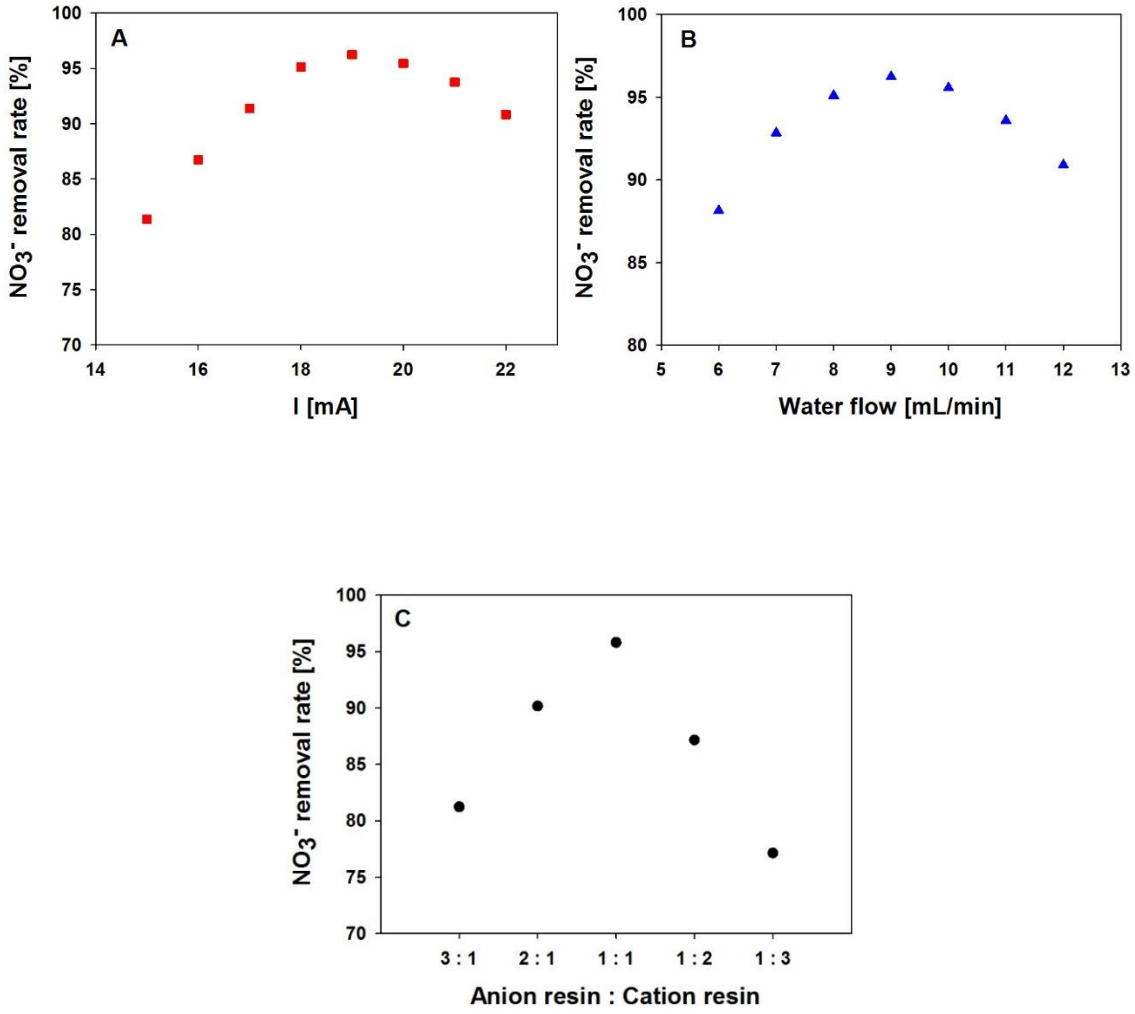

Fig. 4.3. Percent removal of NO_3^- ions in dilute compartment of EDI with variation of (A) applied current, (B) water flow rate, (C) mixed resins ratio.

of water could be enhanced [45]. By having a 1:1 ratio of mixed-bed ion exchange resins, water dissociation could theoretically disperse evenly across the entire dilute compartment. Thus, the regeneration of the resins in a uniform manner might achieve an optimal removal rate. Interestingly, anion to cation resin ratios of 2:1 and 3:1 exhibited improved results over the ratios 1:2 and 1:3, respectively. This might be explained by the anion exchange resin alone, which could absorb portions of the NO_3^- ions during the process. Thus, the optimum ratio of the mixed anion and cation exchange resins was determined to be 1:1 by weight.

4.3.4 The EDI process with nitrate and hardness ions

To investigate the nitrate removal from water in the presence of hardness ions in the EDI process, a series of experiments were performed. All resins were completely saturated with a calcium nitrate and magnesium nitrate solution prior to the experiments. Subsequently, a 1 L solution that contained 200 ppm NO_3^-, 50 ppm Ca^{2+} and 50 ppm Mg^{2+} was circulated in the dilute compartment, while two 250 mL of 0.1 M H_2SO_4 solutions were recycled through the cation concentrate compartment and anion concentrate compartment, respectively, under the optimal experimental conditions (applied current: 19.0 mA; flow rate: 9 mL/min; mixed resins ratio: 1:1). Fig. 4.4A depicts the nitrate removal in the dilute compartment, as well as nitrate recovery in the concentrate compartment with time variations. It was revealed that only 7.5 ppm NO_3^- remained in the dilute compartment following a 4-hour treatment, which already met the requirement of MAC in potable water, i.e., 45 ppm of nitrate. Meanwhile, NO_3^- ions were concentrated in the anionic compartment, where 772 ppm of nitrate was recovered. The EDI process was evaluated in terms of the removal rate (RR) and mass transfer rate (MTR), which were calculated from equations (4.1) and (4.2):

$$RR = \frac{C_0 - C_d}{C_0} \times 100\% \qquad (4.1)$$

$$MTR = \frac{C_c}{(C_0 - C_d) \times n} \times 100\% \qquad (4.2)$$

where C_0 and C_d represent the ion concentrations in the dilute compartment prior to and following treatment, and C_c is the concentration in the concentrate compartment subsequent to treatment, respectively. Since the volume of the treated solution (1 L) recycled in the dilute compartment was four times larger than the volume of the solution (250 mL) that was circulated in the concentrate compartment, n = 4 in equation (4.2). As for the nitrate removal rate (RR), 96.25% was achieved following a 4-hour treatment. The mass transfer rate (MTR) was calculated to be 100.35%, and the removal of Ca^{2+} and Mg^{2+} over time are depicted graphically in Fig. 4.4B. Based on the equations (4.1) and (4.2), the RR and MTR of Ca^{2+} and Mg^{2+} were calculated to be 96.69% and 101.97%, 96.13%, and 102.38%, respectively. As can be seen, both Ca^{2+} and Mg^{2+} were effectively removed from the dilute compartment and concentrated in cationic compartment. However, the removal of Ca^{2+} exhibited slightly better performance than Mg^{2+}. This might be explained by the general selective separation trends of identical valence ions, where the higher the atomic number is, the more selective it will be (e.g., $Mg^{2+} < Ca^{2+} < Sr^{2+} < Ba^{2+}$). It is notable that all of the MTR results calculated from the equation 4.2 were higher than 100%, which was attributed to the fact that some of the NO_3^-, Ca^{2+}, and Mg^{2+} ions from the initially saturated ion exchange materials were transferred into the concentrate compartment due to the resin regeneration during the EDI process.

The pH variations over time in three different compartments were observed, and are depicted in Fig. 4.5. The precipitation of insoluble hydroxides such as $Ca(OH)_2$ and $Mg(OH)_2$ in the cationic compartment was avoided, as 0.1 M H_2SO_4 was employed as the electrolyte. In the dilute compartment, the pH was measured and found to increase at first, but was

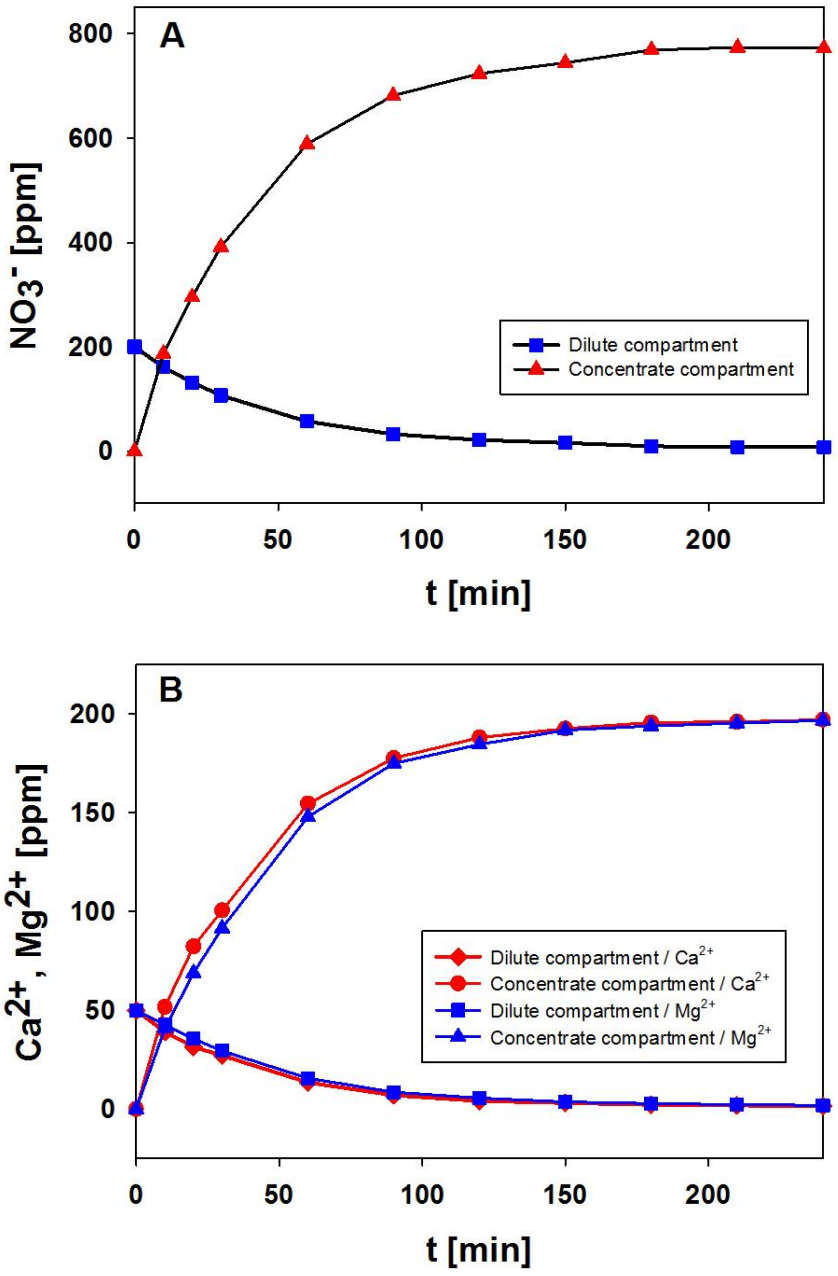

Fig. 4.4. Variation of ion concentration in dilute and concentrate compartment of EDI cell between: (A) NO_3^-, (B) Ca^{2+} and Mg^{2+}.

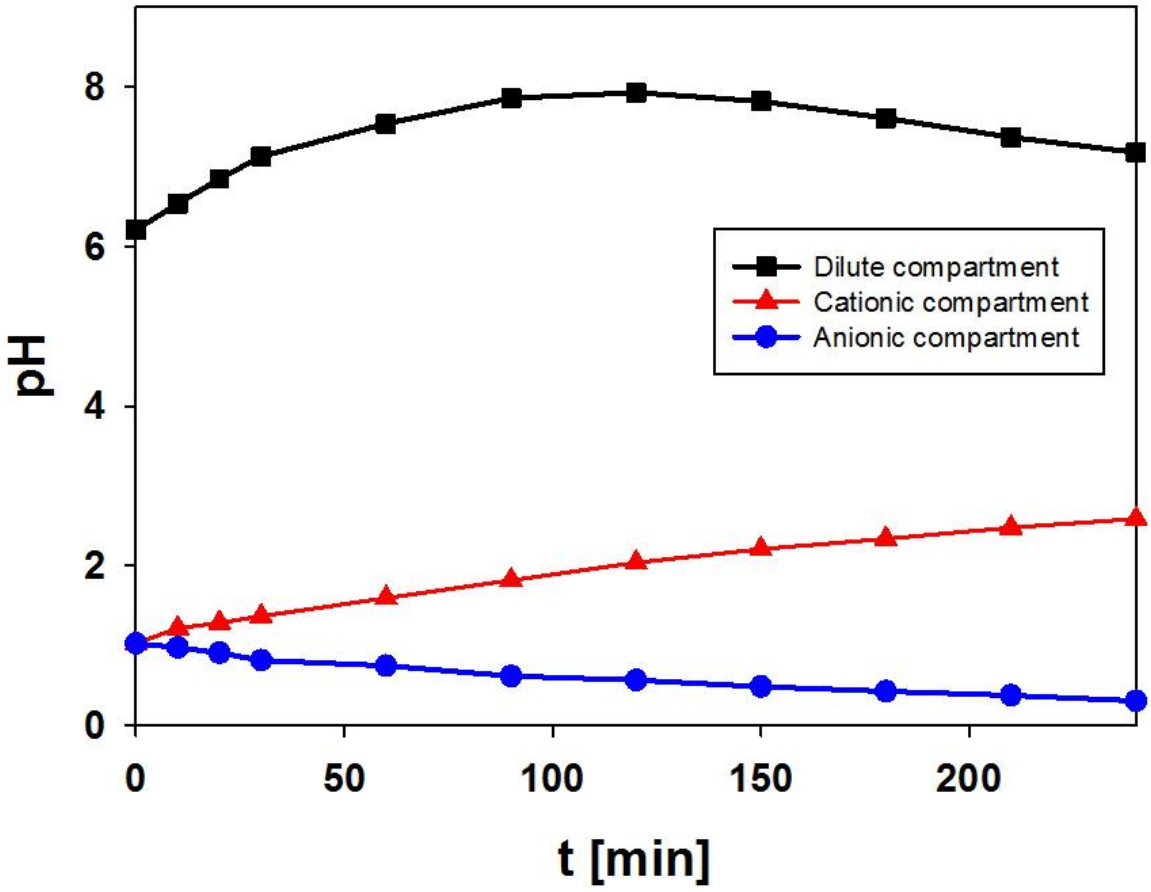

Fig. 4.5. Variation of pH in the dilute, anionic and cationic concentrate compartments with time.

subsequently decreased. This was due to the onset of water dissociation, whereby a significant amount of H^+ and OH^- ions were produced, and it is well known that the migration rate of the H^+ ions is more rapid than that of OH^- ions, which results in the elevation of pH. However, following four hours of treatment the ion equilibrium was attained, at which point the pH dropped back to ~7. Similarly, a portion of the H^+ ions from the electrode rinse compartment migrated to the anionic compartment, which initiated a decrease in pH, while the OH^- ions from the other electrode rinse compartment resulted in an increase of pH in the cationic compartment.

4.3.5 Analysis of real samples

Actual groundwater, which was obtained from an agricultural field in the city of Thunder Bay, Ontario, Canada, was collected and tested through the EDI process. The initial and final concentrations of all species are presented in Table 4.2, where the experiments were repeated

Table 4.2. EDI results of Thunder Bay ground water treatment, showing the initial and final concentrations and removal rate of all species after 4 hours.

Species	Initial Concentration (ppm)	Final Concentration ± SD (ppm)	Removal Rate ± SD (%)
Calcium	36.53	1.34 ± 0.03	96.33 ± 0.08
Magnesium	17.27	0.75 ± 0.02	95.65 ± 0.12
Sodium	7.44	0.48 ± 0.01	93.55 ± 0.13
Potassium	2.25	0.13 ± 0.01	94.22 ± 0.44
Silicon	7.38	0.27 ± 0.01	96.34 ± 0.14
Nitrate	87.83	8.16 ± 0.13	90.71 ± 0.15

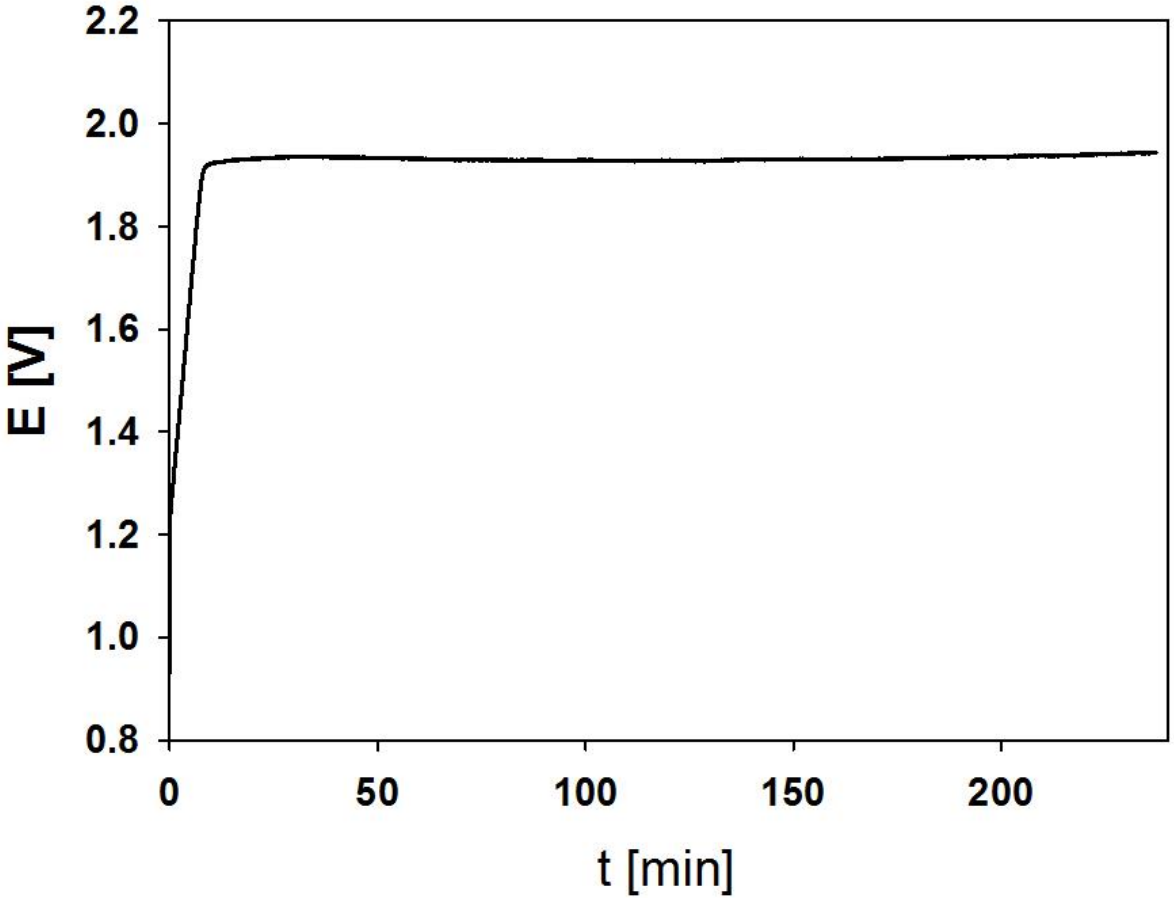

Fig. 4.6. Voltage-time curve of the EDI cell at the applied current 19.0 mA for 4 hours.

four times. The results indicated that following four hours of operation, the EDI system had the capacity to effectively reduce the nitrate concentration below the allowable 50 ppm level. Simultaneously, it was possible to remove the hardness ions to a very low level. Fig. 4.6 displays the EDI cell voltage of the groundwater treatment over four hours, demonstrating that the energy consumption remained stable, which was nearly constant and fairly low at about 1.9 V. Overall, the proposed EDI system in this study exhibited excellent efficiency and low energy consumption for the separation of nitrate and hardness ions, demonstrating that it could be successfully applied in practice.

4.4 Conclusions

In summary, the experiments performed in this study demonstrated that an EDI system is capable of greatly decreasing nitrate content of groundwater, while removing hardness ions. UV-Vis spectroscopy was employed to quantify the concentration of nitrate, while the ICP-AES was used to monitor the concentration of hardness ions. The limiting current was systemically investigated by measuring the current - voltage relationship, and determined to be 19.0 mA. Additionally, a range of operational variables, including the applied current, water flow rate, and mixed resin ratios, were investigated and the optimal experimental parameters were determined. As relates to the continuous separation and recovery of nitrate and hardness ions, high removal rates of NO_3^- (96.25%), Ca^{2+} (96.69%), and Mg^{2+} (96.13%) were achieved, and ions were concentrated in the anionic and cationic compartments. Moreover, the efficient removal rate and low energy consumption in the treatment of actual samples makes the EDI process very promising for a wide range of practical applications.

References

[1] Canter, L. W. *Nitrates in groundwater*, *CRC press*. **1996**.

[2] Park, H. I.; Kun kim, D.; Choi, Y. J.; Pak, D. *Process Biochem*. **2005**, *40*, 3383.

[3] Mikusˇka, P.; Vecˇerˇa, Z. *Anal. Chim. Acta.* **2003**, *495*, 225.

[4] White, P.; Ruble, C. L.; Lane, M. E. *Environ. Monitor. Assess.* **2013**, *185*, 643.

[5] Van der Hoek, J. P. *Environ. Technol.* **1987**, *2*, 593.

[6] Mateju, V.; Cizinska, S.; Krejci, J.; Tomas, J. *Enzyme. Microb. Techonol.***1992**, *14*, 170.

[7] Elmidaoui, A.; Menkouchi Sahli, M. A.; Tahaiki, M.; Chay, L.; Taky, M.; Elmghari, M.; Hafsi, M. *Desalination*. **2002**, *153*, 389.

[8] Golder, A. K.; Chanda, A. K.; Samanta, A. N.; Ray, S. *Sep. Purif. Technol.* **2011**, *76*, 345.

[9] Schoeman, J. J.; Steyn, A. *Desalination.* **2003**, *155*, 15.

[10] Bailey, D. A.; Jones, K. *W.P.C.* **1974**, *73*, 353.

[11] Boumediene, M; Achour, D. *Desalination.* **2004**, *168*, 187.

[12] Basha, C. A.; Ramanathan, K.; Rajkumar, R.; Mahalakshmi, M.; Kumar, P. S. *Ind. Eng. Chem. Res.* **2008**, *47*, 2279.

[13] Reddy, K. R.; Cameselle, C. *Electrochemical remediation technologies for polluted soils, sediments and groundwater*. **2009**.

[14] Kabay, N.; Yüksel, M.; Samatya, S.; Arar, Ö.; Yüksel, Ü. *Sep. Sci. Technol*. **2007**, *42,* 2615.

[15] Elmidaoui, A.; Elhannouni, F.; Sahli, M. M.; Chay, L.; Elabbassi, H.; Hafsi, M.; Largeteau, D. *Desalination*. **2001**, *136*, 325.

[16] Alvarado, L.; Chen, A. C. *Electrochim. Acta.* **2014**, *132*, 583.

[17] Lüdtke, K.; Peinemann, K. V.; Kasche, V.; Behling, R. D. *J. Membr. Sci*. **1998**, *151*, 3.

[18] Kapoor, A.; Viraraghavan, T. *J. Environ. Eng*. **1997**, *123*, 371.

[19] Coca, M.; Mato, S.; Gonzalez-Benito, G.; Urueña, M. A.; Garcia-Cubero, M. T. *J. Food Eng.* **2010**, *97*, 569.

[20] Nataraj, S. K.; Hosamani, K. M.; Aminabhavi, T. M. *J. Appl. Polym. Sci.* **2006**, *99*, 1788.

[21] Alvarado, L.; Torres, I. R.; Chen, A. C. *Sep. Purif. Technol.* **2013**, *105*, 55.

[22] Arar, Ö.; Yüksel, Ü.; Kabay, N.; Yüksel, M. *Desalination.* **2014**, *342*, 16.

[23] Zhang, Z. Y.; Liba, D.; Alvarado, L.; Chen, A. C. *Sep. Purif. Technol.* **2014**, *137*, 86.

[24] Bi, J.; Peng, C.; Xu, H.; Ahmed, A. S. *Desalin. Water Treat*. **2011**, *34*, 394.

[25] Meng, H.; Peng, C.; Song, S.; Deng, D. *Surf. Rev. Lett.* **2004**, *11*, 599.

[26] Mahmoud, A.; Hoadley, A. F. A. *Water Res.* **2012**, *46*, 3364.

[27] Walters, W. R.; Weiser, D. W.; Marek, L. J. *Ind. Eng. Chem*. **1955**, *47*, 61.

[28] Glueckauf, E. *British Chem. Eng*. **1959**, *4*, 646.

[29] Arar, Ö.; Yüksel, Ü.; Kabay, N.; Yüksel, M. *Desalination.* **2011**, *277*, 296.

[30] Strathmann, H. *Ion-exchange membrane separation processes (Vol. 9). Elsevier*. **2004**.

[31] Bouhidel, K. E.; Lakehal, A. *Desalination.* **2006**, *193*, 411.

[32] Liang, L.; Wang, L. *Semiconductor Pure Water and Chemicals Conference, Monterey, Calif.* **2001**.

[33] Rozhdestvenska, L. M.; Dzyazko, Y. S.; Belyakov, V. N. *Desalination.* **2006**, *198*, 247

[34] Hu, J. Fang, Z. Jiang, X. Li, T. Chen X. *Sep. Purif. Technol.* **2015**, *144*, 90.

[35] Peng, C. Jin, R. Li, G. Li, F. Gu, Q. *Sep. Purif. Technol.* **2014**, *136*, 42.

[36] Shen, X. Li, T. Jiang, X. Chen, X. *Sep. Purif. Technol.* **2014**, *128*, 39.

[37] Meyer, N.; Parker, W. J.; Van Geel, P. J.; Adiga, M. *Desalination*. **2005**, *175*, 153.

[38] Meyer, N.; Parker, W. J.; Van Geel, P. J.; Adiga, M. *Desalination*. **2005**, *175*, 167.

[39] Chen, A. C.; Miller, B. *J. Phys. Chem. B,* **2004**, *108*, 2245.

[40] Asmussen, R. M.; Tian, M.; Chen, A. C. *Environ. Sci. Technol.* **2009**, *43*, 5100.

[41] Tian, M.; Wen, J. L; MacDonald, D.; Asmussen, R. M.; Chen, A. C. *Electrochem. Commun.* **2010**, *12*, 527.

[42] Martí-Calatayud, M. C.; García-Gabaldón, M.; Pérez-Herranz, V.; Ortega, E. *J. Membr. Sci.* **2011**, *379*, 449.

[43] Ganzi, G. C.; Egozy, Y.; Giuffrida, A. J.; Jha. A. D. *Ultrapure Water*. **1987**, *4*, 43.

[44] Ganzi, G. C.; Jha, A. D.; DiMascio, F.; Wood. J. H. *Ultrapure Water*. **1997**, *14*, 64.

[45] Wood, J.; Arba, J.; Shaw, M. *Desalination.* **2010**, *250*, 973.

Chapter 5 The electrochemical reduced nanoporous TiO_2 electrode for the determination of chemical oxygen demand

5.1 Introduction

The environmental monitoring of organic pollution in water (e.g., industrial wastewater, lakes and rivers) is undoubtedly critical for the assessment of water quality. The amount of organic compounds in wastewater is generally evaluated via a chemical oxygen demand (COD), biological oxygen demand (BOD), and total organic carbon (TOC) tests. Of these three tests, BOD measurements are not suitable for heavily polluted water bodies, while TOC measurements often require expensive analyzers. Consequently, COD has been extensively employed as one of the most important indicators of the organic contamination of water [1], which is defined as the demand of oxygen required for the oxidative degradation of organic compounds by potent oxidizing agents (e.g., dichromate, permanganate) [2]. Despite its common use, this standard method has several inherent drawbacks [3, 4], encompassing a time-consuming process (2 - 4 hours), the requirement for expensive (Ag_2SO_4), highly corrosive (concentrated H_2SO_4) and toxic ($Cr_2O_7^-$) chemicals, and the incomplete oxidation of volatile compounds. Because of these limitations, the conventional COD method is difficult to implement for the rapid, inexpensive, on-site evaluation of organic water pollution levels.

In view of the disadvantages of conventional COD methods, a great deal of effort has been invested toward the development of an alternative, such as electrochemical techniques, which show promise [5-8]. Therefore, various electrode materials, such as boron-doped diamond [9, 10], Cu/CuO [11], F-doped PbO_2 [12], RhO_3/Ti [13], and bifunctional TiO_2/Ti/TiO_2-Pt electrodes [14], have been investigated and applied in the determination of COD. Advanced

oxidation methods for COD analysis, based on either electrocatalytic or photocatalytic oxidation principles [15-19], have demonstrated advantages such as rapid response times, direct acquisition of analytical signals, low cost, and ease of incorporation into online monitoring, when compared with traditional COD methods. However, their pragmatic application may be limited by the fact that the electrocatalytic method is incapable of oxidizing a wide spectrum of organic compounds, while photocatalytic methods suffer from a narrow dynamic working range, due to a tendency for the recombination of photogenerated electron-hole pairs. An alternate method, referred to as photoelectrocatalysis [20-23], overcomes insufficient oxidation capabilities and reduces the propensity for photogenerated electron-hole recombination through the application of potential bias [24]. The principle of the photoelectrocatalytic process is built on the fact that photogenerated holes and electrons participate in redox reactions with organic compounds that are present in solution. When the appropriate electrode is illuminated with UV light, decomposed substances release electrons that transfer to the working electrode, which generate an analytical signal. Subsequently, an electrochemical workstation is applied to record current variations, resulting in the quantification of COD values.

In recent years, TiO_2-based photoelectrocatalytic sensing techniques have quickly become a research focus for environmental monitoring and protection [25], due to their strong capacity for the oxidization of organic compounds under UV illumination. Among the various COD measurement techniques, electrodes comprised of TiO_2 stand out as the most promising, due to their super oxidizing abilities under UV illumination, as well as high stability, low cost, non-toxicity, chemical inertness, and environmental tolerance [26-30]. Nevertheless, as photogenerated electron-hole pairs in discrete TiO_2 nanoparticles and coated

nanofilms readily recombine (resulting in low sensitivity and poor catalytic efficiency); improvements are still required in terms of photoelectrocatalytic activity and stability [31, 32].

In the present work, highly ordered nanoporous TiO_2 electrodes were directly grown on a Ti substrate via a three-step anodization process, and subsequently treated by electrochemical (EC) reduction. The as-prepared and the electrochemically reduced nanoporous TiO_2 electrodes were characterized utilizing a series of material characterization and electrochemical techniques, such as field-emission scanning electron microscopy (FE-SEM), energy dispersive spectroscopy (EDS), X-ray diffraction (XRD), X-ray photoelectron spectroscopy (XPS), cyclic voltammetry (CV), linear voltammetry (LV) and chronoamperometry, to investigate their morphology, composition, structure, and electrochemical activity. Our study indicated that photoelectrocatalytic activity associated with the oxidation of various organic compounds was significantly enhanced on the reduced nanoporous TiO_2 electrodes. Moreover, the optimal applied potential was determined in a three-electrode photoelectrochemical cell. Under the optimized experimental conditions, reduced nanoporous TiO_2 electrodes were employed to measure the COD concentration of numerous synthetic and actual samples by the photoelectrocatalytic method, where the relationship between the theoretical and measured COD analytical signal values was experimentally validated. In comparison with other electrode materials, the reduced nanoporous TiO_2 electrodes not only reduced analysis times, but also lowered the cost of the electrode materials. Further, the combination of photoelectrocatalytic methods for the measurement of COD, in conjunction with the reduced nanoporous TiO_2 electrodes promoted

the development of an inexpensive, real time, on-site, environmentally compatible COD analysis testing system.

5.2 Experimental

5.2.1 Materials and reagents

Five organic compounds were selected in the preparation of standard samples with known COD values: D-glucose, potassium hydrogen phthalate (KHP), lactic acid, phenol, and acetic acid, and all reagents were purchased from Sigma-Aldrich. The actual test samples were collected from local industrial sites and ambient lake water. When necessary, both synthetic and actual samples were diluted to appropriate concentrations prior to analysis. All other utilized chemicals were of analytical grade and used as received. Titanium plates (99.2%) were purchased from Alfa Aesar. The water used in the preparation of all solutions was purified by a Nanopure® Diamond Water System (18.2 MΩ cm).

5.2.2 Preparation and characterization of reduced nanoporous TiO_2 electrodes

5.2.2.1 Fabrication of nanoporous TiO_2 electrodes

Highly uniform nanoporous TiO_2 were grown directly on titanium plates utilizing a three-step anodic oxidation process. Briefly, pure titanium plates were initially sonicated in acetone for 15 min, rinsed with pure water, and then etched in an 18% HCl solution at 85 ^oC for 10 min. Subsequently, in the first step, the etched titanium plates were anodized in a one-compartment, two-electrode (titanium plate anode and platinum mesh cathode) cell in a solution containing ethylene glycol, 0.3 wt.% NH_4F, and 2 wt.% H_2O at 50 V for five hours.

Afterward, the roughly surface grown nanoporous TiO_2 layer was removed via masking tape, and the same titanium plate was treated by a second-step anodization at the same voltage for another two hours. For the third step, the fabricated nanoporous layer was again peeled with masking tape after which the titanium plate was anodized at 50 V for 15 min. Finally, a highly self-organized nanoporous TiO_2 was achieved. As an anatase TiO_2 structure is known to be the most efficient for photoelectrocatalysis [33, 34], the fabricated nanoporous TiO_2 electrodes subsequently underwent thermal treatment at 450 °C for three hours.

5.2.2.2 Electrochemical reduction of nanoporous TiO_2

In order to enhance the photoelectrocatalytic activity of the nanoporous TiO_2 electrodes, a three-electrode cell system was employed for the electrochemical reduction treatment. A Pt coil with a 10 cm^2 surface area was utilized as the auxiliary electrode, whereas an Ag/AgCl electrode was used as the reference electrode. Our previous studies have shown that the optimal conditions for the electrochemical reduction treatment of nanoporous TiO_2 electrodes requires their immersion in a 0.1 M H_2SO_4 solution at a cathodic current density of -5 mA cm^{-2} for 10 min [35]. The experiments were carried out at room temperature (20 ± 2 °C) and the solution in the electrochemical cell system was bubbled with argon throughout the process.

5.2.2.3 Characterization of the synthesized reduced nanoporous TiO_2 electrodes

The surface morphology of the synthesized reduced nanoporous TiO_2 electrode was observed using SEM (JEOL, Model 5900LV). The surface composition was characterized by

EDS (Oxford Links ISIS). The X-ray diffraction spectra of the electrode were performed with a Philips PW 1050-3710 diffractometer under Cu Ka radiation.

5.2.3 Electrochemical and photoelectrochemical measurements

Electrochemical and photoelectrochemical experiments (e.g., cyclic voltammetry (CV), linear voltammetry (LV) and chronoamperometry), were performed at room temperature in a three-electrode cell that was interfaced with an electrochemical workstation (PGZ301 Universal Potentiostat). The electrochemically reduced nanoporous TiO_2 electrode was employed as the working electrode (1.25 cm × 0.8 cm × 0.5 mm). A platinum coil with a 10 cm^2 surface area and an Ag/AgCl (saturated KCl) electrode were utilized as the counter and reference electrodes, respectively. The UV illumination source was a CureSpot 50 (ADAC systems), which was equipped with a Hg lamp with a measured light irradiance of 2.0 mW cm^{-2}. A rubber lid with an appropriate opening, in order to physically secure the light source and guide the light onto the surface of the nanoporous TiO_2 electrode, was employed for the electrochemical cell.

5.2.4 Photoelectrocatalytic measurement for COD determination

The photoelectrocatalytic measurements of COD were carried out in a custom lab-made, three-electrode cell reactor, containing 5 mL of 0.1 M Na_2SO_4 (pH 7.9), and stirred by a magnetic stirrer. When a proper potential bias was applied, chronoamperometry was employed to record the corresponding increase in current which was the result of the photoelectrocatalytic degradation of organic compounds. Because the photocurrent generated during this process is proportional to the substrate concentration [36], by measuring current

variations in association with organic concentrations, changes in current could be easily converted into equivalent COD values.

5.3 Results and discussion

5.3.1 Surface characterization of the reduced nanoporous TiO_2 electrodes

The morphologies and compositions of the reduced nanoporous TiO_2 electrodes were examined by scanning electron microscopy (SEM) and energy dispersive X-ray spectroscopy (EDS). The crystallographic structures of the synthesized electrodes were identified using X-ray diffraction (XRD). Figure 5.1A depicts a typical SEM image of the reduced nanoporous TiO_2 surface. It is apparent that the nanoporous structures are highly ordered and well aligned, with a uniform outer pore diameter of ~150 nm, inclusive of two to three inner pores with diameters of approximately 50 nm. Since these nanopores were directly grown from a Ti substrate, the junctions between the nanopores and the substrate was very strong; both the inner and outer surfaces of the nanopores were exposed to the electrolyte. This structural arrangement decreased the diffusion length and thus expedited the separation of photogenerated electron/hole pairs. Moreover, the nanoporous structure at the surface increased the lumens of the pores that were exposed at the top of the layer, which served to enhance photoelectrocatalytic activity. Figure 5.1B shows the EDS spectrum of the reduced nanoporous TiO_2, where only strong O and Ti peaks with a ratio of 2:1 were displayed, showing the formation of TiO_2 nanoporous arrays. Figure 5.1C depicts the XRD patterns of the nanoporous TiO_2 prior to, and following EC reduction. The peaks marked with asterisks were derived from the Ti substrate; all other diffraction peaks were attributed to those of the tetragonal anatase TiO_2 phase, indicating the formation of the anatase structure [37, 38] subsequent to annealing,

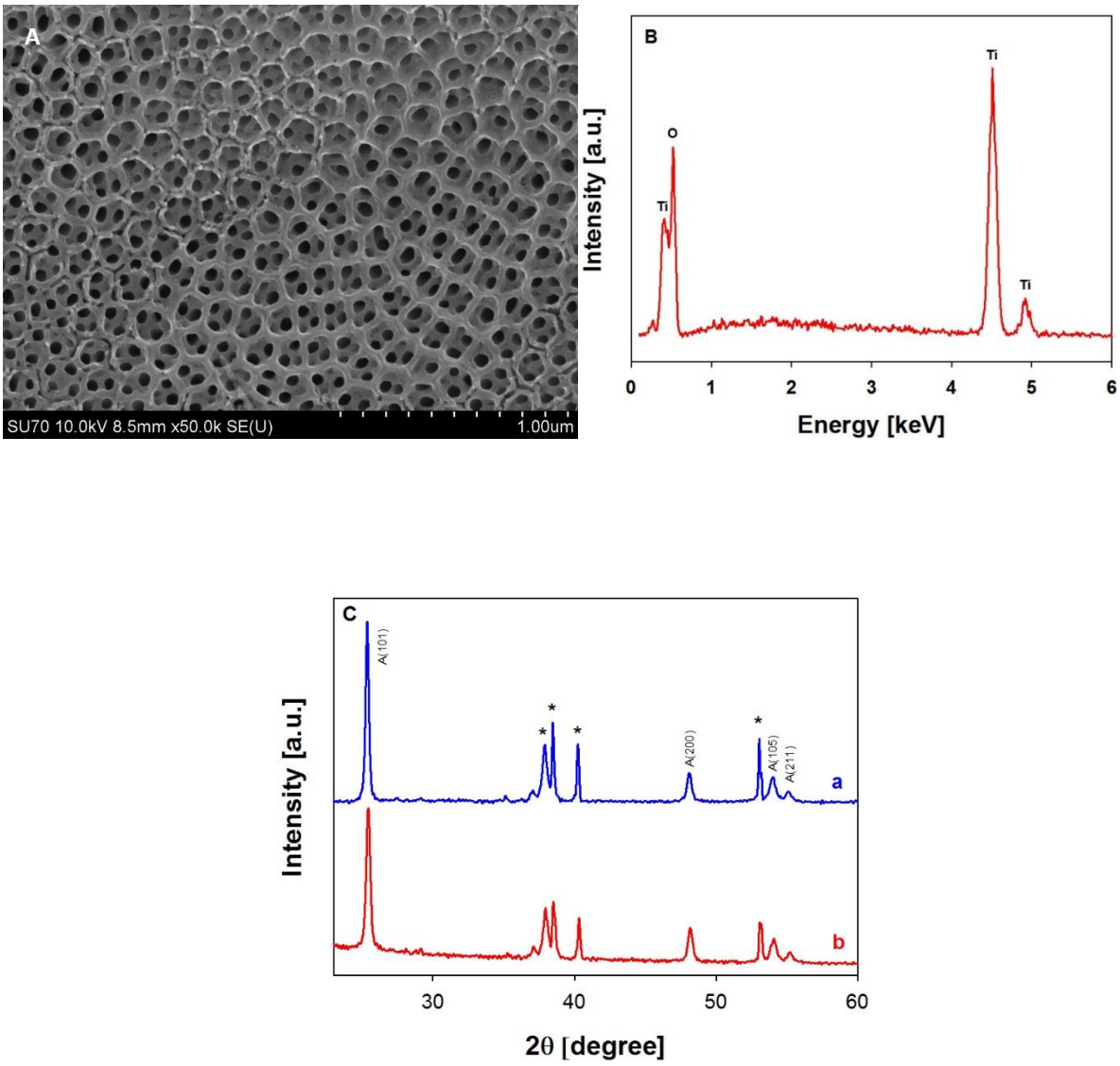

Figure 5.1. (A) SEM image, (B) EDS spectrum and (C) XRD patterns of the (a) reduced and (b) non-reduced nanoporous TiO_2 electrodes

which resulted in higher photocatalytic activity [39]. In addition, no crystalline structural changes were observed during the EC treatment, as the XRD spectra of nanoporous TiO_2 were virtually identical prior to (red), and following (blue) the EC reduction.

5.3.2 Photoelectrochemical behavior of the reduced nanoporous TiO_2 electrodes

Figure 5.2A presents the cyclic voltammograms (CVs) of the nanoporous TiO_2 electrode prior to (red line), and following (blue line) the EC reduction recorded in a 0.1 M H_2SO_4 solution at a potential scan rate of 20 mV s^{-1}. As relates to the nanoporous TiO_2 electrode prior to the EC treatment, the CV observed was between 0 and 0.4 V vs. Ag/AgCl in the cathodic and anodic scans corresponded to hydrogen adsorption and desorption, respectively, while the double-layer charging phenomenon took place at between 0.4 and 1.5 V. The current was significantly increased, following the EC reduction, under an applied current density -5 mA cm^{-2} for 10 min as shown via the blue curve in Figure 5.2A. An almost rectangular CV was observed; particularly, the current for double-layer charging was dramatically increased. Figure 5.2B depicts the CVs following exposure to UV irradiation under identical experimental conditions. The photoelectrocurrent of both the untreated nanoporous TiO_2 (red curve) and the electrochemically reduced nanoporous TiO_2 (blue curve) electrodes increased linearly along with increases in applied potentials, due to the decrease of the recombination of the photogenerated electrons and holes [40]. At a potential of 1.5 V, the photoelectrocurrent of the reduced nanoporous TiO_2 attained 29 mA cm^{-2}, while the electrode without the EC treatment was only 9.5 mA cm^{-2}.

Figure 5.3 presents the photocurrent response of the reduced and non-reduced nanoporous TiO_2 electrodes at an applied electrode potential of 1 V in a 0.1 M Na_2SO_4 solution. In regard

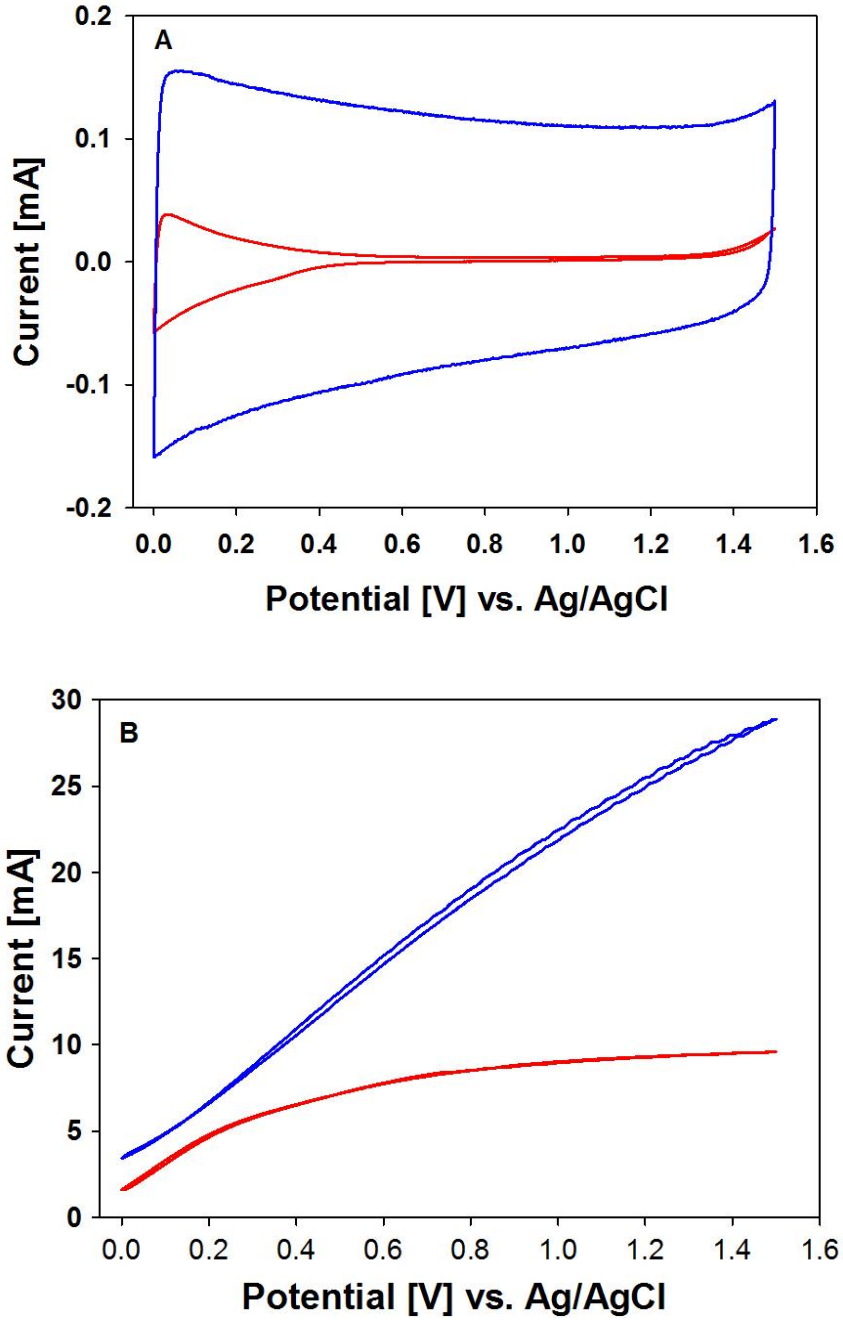

Figure 5.2. Cyclic voltammograms of the nanoporous TiO_2 (red curve) and reduced nanoporous TiO_2 (blue curve) electrodes in 0.1 M H_2SO_2 at a potential scan rate of 20 mV s^{-1} without (A) and with (B) UV irradiation.

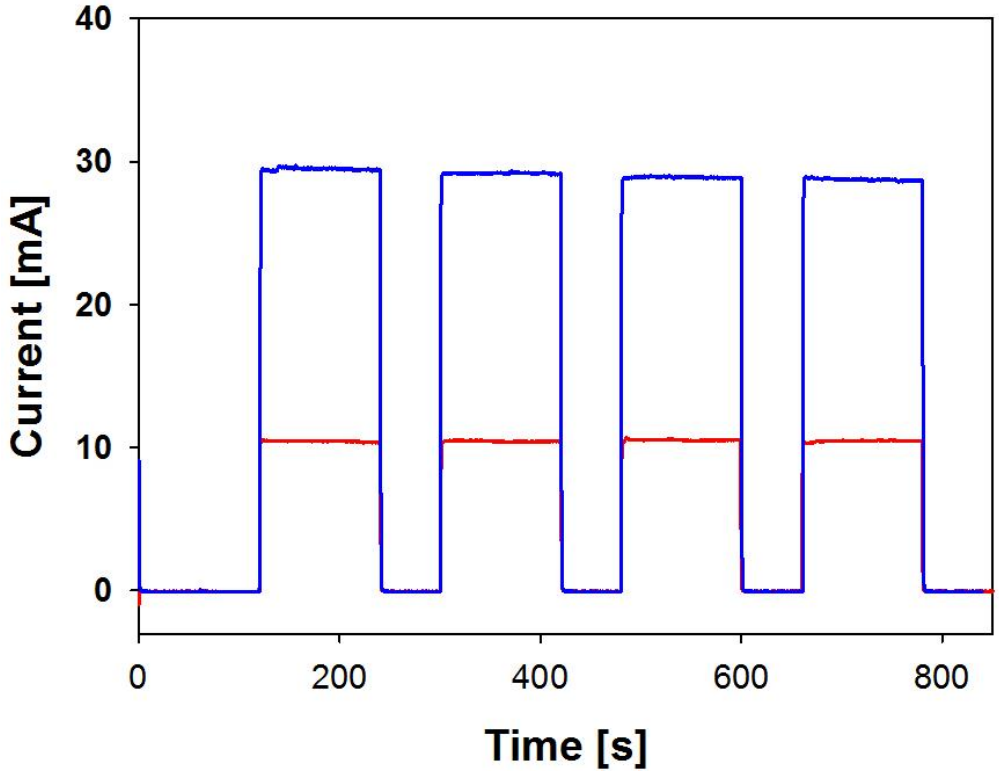

Figure 5.3. Photocurrent responses of the non-reduced (red line) and reduced (blue line) nanoporous TiO_2 electrodes under UV illumination at an applied potential of 1 V vs. Ag/AgCl in 0.1 M Na_2SO_4.

to the non-reduced nanoporous TiO_2 electrode, the photocurrent density was measured to be 0.1 mA cm^{-2} in the absence of UV light, while it was 10.5 mA cm^{-2} under UV illumination. As seen from the baseline, the electrochemical current density was also low (~0.1 mA cm^{-2}) for the reduced nanoporous TiO_2 electrode without UV irradiation; however, a significant instantaneous generation of photocurrent (30 mA cm^{-2}) arose when the electrode was illuminated under low intensity (2.0 mW cm^{-2}) UV light. The photocurrent remained constant when the UV-visible light was switched on, which quickly fell to 0.1 mA cm^{-2} once switched off, indicating the rapid response of the reduced nanoporous TiO_2 electrode to UV light. To investigate the oxidation current response for the degradation of organic matter under the applied potentials, with and without UV irradiation, Figure 5.4A and 5.4B present the linear voltammograms (LVs) of the reduced nanoporous TiO_2 electrodes recorded in 0.1 M Na_2SO_4 solution containing 2 mM glucose at a scan rate of 20 mV s^{-1} without or under the UV illumination, respectively. As can be seen, there was practically no oxidation current response upon the addition of glucose in the absence of UV light (Figure 5.4A), whereas an oxidation current was generated, apparently during the photoelectrocatalytic degradation of the added glucose in the presence of UV light (Figure 5.4B).

The considerably enhanced photoelectrocatalytic activity of the reduced nanoporous TiO_2 electrodes could be attributed to the contributions of two aspects: nanoporous structure and electrochemical reduction treatment. The nanopore arrays serve to significantly enlarge the available surface area, thus increasing the lumen diameters on exposure to UV illumination. Additionally, the method by which the nanoporous TiO_2 electrode was fabricated enabled the nanopores to grow directly from the Ti substrate, which strengthened the interfacial bonds between the nanopores and substrate. In photoelectrocatalytic applications, the diffusion length

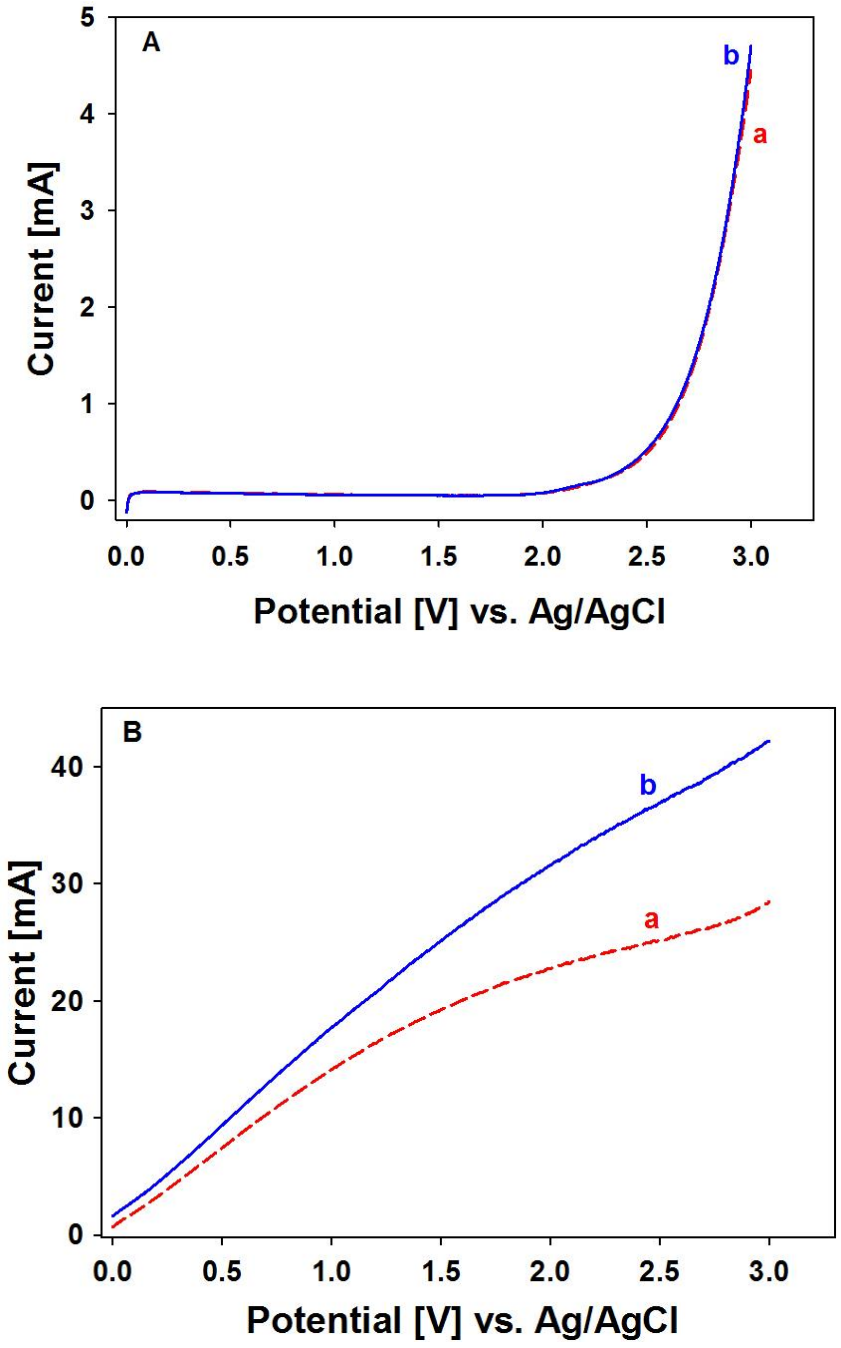

Figure 5.4. Linear voltammograms of (a) 0.1 M Na_2SO_4 and (b) 2 mM glucose in 0.1 M Na_2SO_4 using the reduced nanoporous TiO_2 electrode at a potential scan rate of 20 mV s^{-1} without (A) and with (B) UV irradiation.

was significantly decreased because of the nanoporous structure. Hence, the photoelectrocatalytic properties of the nanoporous TiO_2 electrode were enhanced by facilitating the rapid transport of photoelectrons to the substrate, which expedited the separation of photogenerated electron/hole pairs. The high photoelectrocatalytic activity and stability of the reduced nanoporous TiO_2 electrodes by the EC treatment might be attributed to the increase of Ti^{2+} and Ti^{3+}, as well as the decrease of Ti^{4+} in the nanoporous TiO_2 electrodes during the electrochemical reduction process. Additionally, the increase in oxygen vacancies and the improvement of donor densities might have further enhanced the activity of the reduced nanoporous TiO_2 electrodes [35].

5.3.3 Reaction mechanism and detection principle of the reduced nanoporous TiO_2 electrodes in the determination of COD

In principle, the current generated during the photoelectrocatalytic degradation of organics is proportional to the substrate concentration. It is well-known that when UV illumination is applied, the free photoelectrons in the conduction band and free photoholes in the valence band that are generated from the reduced nanoporous TiO_2 electrode (Eq. 5.1) participate in redox reactions with the organic substances that are present in solution. Photoholes possess strong oxidative capacities (E_g = +3.2 eV), which can mineralize most organic compounds, as shown in Eq. 5.2 [41, 42]. In addition, the photoholes may oxidize the water that is adsorbed on the surface of the reduced nanoporous TiO_2 electrode to create very powerful and non-selectively oxidizing hydroxyl radical agents (Eq. 5.3) [43]. Hydroxyl radicals might also oxidize organic pollutants (see Eq. 5.4) to the point of complete mineralization (i.e., CO_2, water and inorganics) [44]. These reactions are represented as follows:

$$TiO_2 + hv \rightarrow h^+ + e^- \quad (5.1)$$

$$h^+ + R \rightarrow R^{\cdot} \quad (5.2)$$

$$TiO_2 + h^+ + H_2O \rightarrow TiO_2(^{\cdot}OH) + H^+ \quad (5.3)$$

$$TiO_2(^{\cdot}OH) + R \rightarrow TiO_2 + R^{\cdot} + H^+ + e^- \quad (5.4)$$

In a three-electrode system, decomposed organic substances release electrons that were transferred to the reduced nanoporous TiO_2 electrode, and the electrons could appear in the form of current, which is recorded by an electrochemical workstation. Thus, the increase in organic compound concentrations will result in an increase of photoelectrocurrent.

In general, the mineralization (degradation) of organic compounds on the reduced nanoporous TiO_2 electrodes may be summarized as follows:

$$C_aH_bO_cN_dX_g + (2a - c)H_2O \rightarrow aCO_2 + gX^- + dNH_3 + (4a - 2c + b - 3d)H^+ + (4a - 2c + b - 3d - g)e^- \quad (5.5)$$

where X represents a halogen atom and a, b, c, d and g represent the stoichiometric ratio of carbon, hydrogen, oxygen, nitrogen, and halogen in organic compounds, respectively. In a typical photoelectrocatalytic process, Faraday's law can be applied to quantify the concentration by measuring the charge that is passed if the current produced is the result of the photoelectrochemical degradation of organics, which is:

$$Q = \int i\, dt = nFvc \quad (5.6)$$

where i is the current derived from the oxidation of organic matter; n is the number of electrons transferred during the organic substances degradation (relationship n = 4a – 2c + b – 3d – g can be obtained from Eq. 5.5); F is the Faraday constant (96485 C mol^{-1}); v refers to the sample volume while c refers to the concentration of organic compounds. Since one oxygen molecule corresponds to the transference of four electrons:

$$O_2 + 4H^+ + 4e^- \rightarrow 2H_2O \qquad (5.7)$$

according to the COD definition, the equation 5.6 could be converted to a COD value as:

$$\text{COD [mg L}^{-1}\text{ O}_2\text{]} = (Q/\,4Fv) \times 32000 \qquad (5.8)$$

where F is the Faraday constant, and v is the volume of the solution, which is also a constant for a given reactor. It is known that the current generated during the photoelectrocatalytic degradation of organic matter changes proportionally with the concentration of the reactants or COD values.

In order to screen for an appropriate operating potential for the COD measurement, chronoamperometric experiments were performed by injecting 5 μmol glucose into 5 mL of a 0.1 M Na_2SO_4 solution, under UV irradiation, different applied potentials, and stirring. Figure 5.5 reveals that at a constant electrode potential of +1.0 V vs Ag/AgCl, the current response observed was not as clear as that at an applied potential of +1.5 V vs Ag/AgCl, following the addition of the glucose solution. At potentials above +1.5 V vs Ag/AgCl, the current was not stable due to the great disturbance of the oxygen evolution reaction. Considering that both sensitive responses and stable signals are indispensable for precise analysis, an applied potential +1.5 V vs Ag/AgCl was selected for the determination of COD via photoelectrocatalytic processes with the reduced nanoporous TiO_2 electrodes.

5.3.4 Analysis of synthetic and real samples

To validate the proposed methodology a wide range of organic compounds were studied, including glucose, potassium hydrogen phthalate (KHP), lactic acid, phenol and acetic acid. By recording the current increases that were generated through the addition of

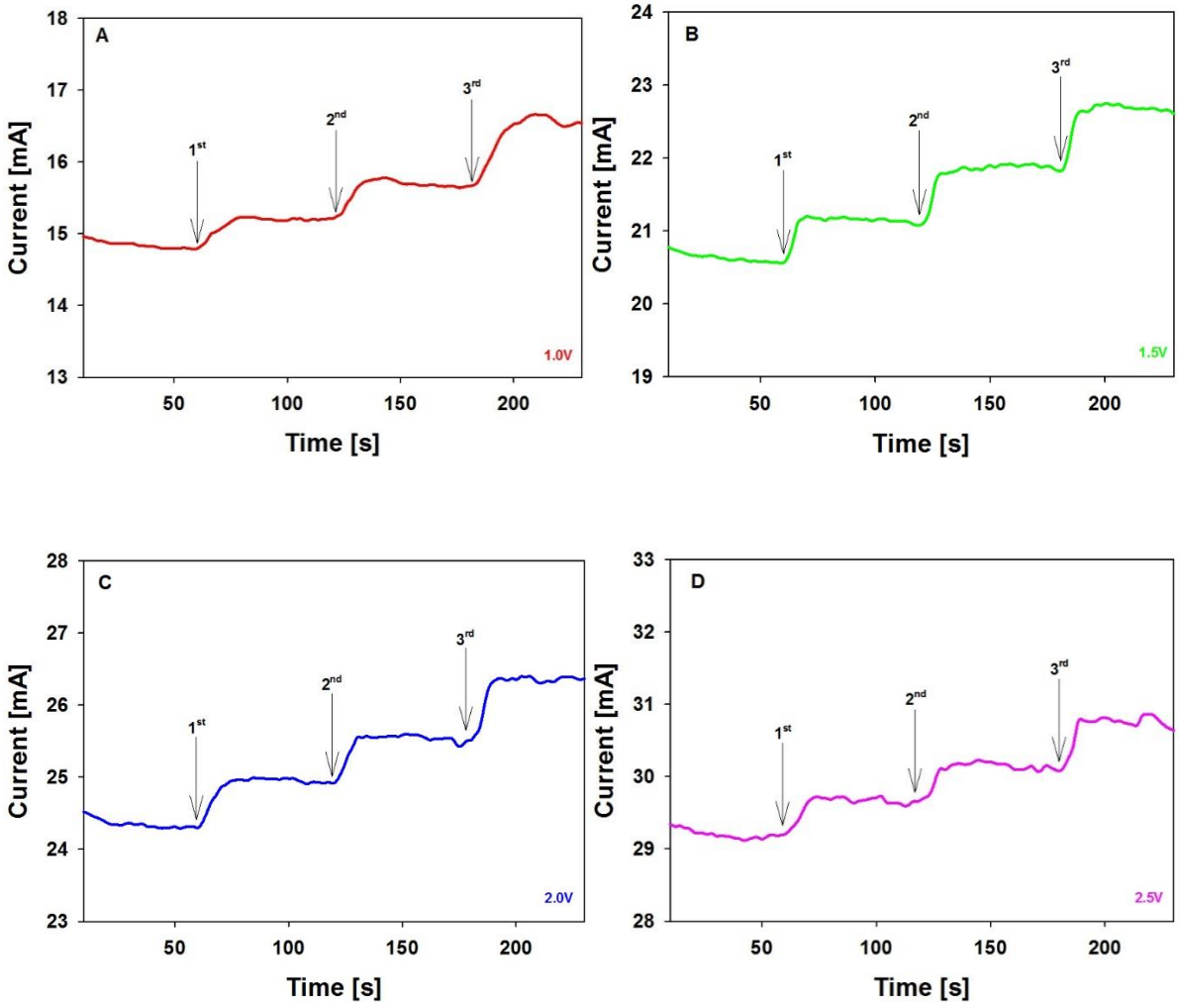

Figure 5.5. Anodic current responses to the injection of glucose samples in the stirred 0.1 M Na_2SO_4 with the reduced nanoporous TiO_2 electrode. Different potentials (A) 1.0 V (B) 1.5 V (C) 2.0 V (D) 2.5 V were applied. The initial solution volume was 5 mL and 5 µmol glucose was injected at each step indicated by an arrow (60 s, 120 s, 180 s).

organic compounds in chronoamperometric experiments, and converting the molar concentrations of individual organic compounds into equivalent theoretical COD concentrations, the relationships between the net current increases (ΔI) and the theoretical COD values (ThCOD) were elucidated (Figure 5.6). As can be seen, during the degradation of various organics in the photoelectrochemical cell using the reduced nanoporous TiO_2 electrode at an applied potential of +1.5 V vs Ag/AgCl, under the constant 2.0 mW cm^{-2} UV illumination, the net current for all organic compounds investigated were well fitted into the linear line $y = 3.8458x$, with $R^2 = 0.9928$, which validated the proposed analytical principle. The results also demonstrated that the COD measurements via the reduced nanoporous TiO_2 electrode were virtually independent of the type of organic species employed. Furthermore, a linear range, from 20 mg L^{-1} to 250 mg L^{-1} COD, and a low detection limit of 8 mg L^{-1} COD (S/N = 3) through the proposed COD measurement method may be obtained. Subsequently, based on the calibration curve plotted in Figure 5.6, ΔI could be easily converted to the COD values of the corresponding organic compounds. The COD values obtained with the reduced nanoporous TiO_2 electrode were compared to the COD values that were determined by the conventional dichromate method. Figure 5.7 demonstrates that the COD values achieved with the dichromate method (COD_{Cr}) were practically identical with the values obtained from the proposed COD measurement technique. It was noted that the conventional COD test included multiple steps encompassing sampling, addition of oxidant reagent (i.e., potassium dichromate), hydrothermal digestion process (two-four hours), and an absorbance measurement, therefore this method is not only time consuming, but also generates secondary pollution. On the other hand, the photoelectrochemical method with the reduced nanoporous TiO_2 electrode is much faster, environmentally compatible, and simple to perform.

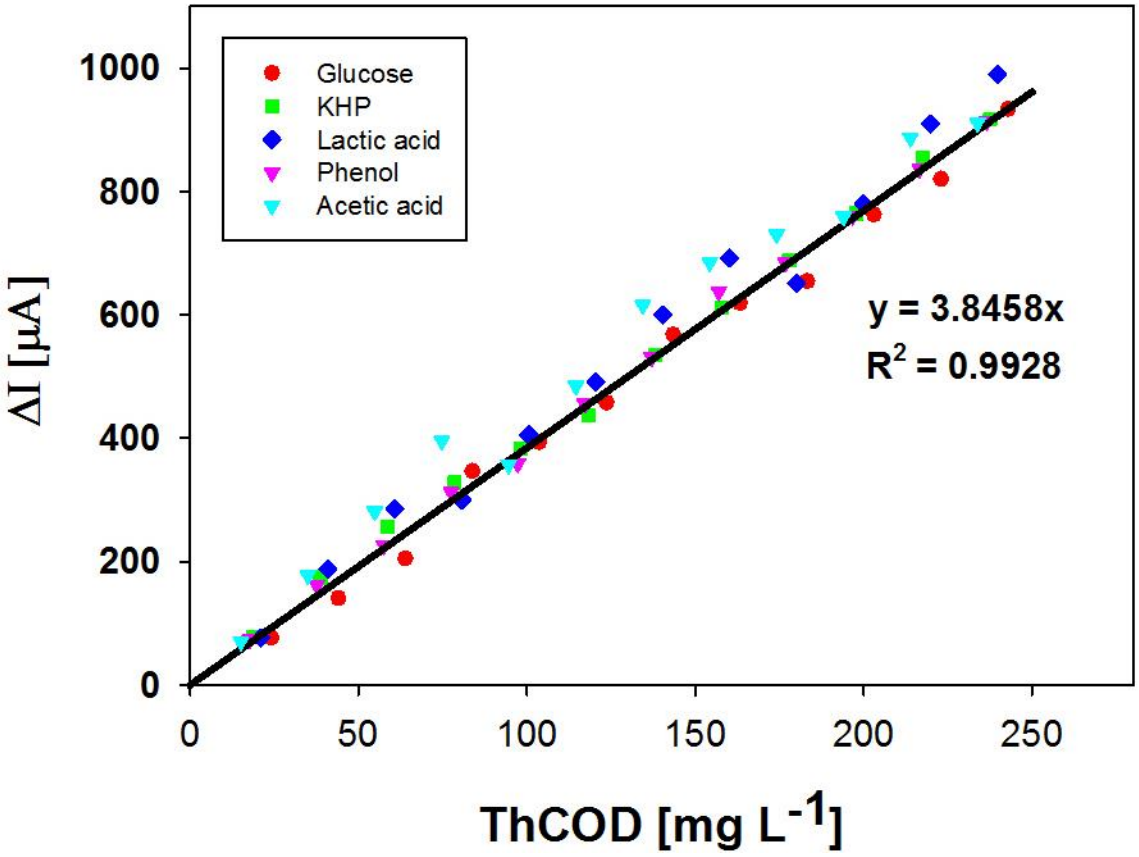

Figure 5.6. Calibration curve of the net current increase (ΔI) and theoretical COD values (ThCOD) of synthetic organic compounds including D-glucose, potassium hydrogen phthalate (KHP), lactic acid, phenol and acetic acid. Supporting electrolyte: 5 mL of 0.1 M Na_2SO_4. Applied potential: 1.5 V (vs. Ag/AgCl).

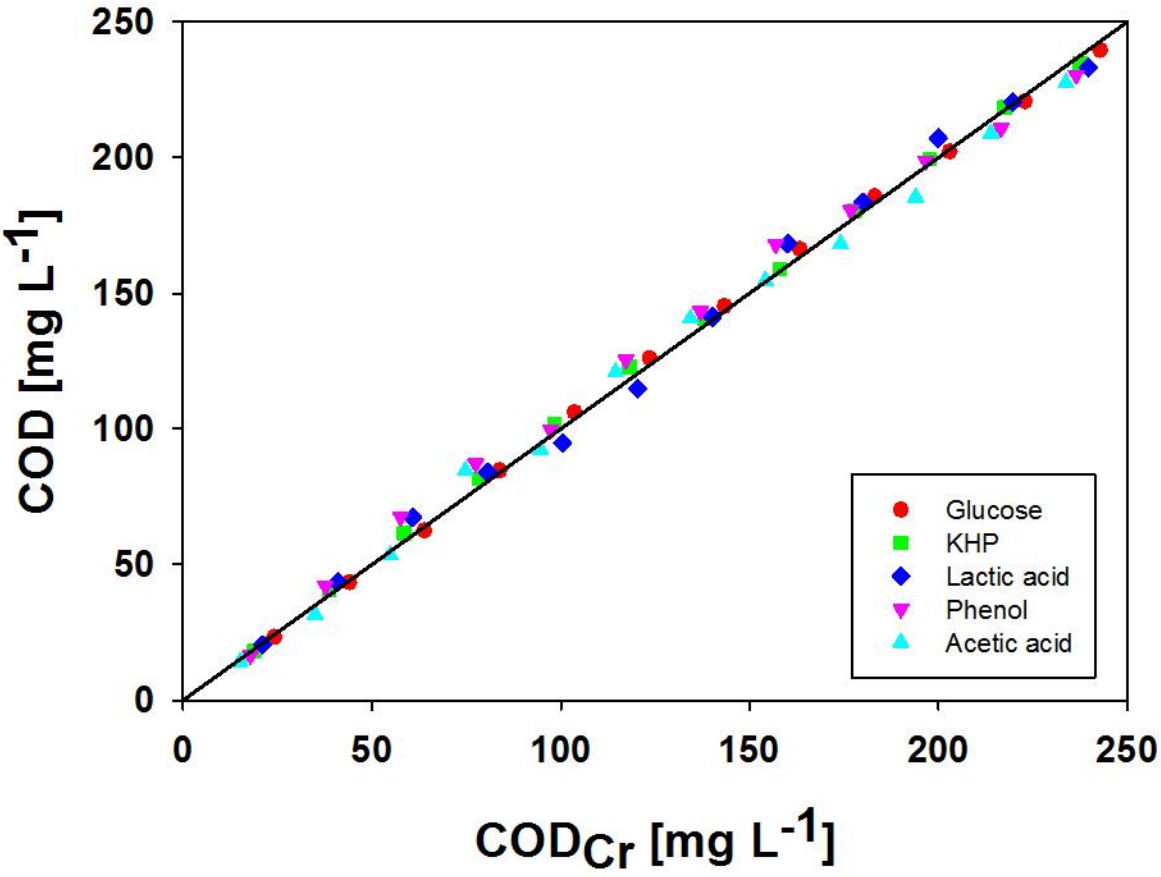

Figure 5.7. Correlation between COD values determined by the reduced nanoporous TiO_2 electrode and the corresponding values measured by the conventional dichromate method (COD_{Cr}).

Additionally, a comparison between the conventional dichromate method and the proposed method for COD measurements was evaluated using actual wastewater samples that were obtained from a local pulp and paper mill and ambient lake water. The samples were diluted to a proper concentration prior to measurements, with the results given in Table 5.1, which shows that all of the relative margins of error for the COD values acquired by these two methods were within ±7%, with relative standard deviations (RSD) of 2.3% and 4.1% for the pulp and paper mill samples, and 5.8% and 5.1% for the ambient lake water samples, respectively. These data indicated that the proposed reduced nanoporous TiO_2 electrode mediated photoelectrochemical method had strong potential for COD measurement applications with good reproducibility in practice.

Table 5.1. Comparison of COD values of real water samples obtained by the proposed method and the conventional dichromate method

Sample	$K_2Cr_2O_7$ method		Reduced nanoporous TiO_2 method		
	Mean ± SD (mg L^{-1})	RSD (%) n = 7	Mean ± SD (mg L^{-1})	RSD (%) n = 7	Relative error (%)
Pulp and paper mill					
Sample 1	1954.3 ± 57.8	3.0	2016.8 ± 63.8	2.3	3.20
Sample 2	1879.7 ± 55.4	3.8	1938.1 ± 51.3	4.1	3.11
Lake water					
Sample 1	28.4 ± 1.17	6.3	30.2 ± 1.26	5.8	6.34
Sample 2	41.5 ± 1.59	5.7	44.3 ± 1.77	5.1	6.75

5.4 Conclusions

In summary, a highly ordered self-organized nanoporous TiO_2 electrode was prepared by a three-step electrochemical anodization and was electrochemically reduced in situ. The EC reduced nanoporous TiO_2 electrode possessed a configuration that was well suited for the efficient separation of photogenerated electron/hole pairs. The electrochemical and photoelectrochemical properties of the electrode were investigated, which indicated that the reduced nanoporous TiO_2 electrode exhibited remarkable photocurrent response, and could effectively oxidize various organic compounds. The considerable enhancement in photoelectrocatalytic activity of the reduced nanoporous TiO_2 electrode was due to the nanoporous configuration, the increase of Ti(II), Ti(III), oxygen vacancies and a significant improvement in the donor density [45, 46]. As a promising material utilized for electroanalysis, the reduced nanoporous TiO_2 electrode was, for the first time, employed for COD determination in a photoelectrocatalytic reactor. In this work, the COD values of both synthetic samples and actual wastewater samples were successfully determined by applying an electrode potential +1.5 V vs Ag/AgCl at the reduced nanoporous TiO_2 electrode under UV illumination. The results also demonstrated that only one to two minutes are required to complete an assay, and that a very low detection limit of 8 mg L^{-1} may be attained. As compared with the conventional COD measurement method, the approach proposed here is performed easily, with rapid analysis, and is environmentally compatible without the discharge of secondary contaminants. All of these advantages suggest that the proposed reduced nanoporous TiO_2 electrodes might be useful in practice for the online monitoring of COD values in wastewater.

References

[1] Jones, B. M.; Sakaji, R. H.; Daughton, C. G. *Anal. Chem.* **1985**, *57*, 2334.

[2] Eaton, A. D.; Franson, M. A. H.; A. P. H. Association; Washington, DC, **2005**.

[3] Westbroek, P.; Temmerman, E. *Anal. Chim. Acta.* **2001**, *437*, 95.

[4] Zhang, S. Q.; Li, L. H.; Zhao, H. J.; Li, G. Y. *Sens. Actuators B* **2009**, *141*, 634.

[5] Ai, S.; Gao, M.; Yang, Y.; Li, J.; Jin, L. *Electroanal.* **2004**, *16*, 404.

[6] Cheng, Q.; Wu, C.; Chen, J.; Zhou, Y.; Wu, K. *J. Phys. Chem. C* **2011**, *115*, 22845.

[7] Zhou, Y.; Jing, T.; Hao, Q.; Zhou, Y.; Mei, S. *Electrochim. Acta.* **2012**, *74*, 165.

[8] Yang, J.; Chen, J.; Zhou, Y.; Wu, K. *Sens. Actuators B* **2011**, *153*, 78.

[9] Takeshi, K.; Yusuke, T.; Masaki, H.; Takeshi, W.; Tatsuo, A.; Makoto, Y.; Yasuaki, E. *Anal. Chem.* **2014**, *86,* 8066.

[10] Bogdanowicz, R.; Czupryniak, J.; Gnyba, M.; Ryl, J.; Ossowski, T.; Sobaszek, M.; Darowicki, K. *Sens. Actuators B* **2013**, *189*, 30.

[11] Silva, C. R.; Conceic¸o, C. D. C.; Bonifácio, V. G.; Filho, O. F.; Teixeira, M. F. S. *J. Solid State Electrochem.* **2009**, *13*, 665.

[12] Li, J.; Li, L.; Zheng, L.; Xian, Y.; Ai, S.; Jin, L. *Anal. Chim. Acta*. **2005**, *548*, 199.

[13] Li, J. Q.; Li, L. P.; Zheng, L.; Xian, Y. Z.; Jin, L. T. *Meas. Sci. Technol.* **2006**, *17*, 1995.

[14] Qu, X.; Tian, M.; Chen, S.; Liao, B. Q.; Chen, A. C. *Electroanal.* **2011**, *23*, 1267.

[15] Wang, H.; Zhong, S.; He, Y.; Song, G. *Sens. Actuators B* **2011**, *160*, 195.

[16] Zhang, Z.; Yuan, Y.; Fang, Y.; Liang, L.; Ding, H.; Jin, L. *Talanta.* **2007**, *73*, 523.

[17] Han, Y.; Qiu, J.; Miao, Y.; Han, J.; Zhang, S.; Zhang, H.; Zhao, H. *Anal. Methods* **2011**, *3*, 2003.

[18] Quan, X.; Yang, S. G.; Ruan, X. L.; Zhao, H. M. *Environ. Sci. Technol.* **2005**, *39*, 3770.

[19] Fierro, S.; Abe, K.; Christos, C.; Einaga, Y. *J. Electrochem. Soc.* **2011**, *158*, F183.

[20] Fang, Y. J.; Zhang, H. Z.; Yuan, Y.; Ding, H. C.; Jin, L. T. *Modern Sci. Instrum.* **2006**, *4*, 41.

[21] Liang, L. H.; Zhang, Z. H.; Yuan, Y.; Zeng, L. P.; Jin, L. T. *Chem. Sens.* **2008**, *28*, 57.

[22] Wang, C.; Wu, J. C.; Wang, P. F.; Ao, Y. H.; Hou, J.; Qian, J. *Sens. Actuators B* **2013**, *181*, 1

[23] Li, S. X.; Zheng, F .Y.; Cai, S. J.; Liang, W. J.; Li, Y. C. *Sens. Actuators B* **2013**, *188*, 280.

[24] Leng, W. H.; Zhang, Z.; Zhang, J. Q.; Cao, C. N. *J. Phys. Chem. B* **2005**, *109*, 15008.

[25] Sun, Z.; Kim, J. H.; Zhao, Y.; Bijarbooneh, F.; Malgras, V.; Lee, Y.; Kang, Y. M.; Dou, S. X. *J. Am. Chem. Soc.* **2011**, *133*, 19314.

[26] Tian, M.; Wu, G. S.; Chen, A. C. *ACS Catal.* **2012**, *2*, 425.

[27] Wu, G. S.; Nishikawa, T.; Ohtani, B.; Chen, A. C. *Chem. Mater.* **2007**, *19*, 4530.

[28] Yu, Y.; Ren, J.; Liu, D.; Meng, M. *ACS Catal.* **2014**, *4*, 934.

[29] Luan, Y.; Jing, L.; Xie, Y.; Sun, X.; Feng, Y.; Fu, H. *ACS Catal.* **2013**, *3*, 1378.

[30] Chen, A. C. *Can. J. Chem.* **2014**, *92*, 581.

[31] Qu, J.; Zhao, X. *Environ. Sci. Technol.* **2008**, *42*, 4934.

[32] Stotter, J.; Show, Y.; Wang, S.; Swain, G. *Chem. Mater.* **2005**, *17*, 4880.

[33] Gong, J. J.; Lai, Y. K.; Lin, C. J. *Electrochim. Acta.* **2010**, *55*, 4776.

[34] Ye, M. D.; Xin, X. K.; Lin, C. J.; Lin, Z. *Nano Lett.* **2011**, *11*, 3214.

[35] Chang, X.; Thind, S. S.; Chen, A. C. *ACS Catal.* **2014**, *4*, 2616.

[36] Bai, J.; Zhou, B. X. *Chem. Rev.* **2014**, *114*, 10131.

[37] Beranek, R.; Tsuchiya, H.; Sugishima, T.; Macak, J. M.; Taveira, L.; Fujimoto, S.; Kisch, H.; Schmuki, P. *Appl. Phys. Lett.* **2005**, *87*, 243114.

[38] Tian, M.; Wen, J. L.; MacDonald, D.; Asmussen, R. M.; Chen, A. C. *Electrochem. Commun.* **2010**, *87*, 527.

[39] Macak, J. M.; Zlamal, M.; Krysa, J.; Schmuki, P. *Small* **2007**, *3*, 300.

[40] Wu, G. S.; Wang, J. P.; Thomas, D. F.; Chen, A. C. *Langmuir* **2008**, *24*, 3503.

[41] Qiu, J. X.; Zhang, S. Q.; Zhao, H. J. *J. Hazard. Mater.* **2012**, *211*, 381.

[42] Bai, J.; Li, J. H.; Liu, Y. B.; Zhou, B. X. *Appl. Catal. B* **2010**, *95*, 408.

[43] Comninellis, Ch. *Electrochim. Acta.* **1994**, *39*, 1857.

[44] Konstantinou, I. K.; Albanis, T. A. *Appl. Catal. B*, **2004**, *49*, 1.

[45] Chen, X. B.; Liu, L.; Yu, P. Y.; Mao, S. S. *Science* **2011**, *331*, 746.

[46] Chang, X.; Thind, S. S.; Tian, M.; Hossain, M. M.; Chen. A. C. *Electrochim. Acta* **2015**, *173*, 728.

Chapter 6 Summary and future work

In consideration of the rapidly increasing quantities of pollutants that are directly or indirectly discharged into ambient water bodies, conventional treatments for wastewater can no longer meet the requirements of financial and social pressures for sustainable development. Over the past decade, more potent, robust and environmentally compatible wastewater treatment methods and water quality assessment techniques have quickly become an intense research focus. In this M.Sc. thesis project, the primary interest was to investigate electrodeionization (EDI) as a viable approach for wastewater treatment, as well as the photoelectrochemical method for the rapid determination of COD based on reduced nanoporous TiO_2 electrodes. The primary results obtained are summarized below.

6.1 Separation and recovery of Cr(III) and Cr(VI) using electrodeionization as an efficient approach

Chromium(VI) is carcinogenic, while Cr(III) is considered to be less toxic, and Cr species with combined oxidation states are often found in industrial effluent. It is thus critical to develop techniques that have the capacity for the efficacious removal of both Cr(VI) and Cr(III). In Chapter 3, we investigated the continuous separation and recovery of Cr(III) and Cr(VI) using electrodeionization (EDI) as an advanced and efficient approach. Firstly, we developed a new analytical method, which integrates UV-Visible spectroscopy and Inductively Coupled Plasma Atomic Emission Spectroscopy (ICP-AES), for determining the concentrations of both Cr(VI) and Cr(III) in a mixed solution, and for monitoring the EDI process. Secondly, we determined the limiting current and systematically studied the effects of different applied currents on the removal of Cr(VI), as well as on the recovery of Cr(III)

and Cr(VI). Thirdly, the influence of the level of saturation of ion-exchange resins was assessed in terms of both removal efficiency and energy consumption. It was revealed that the use of fresh ion exchange resins for the EDI process, initially exhibited very effective removal of both Cr(VI) and Cr(III). Both resins became increasingly saturated subsequent to each cycle, resulting in a gradual lowering of the cell voltage. The continuous and highly efficacious removal of highly toxic Cr(VI) (> 99%), and low energy consumption make the EDI process attractive for the separation and recovery of Cr(VI) and Cr(III).

6.2 Removal of nitrate and hardness ions from ground water using electrodeionization

Nitrate concentrations in groundwater frequently exceed the permissible level for potable water in intensive agricultural regions. It is critical to develop strategies for the removal of nitrates at low cost, high efficiency, and without the addition of chemicals. In Chapter 4, a series of experiments were performed with an advanced and efficient approach known as electrodeionization (EDI). It was learned that the EDI system may effectively remove and concentrate nitrate with low energy consumption. An additional desired side effect of this process was that hardness ions, such as Ca^{2+} and Mg^{2+}, were also removed from the dilute compartment and recovered in the concentrate compartment. Furthermore, the limiting current was systematically investigated and the effects of different applied currents, water flow rates, and ratios of cationic and anionic exchange resins on the performance of nitrate removal were studied. When treating actual groundwater samples, the EDI system exhibited an excellent removal rate for all ions (> 90%) under a low and constant cell voltage. The results confirmed that the EDI process was suitable for the continuous and highly efficacious removal and recovery of nitrates and hardness ions in groundwater.

6.3 Electrochemically reduced nanoporous TiO_2 electrode for the determination of chemical oxygen demand

In Chapter 5, a novel, rapid, and environmentally compatible technique for the determination of chemical oxygen demand (COD) using a reduced nanoporous TiO_2 electrode was developed. Highly ordered nanoporous structures were grown directly onto a Ti plate using a three-step anodic oxidation process. Subsequent to electrochemical reduction, the electrochemical behaviour of the reduced nanoporous TiO_2 demonstrated a significant enhancement in photoelectrocatalytic activity. For the first time, a reduced nanoporous TiO_2 electrode was employed to measure COD values in wastewater using a photoelectrochemical method, and the COD values of both the synthetic and actual samples were successfully measured. A typical processing period of one to two minutes, a practical detection limit of 8 mg L^{-1}, and a linear range of 20 mg L^{-1} to 250 mg L^{-1} COD were achieved. More importantly, the proposed method was in excellent agreement with the standard $K_2Cr_2O_7$ COD determination technique, while exhibiting a more rapid analysis period. Additionally, no toxic ($Cr_2O_7^-$) and highly corrosive (H_2SO_4) reagents were required, combined with simple and automatic operation, and environmental compatibility.

6.4 Concluding remarks and future work

In summary, the EDI process has been verified as a green, versatile, environmentally compatible technology to separate and recover ions from wastewater. It has a promising future. Its advantages are that it does not generate residues, consumes low energy while in operation to facilitate cost reductions, and performs highly efficacious ionic separation. Previous studies of EDI have typically only considered synthetic wastewater containing target

compounds, which diminished its industrial significance. To make the EDI process more attractive for industrial applications, a variety of actual wastewater samples should be used in future studies. Furthermore, improvements in EDI systems, such as novel electrode coatings with enhanced activities and higher surface areas, and modified ion exchange materials with better target selectivity and stability, are required to significantly increase the efficacy of EDI systems for a broad range of applications at a global scale.

The rapid determination of COD based on reduced nanoporous TiO_2 electrodes by means of a photoelectrochemical method was successfully developed. As compared to traditional monitoring methods, the proposed approach is simple to operate, lends itself to rapid analysis, and is environmentally compatible without discharging secondary pollutants. Nevertheless, due to the complexity of industrial wastewater, a wider electrode working range with improved photoelectrochemical sensitivity is required in the future. Additionally, microfabrication processes should be developed to commercialize the application. Simplified, modular, and portable devices for the accurate and rapid measurement of COD should be investigated in future work.